



A VARIABLE FLUID-TRANSFORMER FOR  
INCREASING EFFICIENCY IN  
HYDRAULIC CONTROL SYSTEMS

by

STEPHEN LANG DICKERSON

B.S. Mechanical Engineering, Illinois Institute of Technology  
(1962)

M.S. Mechanical Engineering, University of California  
(1963)

SUBMITTED IN PARTIAL FULFILLMENT  
OF THE REQUIREMENTS FOR THE  
DEGREE OF  
DOCTOR OF SCIENCE

at the  
MASSACHUSETTS INSTITUTE OF TECHNOLOGY  
June, 1965

Signature of Author . . . . .  
Department of Mechanical Engineering, May 14, 1965

Certified by . . . . .  
Thesis Supervisor

Accepted by . . . . .  
Chairman, Department Committee on Graduate Students

088

ABSTRACT

A VARIABLE FLUID-TRANSFORMER FOR  
INCREASING EFFICIENCY IN  
HYDRAULIC CONTROL SYSTEMS

STEPHEN LANG DICKERSON

Submitted to the Department of Mechanical  
Engineering on May 14, 1965, in partial  
fulfillment of the requirements for the  
Degree of Doctor of Science

This thesis investigates a variable fluid transformer as a device for controlling the dynamic flow of fluid power in hydraulic control systems. The variable transformer takes the form of a variable jet-pump (VJP).

The advantage of the VJP over the variable orifice as a modulator of fluid power is the reduction in hydraulic power that can be realized. Typically, use of the VJP will halve system power requirements.

Two principal tasks are completed in the thesis. First, a workable VJP design and its static and dynamic characteristics are determined. Analytical models to describe the characteristics are given together with supporting experimental results. Second, the feasibility of such a device in improving the power efficiency of a hydraulic control system is demonstrated. In this respect a particular application--the four-way constant-supply-pressure control system--is studied in detail with regard to efficiency and dynamic control considerations. The experimental results using a position control system are included.

Thesis Supervisor: Shih-Ying Lee  
Title: Associate Professor of Mechanical Engineering

## ACKNOWLEDGEMENTS

The author thanks Professor Shih-Ying Lee for inspiring my initial interest in hydraulic controls and his continuous assistance in preparing this thesis. The patient listening to problems and progress and the helpful suggestions of Professors George A. Brown and Herbert H. Richardson are greatly appreciated. Many former teachers at M.I.T., the University of California, and Illinois Institute of Technology also have my gratitude. Finally, I thank my wife for typing the thesis under pressure of time limits.

This work was done in part at the M.I.T. Computation Center. The author was supported by a Cooperative National Science Foundation Fellowship during the thesis work. A Chandler-Evans grant-in-aid supplied funds for research expenses.

TABLE OF CONTENTS

ABSTRACT . . . . . ii

ACKNOWLEDGEMENTS . . . . . iii

TABLE OF CONTENTS . . . . . iv

TABLE OF SYMBOLS . . . . . vii

INTRODUCTION . . . . . 1

I. STEADY-STATE VJP CHARACTERISTICS . . . . . 4

    Introduction . . . . . 4

    Nozzle Flow . . . . . 6

    Induced Flow . . . . . 10

    Choked Flow . . . . . 18

    Blocked Flow . . . . . 23

    Cone Force and Pressure . . . . . 25

    Summary of VJP Characteristics . . . . . 29

    Experimental Apparatus . . . . . 31

II. DYNAMICS OF THE VJP . . . . . 33

    Purpose . . . . . 33

    Conclusion . . . . . 33

    Normal Operating Conditions of VJP . . . . . 34

    Assumption of Lumped Effects . . . . . 35

    Lumped Capacitance and Inertial Effects  
    in Induced and Blocked Flow Condition . . . . . 38

    The Choked Flow Condition . . . . . 40

    Interpretation of Results . . . . . 54

The Effect of the Check Valve . . . . .	56
Experimental Purpose . . . . .	61
Method of Attack . . . . .	61
Experimental Apparatus . . . . .	62
Experimental Results . . . . .	64
III. CONTROL SYSTEM CONSIDERATIONS IN VJPV DESIGN . . . . .	70
Introduction . . . . .	70
Mechanical Arrangement . . . . .	70
Limiting the number of Parameters . . . . .	73
Schematic Representation of the 4-way VJPV . . . . .	73
Analytic Description of VJPV Pressure-Flow Characteristics . . . . .	74
Effect of Parameters on VJPV Characteristics . . . . .	79
Examples of VJPV Characteristics . . . . .	83
State Space Analysis of a Simple Control System . . . . .	84
IV. RELATIVE POWER EFFICIENCY OF VJPV CONTROL SYSTEMS . . . . .	88
Introduction . . . . .	88
Index of Relative Efficiency . . . . .	88
Simple Cyclic Examples . . . . .	91
Interpretation of Numerical Examples . . . . .	95
Other Efficiency Considerations . . . . .	96
Conclusions . . . . .	97
V. EXPERIENCE WITH A 4-WAY VJPV . . . . .	98
Introduction . . . . .	98
Apparatus . . . . .	98
VJPV Parameters . . . . .	100

Efficiency . . . . .	101
Closed Loop Dynamic Response . . . . .	102
Dynamic Spool Position-Flow Tests . . . . .	103
Conclusion . . . . .	104
VI. OTHER APPLICATIONS AND SUGGESTED FUTURE RESEARCH . . . . .	105
FIGURES . . . . .	108
REFERENCES . . . . .	150
BIOGRAPHICAL NOTE . . . . .	151
APPENDIXES	
One: Geometry Considerations . . . . .	152
Two: Reynolds Number and Normalizing Flow . . . . .	155
Three: VJPV Pressure-Flow Equations . . . . .	157

## SYMBOLS

### Notes

1. Given below are the usual meanings of the symbols. Symbols defined and used only in short sections of the thesis are not listed.
2. It is important to realize that pressures are usually expressed as gage pressures referred to  $P_e \equiv 0$ . In absolute terms  $P_e$  is generally greater than atmospheric.

### Symbols

A	area, with subscript
$\bar{A}$	normalized area $\equiv A/A_T$
$C_v, c_v$	coefficient of velocity for exhaust "nozzle," induced flow and choked flow respectively
$C_d$	nozzle coefficient of discharge
D	diameter of throat
d	diameter of nozzle hole
H	upstream stagnation pressure in converging-diverging section
I	index of relative efficiency
$K_v, k_v$	coefficient of velocity for exhaust nozzle, induced and choked flow respectively
K	solubility constant
$\kappa$	modified solubility constant K/SR
$K_c$	normalized check valve constant
$K_o$	normalized orifice constant
$K_f$	normalized fixed orifice constant

$P, p$	pressure, usually gage referred to $P_e \equiv 0$	
$\mathcal{P}$	normalized pressure $\frac{P}{P_s}$	
$p_o$	absolute vapor pressure of dissolved gases in hydraulic fluid	
$\mathcal{P}$	power	
$Q$	volumetric flow	
$q$	normalized flow $\frac{Q}{A_{ref} \sqrt{\frac{2p_s}{\rho}}}$	$A_{ref} = A_T$ in defining $q_L, q_s,$ and $q_e$
		$A_{ref} = A_N$ in defining $q_N$
$q_{eo}$	linearizing exhaust flow	
$q_{No}$	leakage flow in VJP	
$R$	Reynolds number	
$s$	Laplace variable	
(SR)	slip ratio	
$T$	a delay, transmission, or propagation time	
$t$	time	
$V$	velocity	
$v$	volume or specific volume depending on context	
$w$	angular frequency	
$x$	linear dimension giving position of slider	
$\chi$	normalized $x(\equiv \frac{x}{x_{ref}})$	
$\alpha$	liquid fraction of mixed phase <u>or</u> an angle	
$\Delta$	angular delay of a check valve <u>or</u> increment of a value (i.e., $\Delta t$ )	
$\eta$	efficiency of mixing section and diffusor	



$\mu$	viscosity
$\psi$	exhaust flow momentum coefficient
$\rho$	density
$\nu$	kinematic viscosity

### Subscripts

e	exhaust (not blocked)
eb	exhaust (blocked)
g	gaseous phase
L	load
l	liquid phase
max	maximum
min	minimum
N	nozzle <u>or</u> normalizing ( $Q_N$ )
ref	reference
s	supply <u>or</u> occasionally shock
sat	saturation, refers to vapor pressure of pure fluid
T	throat
vap	vapor, refers to vapor pressure of dissolved gases
1	at section 1
2	at section 2
3	at section 3

### Abbreviations

VJP	variable jet pump
VJPV	variable jet pump valve

### Special Functions

$F_1(\mathcal{P}_L, \chi, Q_L) = 0$  or  $F_1(P_L, x, Q_L) = 0$  is the characteristic function of a VJP in normalized and ordinary form respectively.

$F_2(\mathcal{P}_L, \chi, q_s) = 0$  or  $F_2(P_L, x, Q_s)$  is the supply flow characteristic function of a VJP.

$F_3(\mathcal{P}_L, q_L, q_s) = 0$  or  $F_3(P_L, Q_L, Q_s)$  is the derived characteristic function of the VJP.

$G_1$ ,  $G_2$  and  $G_3$  are the corresponding functions for a VJPV. The notation  $\chi = F_1(\mathcal{P}_L, q_L)$  or  $Q_s = F_3(P_L, Q_L)$  for instance will also be used to indicate the functional relationships.  $f(\chi)$  is a normalized function giving the apparent area of the variable nozzle as a function of the normalized slider position.

## Introduction

There are several conventional methods of controlling the flow of fluid power. In the area of direct modulation of fluid streams the variable orifice occupies a preeminent place. Other means include the jet-pipe valve and the fluid amplifier. Each of these devices control power by dissipating a large part of it. The variable orifice is analogous to a variable resistor. The flow times the pressure drop through the orifice represents a power loss. The jet-pipe valve and fluid amplifier require a constant power input whether any output work is being done or not.

This thesis investigates a more efficient alternative to these devices. Clearly the ideal modulation of fluid power from an efficiency standpoint is a variable transformer which can dynamically match the flow and pressure requirements of a load with the flow and pressure characteristics of a source of hydraulic power with a minimum of power loss. The jet-pump is a crude fluid transformer in that it can convert a fluid stream of a high pressure (relative to a common low pressure stream) to a fluid stream at lower pressure and higher flow. A variable jet-pump (VJP) in which the primary flow can be varied is a dynamic control device which, although far from a loss-less transformer, does enable more efficient control systems than with other means of direct fluid modulation.

The operating principal of a VJP is straightforward. A modulated circular jet propelled by a high pressure source enters a region of low pressure fluid, then a tubular straight section (mixing section), and finally a diffusor. The low pressure fluid is entrained with the jet

and also passes into the mixing section and diffuser. The pressure and flow at the output of the diffuser depends on the size of the primary circular-jet and the amount of induced flow. The primary jet is modulated by moving a cone axially in the hole through which the jet stream is passing. This is very similar to the variable nozzles on some Pelton wheels.

Although this appears to be the first systematic study of the VJP, a 1948 patent<sup>7</sup> incorporates a VJP in regulating the pressure output from a pump. Cunningham<sup>2</sup> suggests that a VJP might have application as a lubricating oil scavenge pump for aircraft engines. Recent literature on liquid jet-pumps is quite sparse; however, Cunningham makes a rather thorough investigation using liquids similar to hydraulic fluids. A recent thesis by Murdock<sup>8</sup> is a valuable aid in understanding the phenomena of jet-pump choking.

There are several books dealing with the general subject of hydraulic control.<sup>1,6</sup> The author made extensive use of Blackburn et. al.<sup>1</sup> in this regard.

Chapters 1 and 2 of this thesis deal with the VJP itself. Chapter 1 is concerned with the static or steady state properties. Chapter 2 deals with dynamic considerations.

Chapters 3 through 6 are concerned with applications, principally the four-way constant-supply-pressure variable jet-pump valve (VJPV). Chapter 3 deals with the design and control considerations. Chapter 4 with the relative power requirements of the VJPV controlled system and the ordinary

---

\* Superscripts indicate a Reference found on page 150.

orifice valve controlled system. Chapter 5 relates the experimental results using a bread-board VJPV in a position control system. Chapter 6 very briefly indicates other applications and areas of possible future investigations.

## Chapter 1

## STEADY STATE VJP CHARACTERISTICS

Introduction

In this chapter the steady state characteristics of a variable jet pump (VJP) are investigated. It is desired to be able to relate analytically  $P_L$ ,  $P_s$ ,  $P_e$ ,  $Q_s$ ,  $Q_e$ ,  $Q_L$ ,  $x$ ,  $d$  and  $D$  for such a device. Referring to Fig. 1.1 the pressures  $P_L$ ,  $P_s$ , and  $P_e$  are the stagnation pressures at the three fluid ports of the VJP and are the load, supply, and exhaust pressures respectively.  $Q_L$ ,  $Q_s$ , and  $Q_e$  are respective flows through these ports.  $D$  and  $d$  are characteristic dimensions of the VJP and are the throat diameter and slider diameters respectively. All other dimensions of the VJP are specified in terms of  $D$ .  $x$  is the opening of the nozzle cone and is defined pictorially in Fig. 1.3. In particular, in any given application  $P_s$ ,  $P_e$ ,  $d$ , and  $D$  are considered given, and what is needed is a function of the form  $F_1(P_L, x, Q_L) = 0$ . In popular hydraulic control work  $F_1$  is said to describe the "characteristics of the valve." Since this is not an ordinary orifice valve,  $Q_L$  is not equal to  $Q_s$  in general. Therefore, one also needs a function of the form  $F_2(P_L, x, Q_s) = 0$  or  $F_3(P_L, Q_L, Q_s) = 0$  to completely specify its performance. Note that by continuity  $Q_L = Q_s + Q_e$  at least in the steady state.

The VJP exhibits three distinct operating modes. At sufficiently low load pressures,  $P_L$ , the output flow does not depend on  $P_L$ . This is the choked condition. At sufficiently high load pressures there is no

pumping action ( $Q_e \leq 0$ ) and, therefore, it is desirable to block the exhaust port so that  $Q_e = 0$  in order to improve energy efficiency. This is the blocked condition. In between these two extremes is a condition of induced flow where a decrease in  $P_L$  is accompanied by an increase in  $Q_L$  and  $Q_e$ . This latter is the usual jet pump or ejector action and is called the induced flow condition.

The particular geometry of the VJP (see Fig. 1.1) except for the scale factors  $d$  and  $D$  was determined after trying a variety of geometries. In particular, 5 different mixing sections, 2 different nozzle plates, and 3 different sliders were tried. The final geometry is a compromise between performance, ease of manufacture, control considerations, and a desire to have a good performance over a wide range of operating Reynold's numbers. No actual attempt to mathematically optimize was made however.

The text is divided into six sections.

- First: the variable nozzle characteristics are discussed under conditions of induced or choked flow.
- Second: the performance of the jet-pump in the region of induced (but not choked) flow is analyzed.
- Third: the phenomena of choking is investigated.
- Fourth: the characteristics of the jet pump under conditions of blocked exhaust port is presented.
- Fifth: the pressures and forces on the nozzle cone are discussed.
- Sixth: the experimental apparatus is presented.

In each section the theory and experimental "verification" are presented together. Insufficient data has been taken for a complete empirical description over all likely operating conditions.

### Nozzle Flow Characteristics

The purpose here is to relate the nozzle flow,  $Q_s = Q_N$ , to  $x$  given  $P_s$ ,  $P_e$ , and  $P_L$ ,\* under conditions of induced and choked flow. The following assumptions are made:

1. The flow depends on  $x$ ,  $P_s$ , and  $P_e$  and not  $P_L$ .
2. The flow is restricted predominantly by inertial effects and not viscous effects. Thus, Bernoulli's equation is approximately correct and more particularly the orifice equation applies.

$$Q_N = C_d A_N \sqrt{\frac{2(\Delta P)}{\rho}} \quad 1.1$$

3. The  $A_N$  above is a function of only  $x$  and  $d$ . Thus,  $f_1(A_N, x, d) = 0$  or by dimensional analysis  $f_2(C_1 \frac{A_N}{d^2}, C_2 \frac{x}{d}) = 0$  where  $C_1$  and  $C_2$  are constants. In particular then, take:

$$\frac{A_N}{\frac{\pi d^2}{4}} \equiv f(\chi) \quad \text{where} \quad \chi \equiv \frac{x}{x_{\text{ref}}} \equiv \frac{x}{d/2} \quad 1.2$$

Using assumption 1. and Eq. 1.2, Eq. 1.1 becomes:

$$Q_N = C_d \frac{\pi}{4} d^2 f(\chi) \sqrt{\frac{2(P_s - P_e)}{\rho}} \quad 1.3$$

or recalling that  $P_e \equiv 0$

$$q_N = C_d f(\chi) \quad \text{where} \quad q_N \equiv \frac{Q_N}{\left(\frac{\pi}{4} d^2\right) \sqrt{\frac{2P_s}{\rho}}} \quad 1.4$$

---

\*This section deals with the VJP nozzle flow except when the exhaust port is blocked. See section 4.



Both  $q_N$  and  $f(\chi)$  have convenient physical interpretations.  $q_N$  is proportional to  $Q_N$  and equal to 1 when  $Q_N$  is that flow that would be realized when the fluid flows at its potential velocity,  $\sqrt{\frac{2P}{\rho}}$ , through the entire nozzle area,  $\frac{\pi}{4} d^2$ . Thus,  $0 \leq q_N < 1$ .  $f(\chi)$  is the ratio of the "apparent" area of the nozzle with the area of the entire nozzle hole.

Several possible "apparent" areas suggest themselves and were tried. These are: (see Fig. 1.3)

1. perpendicular area
2. minimum area
3. radial area
4. angular area (1 and 2 are special cases of this).

None of these are found to be satisfactory for all values of  $\chi$  but the radial area fits very good over the range  $\chi \leq 1$  which is the range of values of interest because for  $\chi > 1$  the gain of the variable nozzle is small (i.e.,  $\frac{df}{d\chi}$  is small) and of little use for control purposes.

Of course,  $f(\chi)$  could be defined entirely empirically and not rely on a corresponding physical area and where extreme accuracy is needed this may be necessary. But for feedback control applications, the radial area interpretation is satisfactory and has the advantage of a physical interpretation. Hence, we will take:

$$f(\chi) = \frac{\frac{\pi}{4} d^2 - \frac{\pi}{4} (d - 2x)^2}{\frac{\pi}{4} d^2} = \frac{4dx - 4x^2}{d^2} = 2\chi - \chi^2 \quad (\chi > 0)$$

$$= 0 \quad (\chi \leq 0)$$

Because in the real case the clearance between the slider and the nozzle plate is not reduced to zero for  $\chi \leq 0$ , Eq. 1.4 is modified to:

$$q_N = C_d f(\chi) + q_{No} \quad 1.6$$

$q_{No}$  is easily determined experimentally by measuring  $q_N$  for  $\chi \leq 0$  where  $f(\chi) = 0$ .

$C_d$  is an experimentally determined constant which for a given geometry is a weak function of the Reynold's number  $R_N$ .

$$R_N \equiv \frac{V_{ref} d \rho}{\mu} \quad \text{where } V_{ref} \equiv \sqrt{\frac{2P_s}{\rho}} \quad 1.7$$

thus:

$$R_N \equiv \frac{\sqrt{2P_s \rho} d}{\mu} \quad 1.8$$

This definition has the advantage of not depending on a measured velocity and, more important, not depending on  $x$ .

Although the geometry of Fig. 1.1 has been assumed throughout, experimental evidence indicates that Eq. 1.6 applies to any nozzle of the general form of Fig. 1.3 where  $\beta > \alpha$ ,  $\alpha \leq 45^\circ$ ,  $\beta \leq 90^\circ$ , where a more general form of Eq. 1.2 should be used. Namely,

$$\chi \equiv \frac{x}{x_{ref}} = \frac{x}{\frac{d}{2} \cot(\alpha)} \quad 1.9$$

Fig. 1.5 gives plots of  $q_N$  vs.  $\chi$  (and  $x$ ) for 3 different  $R_N$  and superimposes Eq. 1.6 for various values of  $C_d$ . The desired value of  $C_d$  is approximately given by:

$R_N$	$C_d$
21,400	.65
17,500	.64
12,300	.63

In each case  $q_{No} = .03$ , but in well machined variable jet pumps it should approach zero. For instance, in a VJP with slider diameter = 0.10 inches and diametrial clearance 0.0002 inches,  $q_{No}$  should be < .004. It is easy to verify that  $q_{No}$  must be less than

$$\left[ \frac{\text{area of clearance}}{\text{total area of nozzle hole}} \right] \approx 2 \cdot \left[ \frac{\text{diametrial clearance}}{\text{diameter}} \right] .$$

Having related slider position to supply flow through Eq. 1.6, it will be convenient to work with  $Q_s$  or  $q_s$  in most of the remaining discussions (i.e., work with  $F_3$ ) rather than  $x$ , (i.e.,  $F_1$  or  $F_2$ ) thus the following definition is pertinent.

$$q_s \equiv \frac{Q_s}{\frac{\pi}{4} D^2 \sqrt{\frac{2P_s}{\rho}}} \quad \text{which since } Q_s = Q_N \quad 1.10$$

$$\text{and } q_N \equiv \frac{Q_N}{\frac{\pi}{4} d^2 \sqrt{\frac{2P_s}{\rho}}}$$

$$q_s = \left(\frac{d}{D}\right)^2 \cdot q_N = \left(\frac{d}{D}\right)^2 (C_d f(\chi) + q_{No})$$

Thus, we are led to an equation of the form  $F_2 (\mathcal{P}_L, \chi, q_s) = 0$  for the region of induced and choked flow, namely Eq. 1.10.

### Region of Induced Flow

The calculation of the amount of flow induced into the VJP,  $Q_e$ , is the most difficult fluid dynamics problem associated with the VJP. This is the area of concern for most of the literature on jet-pumps. The most often cited reference in the field of incompressible-flow jet-pumps is the Gosline and O'Brien.<sup>3</sup> The most pertinent to this work is Cunningham.<sup>2</sup> Both arrive at the same expression in slightly different form. This expression is cumbersome to work with, especially when the jet-pump has a variable nozzle. Both Gosline and O'Brien, and Cunningham (and all studies of jet pumps known to the author) are concerned with jet-pumps with fixed-area, uniform-diameter nozzles. Their expression, in terms of the variables used in this report is:

$$P_L = 2q_s C_V + \frac{2q_e^2}{1 - \frac{q_s}{C_V}} - (2 - \eta) q_L^2 - \frac{q_e^2}{K_v^2 \left(1 - \frac{q_s}{C_V}\right)^2} \quad 1.11$$

where  $C_V$ ,  $\eta$ ,  $K_v$  are empirical coefficients. The flows and pressures have been normalized to eliminate terms involving  $P_s$ ,  $P_e$ ,  $d$ , and  $D$  as defined in the symbols table.

In what follows, three distinct models are examined, all of which yield a particular "derived characteristic function" (i.e.,  $F_3$ ) such as Eq. 1.11. Two important properties of these functions will be examined: (1) simplicity and (2) agreement with empirical results. The models differ principally in the choice of control volume around the mixing region of the VJP and the assumptions regarding the nature of the flow.

MODEL 1 (see Fig. 1.2)

The following assumptions are made:

1. Complete mixing takes place in the throat region between sections 1 and 2 (i.e.,  $V_L$  is constant at section 2).
2. The velocity profile at section 1 consists of a central circular core area,  $A_s$ , moving at velocity  $V_s$  that contains the entire supply flow  $Q_s$  and an annular region around  $A_s$  of area  $A_T - A_s$  moving at velocity  $V_e$  that contains the entire flow  $Q_e$ .
3. The "nozzle" or "orifice" equations apply to the flows  $Q_s$  and  $Q_e$ . i.e.,

$$V_s = C_v \sqrt{\frac{2(P_s - P_1)}{\rho}}, \quad v_e = K_v \sqrt{\frac{2(P_e - P_1)}{\rho}} \quad 1.12$$

4. Head losses due to wall friction in the throat and diffuser inefficiency are proportional to  $V_L^2$ .

In equation form, these assumptions become:

$$P_s = P_1 + \frac{\rho V_s^2}{2C_v^2} \quad 1.13$$

$$P_e \equiv 0 = P_1 + \frac{\rho V_e^2}{2K_v^2} \quad (\text{energy}) \quad 1.14$$

$$P_L = P_2 + \frac{\rho V_L^2}{2} \eta \quad 1.15$$

$$(A_T - A_s) V_e + A_s V_s = A_T V_L \quad (\text{continuity}) \quad 1.16$$

$$A_s V_s = Q_s, (A_T - A_s) V_e = Q_e \quad (\text{continuity}) \quad 1.17$$

$$A_T P_1 + (A_T - A_s) \rho V_e^2 + A_s \rho V_s^2 = P_2 A_T + A_T \rho V_e^2 \quad (\text{momentum}) \quad 1.18$$

These equations can quite readily be reduced to the following dimensionless forms:

$$C_v A \sqrt{1 - \mathcal{P}_1} = q_s \quad 1.19$$

$$\text{where } A \equiv \frac{A_s}{A_T}$$

$$(1 - A) k_v \sqrt{-\mathcal{P}_1} = q_e \quad 1.20$$

$$-\mathcal{P}_1 [2K_v^2 + 2A(C_v^2 - K_v^2) - 1] + 2C_v^2 A - (2 - \eta) q_L^2 = \mathcal{P}_L \quad 1.21$$

Unfortunately, this cannot be solved in closed form to give  $F_3(\mathcal{P}_L, q_L, q_s)$  because of the terms  $\sqrt{1 - \mathcal{P}_1}$  and  $\sqrt{-\mathcal{P}_1}$ . However, it can be solved along the important line where  $q_L = q_s$ . This solution is:

$$\mathcal{P}_L = 2C_v q_L - (2 - \eta) q_L^2 = 2C_v q_s - (2 - \eta) q_s^2 \quad 1.22$$

This line, of course, separates the region of induced flow from the region of blocked exhaust flow. It is also useful because data is fairly easy to obtain along this line and thus  $C_v$  and  $\eta$  can be determined, leaving only  $K_v$  to be determined by other means.

## MODEL 2 (see Fig. 1.2)

All the assumptions of Model 1 remain valid except that one assumes:

$$v_s = C_v \sqrt{\frac{2(P_s - P_e)}{\rho}} \quad \text{instead of Eq. 1.12} \quad 1.23$$

$$v_e = K_v \sqrt{\frac{2(P_e - P_1)}{\rho}}$$

This change is hard to justify\* except that a great simplification results.

Thus, if we replace Eq. 1.13 with

$$P_s = P_e + \frac{\rho v_s^2}{2C_v^2} \quad 1.24$$

the final result is the usual jet-pump equation given by Cunningham and others.

$$P_L = 2q_s C_v + \frac{2q_e^2}{1 - \frac{q_s}{C_v}} - (2 - \eta) q_L^2 - \frac{q_e^2}{K_v^2 \left(1 - \frac{q_s}{C_v}\right)^2} \quad 1.25$$

Note that this equation also reduces to Eq. 1.22 when  $q_L = q_s$ .

## MODEL 3 (see Fig. 1.2)

In order to obtain further simplification we take advantage of

the downstream pressure. This implies that in the immediate region of the nozzle, the pressure must be  $P_e$ . The assumptions for this case are:

1. Complete mixing within the control volume.  
I.e.,  $V_L$  is constant at section 3.
2. Along surface 1 the pressure is  $P_e$  and only the nozzle flow crosses this surface. The nozzle velocity is given by:

$$V_s = C_v \sqrt{\frac{2(P_s - P_e)}{\rho}}$$

3. Along the cylindrical surface 2 the velocity profiles are similar for all flows.
4. Head losses due to wall friction in the throat and diffuser inefficiency are proportional to  $V_L^2$ .

In equation form these assumptions become:

$$P_s = P_e + \frac{\rho V_s^2}{2C_v^2} \quad 1.26$$

energy

$$P_L = P_3 + \frac{\rho V_L^2}{2} \eta \quad 1.27$$

$$A_s V_s = Q_s, \quad A_T V_L = Q_L \quad (\text{continuity}) \quad 1.28$$

$$\bar{V}_e = \frac{Q_e}{A_2} \bar{f}(x/x_0) \quad (\text{a vector equation}) \quad 1.29$$

$$P_e A_T + A_s \rho V_s^2 + \rho \int_0^{x_0} -V_{e_r} \cdot V_{e_x} \pi D dx = \rho V_L^2 A_T + P_3 A_T \quad 1.30$$

(momentum)



Eq. 1.29 is a mathematical statement of assumption 3. It is, in fact, a vector equation which can be written:

$$v_{e_x} = \frac{Q_e}{A_2} f_x(x/x_0) \quad 1.31$$

$$v_{e_r} = \frac{-Q_e}{A_2} f_r(x/x_0)$$

Note that by our geometry, Fig. 1.1

$$x_0 = \frac{3}{2} D \quad \text{and} \quad \pi D x_0 = \pi \left(\frac{3}{2} D\right)^2 = A_2 \quad 1.32$$

It has been assumed that  $f(x/x_0)$  does not change for any flow. Thus, if one defines:

$$\psi \equiv \frac{1}{3} \int_0^1 f_x(t) f_y(t) dt = \text{constant} \quad 1.33$$

Eq. 1.30 becomes

$$P_e A_T + A_s \rho v_s^2 + \rho \frac{Q_e^2 3\psi}{A_2} = \rho v_L^2 A_T + P_3 A_T \quad 1.34$$

Equations 1.36, 1.37, 1.38, and 1.34 simplify to

$$p_L = 2C_v q_s - (2 - \eta) q_L^2 + \psi q_e^2 \quad 1.35$$

or using:

$$q_L = q_s + q_e$$

$$\mathcal{P}_L = 2C_v q_s - [2 - \eta - \psi] q_e^2 - (2 - \eta) q_s^2 - (2 - \eta) 2q_s q_e$$

1.36

Eq. 1.35 is a much simpler expression than that derived from Models 1 or 2.

As mentioned previously the criteria for choice of a particular model to describe the flow should be (1) simplicity\* of resulting expressions (2) agreement with empirical data. On the first count, one can certainly eliminate Model 1 because the resulting relationships cannot be expressed in closed form.

Empirically, since all models yield  $\mathcal{P}_L = 2C_v q_L - (2 - \eta) q_L^2$  along the line where  $q_e = 0$ , it is fairly easy to determine suitable values for  $C_v$  and  $\eta$ . Many previous studies are also available for predicting  $C_v$  for simple nozzles and for very high Reynolds numbers. A value of 0.975 is typical.

The data taken indicates that  $C_v = .97$  is good for  $R_N > 12,000$  and probably for lower  $R_N$ .  $\eta$ , as would be expected, is a strong function of  $R_T$  for "low" Reynolds numbers. The empirical results are:

$R_T$	$\eta$
14,000	.54
20,000	.56
25,000	.61

(see Fig. 7a, b, and c)

---

\*If this study were concerned with explaining the mechanics of flow, simplicity would not be a suitable criteria. However, since the resulting expressions here are to be used to analyze control systems using VJP's, simplicity is of essence.

It is important to realize that the  $R_T$  used here is defined by:

$$R_T \equiv \frac{\sqrt{2\rho P_s}}{\mu} D = \frac{V_L D \rho}{\mu} \cdot \frac{1}{q_L} \quad 1.37$$

Thus, the more conventional Reynolds number,  $\rho(V_L D)/\mu$ , is in fact  $q_L$  times  $R_T$ . The reason  $R_T$  is used instead of  $\rho(V_L D)/\mu$  is that the latter is not constant over the entire range of operation. Admittedly  $\eta$  is actually better correlated with  $(V_L D \rho)/\mu$  (and usually is) but to do so would greatly complicate the calculation of the flow characteristics of the VJP since  $\eta$  would not be constant.

Once  $\eta$  and  $C_v$  are determined, all that remains unknown is  $K_v$  in Model 2 and  $\psi$  in Model 3. Cunningham takes  $K_v = 1$ . In Fig. 1.7a is plotted the theoretical curves of Eq. 1.35 and Eq. 1.11 for  $C_v = .97$ ,  $\eta = .61$ ,  $K_v = 1.0$  and  $K_v = .906$ ,  $\psi = .84$ . It can be seen that Eq. 1.11 with  $K_v = 1.0$  provides the best fit with observed data. Eq. 1.35 with  $\psi = .84$  is a close second.

However, it is apparent that the data fits straight lines better than the parabolas provided by Eq. 1.35. Thus, one is tempted to linearize (i.e., approximately by straight lines) one of these equations. If this is done to Eq. 1.35 there results:

$$\mathcal{P}_L = 2C_v q_s - (2 - \eta) q_s^2 - [2(2 - \eta) q_s + (2 - \eta - \psi) q_{e0}] q_e$$

1.38

This, in fact, is a very simple equation since it takes the form of:

$$P_L = A(q_s) - B(q_s) q_e \quad \text{where A, and B are} \quad 1.39$$

functions of  $q_s$

where as we have seen (Eq. 1.10)  $q_s$  is only a function of the slider position.

Furthermore, this linearized equation fits the empirical data very well (better than either model 2 or 3) when  $q_{e0} = .35$ . (see Fig. 1.7a). As seen by Fig. 1.7a, b, and c,  $\psi$  can be considered .84 for all values of  $R_T$  between 14,000 and 25,000. The author surmizes from the way the  $\psi$  enters the derivation, that it can be considered constant for sufficiently\* large  $R_T$ .  $q_{e0}$  on the other hand, depends on the range of values for  $q_e$  for which Eq. 1.38 is to be used. For values of  $q_e$  up to 0.5,  $q_{e0} = 0.35$  appears to be satisfactory.

Because of its simplicity and good agreement with observed data Eq. 1.38 will be taken as the characteristics of the VJP for control system analysis. It is an equation of the form  $F_3(P_L, q_L, q_s) = 0$ .

### Choked Flow

In the operation of a VJP it is observed that (for constant  $x$ ) as the downstream pressure is reduced the supply flow,  $Q_s$ , remains constant and the exhaust flow,  $Q_e$ , increases until a critical value of  $P_L$  is reached. If the value of  $P_L$  is reduced below this value, no change in  $Q_s$  or  $Q_e$  takes place (i.e.,  $Q_L = Q_s + Q_e$  const.). Explanations of this phenomena, called choking, have been made by Cunningham<sup>2</sup> and Murdock.<sup>8</sup>

---

\*The lower bound unknown

Cunningham's analysis is quite accurate, where there is not appreciable dissolved gases in the fluid. Murdock offers a more refined analysis which accurately predicts flow at choking and is intended for the case where the dissolved gases are an important factor in choking. In the case at hand the dissolved gases are the constituent of the hydraulic oil that cause the choking. Hydraulic oils generally have low vapor pressure in their pure state<sup>\*</sup>, but they do dissolve gases from the surroundings until reaching equilibrium.<sup>\*\*</sup> These gases will evolve from the oil whenever the pressure of the oil falls below the pressure at which it is stored in contact with a gaseous atmosphere. In practice this would very frequently be air at 14.7 psia. Even though the dissolved gases cause choking in the VJP, the author believes for reasons put forth in detail in Chapter 2 that Cunningham's general approach is more accurate in this case.

Fig. 1.6d displays the conceptual model. As Cunningham observed, choking sets in when the pressure at section 1, the entrance to the constant cross section throat, falls to some critical pressure. This pressure can be taken as the vapor pressure of the dissolved gases  $P_{\text{vap}}$ , when the following condition is satisfied. Namely:

$$1 - \kappa + \frac{2P_{\text{vap}}^{\kappa}}{P_0} < 0 \quad 2.22a$$

---

\*The vapor pressures of J-43 oil at 100°F is .0029 psia. J-43 oil at approx. 96°F was used in all experiments reported here.

\*\*According to Cunningham a volume of air equal to 11% of the volume of J-43 oil is dissolved at STP.

where  $p_0$  is the absolute vapor pressure of the dissolved gases and  $\kappa$  is a modified solubility constant. In Chapter 2 it is concluded that the above condition is usually satisfied in VJP applications and we will assume so here.

If the flow at Section 1 is considered to be two distinct flows: one containing the supply flow,  $Q_s$ , at velocity,  $V_s$ ; the other containing the exhaust flow,  $Q_e$ , at velocity,  $V_e$ , the following equations apply:

$$P_s = P_1 + \frac{\rho V_s^2}{2C_v^2}, \quad V_s = c_v \sqrt{\frac{2(P_s - P_1)}{\rho}} \quad 1.40$$

$$P_e \equiv 0 = P_1 + \frac{\rho V_e^2}{2k_v^2}, \quad V_e = k_v \sqrt{\frac{-2P_1}{\rho}}$$

where  $c_v$  and  $k_v$  are "coefficients of velocity" often used in nozzle theory to account for observed departure from frictionless flow. The supply flow passes through a circular section at Section 1 of area  $A_s$ . The exhaust flow must pass through an area  $A_T - A_s$ . By continuity:

$$A_s V_s = Q_s, \quad (A_T - A_s) V_e = Q_e \quad 1.41$$

From Eq. 1.40 we can write:

$$A_s c_v \sqrt{\frac{2(P_s - P_1)}{\rho}} = Q_s \quad 1.42$$

$$(A_T - A_s) k_v \sqrt{\frac{2P_1}{\rho}} = Q_e$$

Eq. 1.42 can be written in dimensionless form:

$$q_s = c_v A \sqrt{\frac{P_s - P_1}{P_s}} \quad \text{where } A \equiv \frac{A_s}{A_T}$$

$$q_e = k_v (1 - A) \sqrt{\frac{-P_1}{P_s}} \quad 1.43$$

Eliminating A yields:

$$\frac{q_s}{c_v} \sqrt{\frac{P_s}{P_s - P_1}} + \frac{q_e}{k_v} \sqrt{\frac{P_s}{-P_1}} = 1 \quad 1.44$$

During choked flow  $P_1$  is the vapor pressure of the pure fluid. Thus:

$$\frac{q_s}{c_v} \sqrt{\frac{P_s}{P_s - P_{\text{vap}}}} + \frac{q_e}{k_v} \sqrt{\frac{P_s}{-P_{\text{vap}}}} = 1 \quad 1.45$$

Two constants,  $c_v$  and  $k_v$  in Eq. 1.45 remain to be found experimentally.

There are a great many variables that  $c_v$  and  $k_v$  could depend upon.\*

Fortunately, given that  $R_T$ ,  $R_{\text{vap}}$  are sufficiently large\*\*  $c_v$  appears to be constant  $\approx .99$  and  $k_v \approx .93$ . Equation 1.45 can, of course, be put in two different forms by using the continuity equation:

$$q_L = q_s + q_e$$

---

\*  $P_s$ ,  $P_{\text{vap}}$ ,  $D$ ,  $\mu$ ,  $\rho$ .

\*\*  $R_T = 15,000$ ,  $R_{\text{vap}} = 7,000$  are sufficiently large, but probably much longer than necessary.

Thus:

$$1 = \frac{q_L}{c_v} \sqrt{\frac{P_s}{P_s - P_{vap}}} + q_e \left[ \frac{1}{k_v} \sqrt{\frac{P_s}{-P_{vap}}} - \frac{1}{c_v} \sqrt{\frac{P_s}{P_s - P_{vap}}} \right]$$

1.47

$$1 = \frac{q_L}{k_v} \sqrt{\frac{P_s}{-P_{vap}}} + q_s \left[ \frac{1}{c_v} \sqrt{\frac{P_s}{P_s - P_{vap}}} - \frac{1}{k_v} \sqrt{\frac{P_s}{-P_{vap}}} \right]$$

Equations 1.45, and 1.47 are of the form  $F_3(\mathcal{P}_L, q_L, q_s) = 0$ . Fig.

1.6a, b, and c show experimental results for three different combinations of  $P_s$  and  $P_{vap}$ .

A word is in order to explain why  $c_v \neq C_v$  even though they enter in the same manner in the choked flow and induced flow derivations (note however, they are very close to equal).

First, in the induced flow derivation we are interested in the momentum carried by the streams, i.e.:

$$\rho \int_A V^2 dA \equiv \rho \bar{V}^2 A \quad 1.48$$

in the choked flow derivation we are interested in mass flow, ie,

$$\int_A V dA \equiv \bar{V} A \quad 1.49$$

where in each case the coefficient of velocity, C, is defined by:

$$C(\text{potential velocity}) = C \sqrt{\frac{2P}{\rho}} \equiv \bar{V} \quad 1.50$$



Second, during choking the flow pattern is different.  $C_v$  is evaluated along the line where  $Q_e = 0$ . However,  $c_v$  is evaluated at the maximum  $Q_e$ .

#### Blocked Exhaust Flow

Since the use of the VJP as conceived here is to be an efficient (relative to the variable orifices) modulator of hydraulic power flow, it will be important in most applications to block the exhaust port whenever  $Q_e$  would otherwise be negative. When this port is blocked, the VJP no longer operates as a jet pump, but rather as a variable orifice.

To derive the desired mathematical relationships relating  $Q_s$ ,  $P_L$ ,  $Q_L$  and  $x$ , we note that in the region of blocked exhaust flow:

$$Q_s = Q_L \quad \text{or} \quad q_s = q_L \quad 1.51$$

This is of the form of  $F_3 = 0$ .

The relationship  $F_1 = 0$  (in this case  $F_1$  is identical to  $F_2$ ) can be found using equations of section 1 and 2 where  $P_e$  is set equal to  $P_{eb}$  and  $Q_e = 0$ . Namely, Eq. 1.3 becomes:

$$Q_N = C_d \frac{\pi}{4} d^2 f(x) \cdot \sqrt{\frac{2(P_s - P_{eb})}{\rho}} \quad 1.52$$

or

$$q_N = C_d f(x) \cdot \sqrt{\frac{P_s - P_{eb}}{P_s}} \quad 1.53$$

We must, of course, make the modification for leakage in the real case, which makes Eq. 1.53:

$$q_N = (C_d f(x) + q_{No}) \sqrt{1 - \varphi_{eb}} \quad 1.54$$

and by Eq. 1.10:

$$q_s = \left(\frac{d}{D}\right)^2 (C_d f(x) + q_{No}) \sqrt{1 - \varphi_{eb}} \quad 1.55$$

Eq. 1.34 becomes:

$$P_{eb} A_T + A_s \rho v_s^2 = \rho v_L^2 A_T + P_3 A_T \quad 1.56$$

since  $Q_e = 0$ . Using 1.26 and 1.28 Eq. 1.56 becomes:

$$P_{eb} A_T + Q_s \rho C_v \sqrt{\frac{2(P_s - P_{eb})}{\rho}} = \rho \frac{Q_L^2}{A_T} + P_3 A_T \quad 1.57$$

Dividing by  $P_s A_T$ , this becomes:

$$\varphi_{eb} + 2C_v q_s \sqrt{1 - \varphi_{eb}} = 2q_L^2 + \varphi_3 \quad 1.58$$

From Eq. 1.27

$$\varphi_L = \varphi_3 + \eta q_L^2 \quad 1.59$$

then:

$$\mathcal{P}_{eb} + 2C_v q_s \sqrt{1 - \mathcal{P}_{eb}} = (2 - \eta) q_L^2 + \mathcal{P}_L \quad 1.60$$

Since from Eq. 1.55:

$$1 - \mathcal{P}_{eb} = \left[ \left( \frac{d}{D} \right)^2 (C_d f(\chi) + q_{No}) \right]^{-2} q_s^2 \quad 1.61$$

Eq. 1.60 becomes:

$$\begin{aligned} \mathcal{P}_L = 1 - \{ 2 - \eta + \left[ \left( \frac{d}{D} \right)^2 (C_d f(\chi) + q_{No}) \right]^{-2} - \\ \left[ \left( \frac{d}{D} \right)^2 (C_d f(\chi) + q_{No}) \right]^{-1} \cdot 2C_v \} q_s^2 \end{aligned} \quad 1.62$$

Eq. 1.62 is of the form:

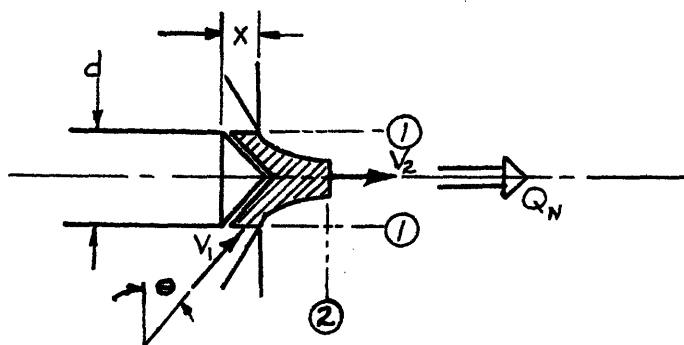
$$\mathcal{P}_L = 1 - A(\chi) q_s^2, \quad (A \text{ is a function of } \chi) \quad 1.63$$

which is as expected, the orifice equation. Since in the derivation of 1.62 no new assumptions were introduced, this equation will be valid if the induced flow analysis and the nozzle flow analysis are valid. Therefore, it is necessary to take no data to verify Eq. 1.62.

#### Cone Forces and Pressure

The hydraulic fluid as it passes through the nozzle will exert a force on the cone face and the supporting uniform diameter shaft. Due to symmetry the total force will be solely in the axial direction. Because the cone's position must be varied in using the VJP as a dynamic control device it is of some importance to know the approximate axial force exerted on it by the fluid.

To determine this force, consider a control volume adjacent to the cone face as shown below.



The fluid enters the C.V. entirely through cylindrical surface 1 and departs entirely through 2. Assume the surface of revolution between 1 and 2 is at pressure  $P_e \equiv 0$ . This assumption is the same one made earlier in considering the induced flow Model 3 and is based on the empirical observation that nozzle flow depends only on  $P_e$  and  $P_s$  but not  $P_L$ . By introducing an average pressure  $P_N$  acting on the nozzle cone the momentum equation for the C.V. writes:

$$P_N \left( \pi \frac{d^2}{4} \right) + \rho QV_1 \sin(\theta) = \rho QV_2 \quad 1.64$$

where we take the velocities across 1 and 2 as constant and given by:

$$V_1 = \frac{Q}{\pi dx \cos(\theta)} \quad , \quad V_2 = C_v \sqrt{\frac{2P_s}{\rho}} \quad 1.65$$

which are, in fact, continuity and Bernoulli respectively. Noting that from Eq. 1.4  $q_N$  is given by:

$$C_d f(x) = q_N \equiv \frac{Q_N}{\pi \frac{d^2}{4} \sqrt{\frac{2P_s}{\rho}}} \quad \text{where } f(x) = 2x - x^2 \quad 1.66$$

$$x \equiv \frac{x}{d/2}$$

Using Eq. 1.66 and 1.65, Eq. 1.64 reduces to

$$\mathcal{P}_N \equiv 2C_v q_N - \tan(\theta) \frac{q_N^2}{x} \quad \text{where } \mathcal{P}_N \equiv \frac{P_N}{P_s} \quad 1.67$$

The right-hand side can be written entirely as a function of  $x$  or  $q_N$  using Eq. 1.66.

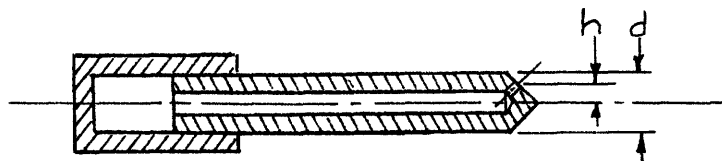
$$\mathcal{P}_N = 2C_v q_N - \tan(\theta) \frac{q_N^2}{1 - \sqrt{1 - \frac{q_N}{C_d}}}$$

or

$$\mathcal{P}_N = 2C_v C_d f(x) - \tan(\theta) \frac{C_d^2 f^2(x)}{x}$$

Experimental measurement of the force on the nozzle cone indicated that  $\theta \approx 51^\circ$ . Fig. 1.14 gives a comparison of the curve given by Eq. 1.68 with experimentally observed data. As expected cone force did not depend on the amount of exhaust flow but only on the nozzle flow.

It may be desirable to balance the force on the cone in some application in order to prevent force feedback. The most obvious scheme to do this, to drill a small hole in the cone face and lead the hydraulic fluid back to a balancing cylinder, is shown.



In order to be in perfect balance the pressure at the hole must equal  $P_N$ , the average pressure on the cone.

It is unlikely that any single point on the cone face would have the average pressure acting on it under all conditions, however, some points probably will give better balancing on the average than others. While this problem needs much more attention, the following qualitative observations were made. By symmetry the pressure on the cone face should only be a function of radius for a given set of conditions. Four separate cones and support shafts equipped with pressure taps were built with holes drilled at  $(h/d)$  equal to 0, 0.21, 0.31, and 0.44. While attempts to measure the pressure distribution with the use of these devices gave erratic results, the indication was that a hole near the outer edge would be best. Two cones with supporting shafts and balancing cylinders were then built. One with a hole in the center, the other was with a hole at  $(h/d) = .35$ . These were then placed in the VJP and manipulated by hand. The one with  $(h/d) = .35$  gave the best results. Its position was easily controlled by hand and required only a few ounces of force. Under the test conditions the unbalanced force on the cone was of the order of 10 pounds. The radius  $(h/d) = 0.35$  also has the conceptual advantage that half the cone area lies within the radius and half outside.

In constructing the dynamic VJP's used in the experimental work in Chapters 2 and 5, the cone forces were balanced using a hole at  $(h/d) = .035$ .

### Summary of VJP Characteristics

#### REGION OF BLOCKED EXIT FLOW

$$\text{here } \mathcal{P}_L > 2C_v q_s - (2 - \eta)q_s^2$$

$$F_2(\mathcal{P}_L, \chi, q_s) \quad \mathcal{P}_L = 1 - \{2 - \eta - \left[\left(\frac{d}{D}\right)^2 (C_d f(\chi) + q_{No})\right]^{-1} \cdot 2C_v \\ + \left[\left(\frac{d}{D}\right)^2 (C_d f(\chi) + q_{No})\right]^{-2}\} q_s^2$$

$$F_3(\mathcal{P}_L, q_L, q_s) \quad q_L = q_s$$

$$F_1(\mathcal{P}_L, \chi, q_L) \quad \text{same as } F_2 \text{ since } q_L = q_s$$

#### REGION OF CHOKED FLOW

$$\text{here } 1 = \frac{q_s}{c_v} \sqrt{\frac{P_s}{P_s - P_{vap}}} + \frac{q_e}{k_v} \sqrt{\frac{P_s}{-P_{vap}}}$$

$$F_2(\mathcal{P}_L, \chi, q_s) \quad q_s = \left(\frac{d}{D}\right)^2 (C_d f(\chi) + q_{No})$$

$$F_3(\mathcal{P}_L, q_L, q_s) \quad 1 = \frac{q_s}{c_v} \sqrt{\frac{P_s}{P_s - P_{vap}}} + \frac{q_e}{k_v} \sqrt{\frac{P_s}{-P_{vap}}}$$

$$F_1(\mathcal{P}_L, \chi, q_L) \quad \text{Substitute } F_2 \text{ in } F_3$$

## REGION OF INDUCED FLOW

$$\text{here} \quad \mathcal{P}_L \leq 2C_v q_s - (2 - \eta) q_s^2$$

$$\text{and} \quad q_e < k_v \sqrt{\frac{-P_{\text{vap}}}{P_s}} - q_s \frac{k_v}{c_v} \sqrt{\frac{-P_{\text{vap}}}{P_s - P_{\text{vap}}}}$$

$$F_2(\mathcal{P}_L, \chi, q_s) \quad q_s = \left(\frac{d}{D}\right)^2 (C_d f(\chi) + q_{\text{No}})$$

$$F_3(\mathcal{P}_L, q_L, q_s) \quad \mathcal{P}_L = 2C_v q_s - (2 - \eta) q_s^2$$

$$- [2(2 - \eta) q_s + (2 - \eta - \psi) q_{e0}] q_e$$

$$F_1(\mathcal{P}_L, \chi, q_L) \quad \text{Substitute } F_2 \text{ in } F_3$$

$$\text{Note that } q_L = q_e + q_s$$

$$f(\chi) = 2\chi - \chi^2$$

## EMPERICAL CONSTANTS

<u>Symbol</u>	<u>Name</u>	<u>Range of Values</u>
$\eta$	"diffusor" efficiency	.54 - .61
$C_v$	nozzle velocity coefficient	.97
$\psi$	exhaust flow momentum coefficient	.84



<u>Symbol</u>	<u>Name</u>	<u>Range of Values</u>
$q_{eo}$	linearizing "average" exhaust flow	.35
$q_{No}$	leakage flow	$\geq 0$
$c_v$	nozzle saturation coefficient of velocity	.93
$k_v$	exhaust saturation coefficient of velocity	.99
$C_d$	nozzle coefficient of discharge	.63 - .65

The values of the above coefficients are subject to the restrictions made in the text. In particular  $\eta$  and  $C_d$  are functions of the appropriate Reynolds numbers,  $q_{eo} = .35$  applies for  $q_e \leq .5$ , and  $c_v$  and  $k_v$  are dependent on fulfilling the condition of Eq. 2.22a.

#### Experimental Apparatus

The apparatus to determine the characteristics of the VJP is quite simple. The VJP itself is constructed as shown in Fig. 1.8. While all results given in this report apply to the standard geometry of Fig. 1.1 where  $D = .125''$  and  $d = .108''$ , the apparatus itself is flexible, and several different geometries were tried as discussed in Appendix 1. The slider position is controlled by a screw with 20 threads/in. The head of the screw has 10 equally spaced machined grooves which are lined up with a machine groove on the VJP housing, giving steps of .005 in. The complete apparatus is indicated in Fig. 1.9. The pressure gages were calibrated with dead weight pressure calibrators. The load flow was measured by 2 rotometers; the exhaust flow by a positive displacement motor driving a D.C. generator connected to a V.T.V.M. The flow measuring devices were compared to each other and found to agree within .1 gpm at all flows.

Photographs of the VJP used to determine the static characteristics are shown in Fig. 1.13.

An adaptor for the VJP of Fig. 1.8 was built to measure cone forces and pressures. This adaptor is shown in Fig. 1.15. The force transducer is a Dynisco 0-25 lb. transducer.

## Chapter 2

### DYNAMICS OF THE VJP

#### Purpose

It is desirable to be able to use the results of the previous chapter in predicting the dynamic performance of a hydraulic control system. In the previous chapter the output pressure,  $P_L$ , of the VJP was functionally related to the output flow,  $Q_L$ , and nozzle cone position  $x$ , given the supply pressure,  $P_s$ , and the exhaust pressure,  $P_e$ . However, this is only for stationary values of  $Q_L$ ,  $x$ , and  $P_L$ . It is the task of this chapter to investigate the contributions of the VJP to the dynamics of a control system.

#### Conclusions

The general conclusion of this study is that under conditions normally encountered in hydraulic control systems, the designer can consider the output pressure,  $P_L$ , as a function of the instantaneous values of  $Q_L$  and  $x$  only, and hence identical to that predicted by the static characteristics.

An important exception to this conclusion occurs in the region of choked flow, where the presence of a mixed phase in the diffusor of the VJP results in rather large compressibility effects and signal transmission delays. These effects are most pronounced in large VJP's operating at relatively low pressures. In most applications the choked flow is the least likely condition of the VJP and the designer may take pains to avoid it altogether if the forementioned dynamic effects will degrade performance. The design of control valves using VJP's is

discussed in the next chapter. The inertial, viscous, and compressibility effects of lines connecting the VJP to various other components in the system are not in general to be ignored. The check valve should be located immediately adjacent to the VJP in order to make the compressibility effects of the fluid volume between the check valve and the VJP mixing region negligible.

The analysis which follows is intended to justify the above conclusion and to indicate the limits on the validity of this conclusion. The experimental section of this chapter is to verify that there are no transient changes in flow regimes (i.e., flow patterns) under dynamic conditions that materially effect the characteristics.

#### Normal Operating Conditions of Hydraulic Control Systems

The expected application of the VJP is in replacing variable orifices in conventional hydraulic control systems. In general, it will be most advantageous to do so when high power flows are involved so that the increased efficiency of the VJP results in an appreciable savings.

In a somewhat arbitrary fashion the normal operating domain of hydraulic control systems will be specified here to provide a basis for subsequent simplifying assumptions.

Range of output horsepower	0 - 100 hp
Operating pressure range, $P_s$	1000 psi - 6000 psi
Vapor pressure of dissolved air in hydraulic fluid	15 psia
Exhaust pressure	$P_e \geq 0.2(P_s - P_e)$ in absolute pressure units
Dynamic response range:	
Under 10 hp	0 - 200 cps
Over 10 hp	0 - 100 cps

In the case where these limits do not apply, most of the simplified assumptions will still hold; however, they should be checked. Output horsepower is defined as that horsepower that would be delivered at  $\mathcal{P} = 0.3$ ,  $q = 0.6$ .

One of the most important parameters in the dynamic study is the characteristic dimension,  $D$ , the VJP throat diameter. Figure 2.1 plots this versus input pressure,  $P_s$ , for lines of constant horsepower.

In this graph, as in all other numerical examples, the density of the fluid,  $\rho$ , is taken as  $7.8 \times 10^{-5} \frac{\text{lb. sec}^2}{\text{in.}^4}$  which is the density of J-43 at 90° F. In numerical examples we will also take the bulk modulus as  $10^5$  psi. This is considerably lower than most hydraulic fluids at room temperature but both dissolved gases and temperature can increase the compressibility.\*

#### Assumption of Lumped Effects

It is extremely convenient to be able to consider the inertial and capacitance effects of the fluid in the VJP as lumped parameters. This assumption is justified if disturbances in the VJP propagate throughout the VJP in a negligible amount of time. Pressure disturbances propagate at the speed of sound relative to the medium. In the cases of blocked or induced flow conditions the VJP is filled with liquid. The speed of sound in hydraulic fluids is of the order of  $3.56 \times 10^4$  in/sec.\*\* The maximum  $D$  of interest from Fig. 2.1 is approximately 0.5 in., hence a disturbance will propagate the length of the VJP (i.e., 5 in.) in

---

\* See pages 57 - 58 of Lewis and Stern<sup>6</sup> for temperature effects. Unpublished work at M.I.T. indicates that dissolved gases can greatly reduce the bulk modulus.

\*\* This is based on density and bulk modulus mentioned in previous section.

$1.4 \times 10^{-4}$  sec. This is a negligible effect since at 100 cps the phase lag will be  $360 \times (1.4 \times 10^{-4}) \times (100) = 5^\circ$ . Most VJP's would be considerably shorter. Thus, we will consider the oil in the VJP as a lumped capacitance and inertia.

In the case of the VJP in a choked condition the discussion is more complicated. A more thorough investigation of this phenomena is postponed to the section on capacitance in the choked condition. In this state disturbances can propagate downstream only, due to supersonic mixed flow in the diffuser. This does not retard the response of  $P_L$  to changes in  $Q_L$  but does affect the response of  $P_L$  to changes in  $x$ . A disturbance originating at the nozzle of the VJP due to a change in  $x$  will propagate through the mixed phase supersonic region at the local speed of sound, plus the velocity of the fluid. The velocity of the fluid will be the greater of these and will be approximately the velocity of the pure liquid phase at the beginning of the diffuser.

As will be shown subsequently the velocity at the beginning of the diffuser (i.e., end of the throat) is simply the flow divided by the area of the throat, since the mixed phase starts at the throat and proceeds down the diffuser. The velocity can be calculated then easily in any particular case. By dividing the length of the mixed phase region by this velocity, the propagation delay can be approximated. Methods of approximating the length of the mixed phase are given later; however, one can easily get an approximate "worst case" delay for any VJP application. The minimum velocity at the throat in the choked condition is given by:

$$V_{\min} = \sqrt{\frac{-2P_{\text{vap}}}{\rho}} \quad 2.1$$

The maximum length of the mixed phase is the length of the diffuser-- which if the standard geometry of Fig. 1.1 is used--is 8 D. Thus, the longest possible propagation time is:

$$T = \frac{8D}{V_{\min}} = 8D \sqrt{\frac{\rho}{-2P_{\text{vap}}}} \quad 2.2$$

This time turns out to be rather significant in the case of large diffusers and small  $P_{\text{vap}}$ . For example in a 100 hp unit with  $P_s = 1000$  psi,  $P_{\text{vap}} = -185$  psi, and  $D = 0.5$ .

$$T = .0023 \text{ sec} \quad 2.3$$

which at 100 cps results in an  $83^\circ$  phase lag!! This is hardly negligible. Hence, in extreme cases the assumption of lumped parameters is questionable. However, the author would expect that since disturbances in the choked condition propagate only downstream that the dynamic performance can be approximated by lumped parameters at each end of the diffuser plus a pure delay for the diffuser proper.

In the case of smaller high pressure VJP's the situation is not so bad. For instance, the 10 hp,  $P_s = 4000$  psi,  $P_{\text{vap}} = -785$  psi unit has

$$T = .00012 \text{ sec} \quad 2.4$$

and the maximum phase lag at 100 cps is  $4.3^\circ$  in which case it probably can be neglected in preliminary analysis at least.

These estimates are conservative since the speed of sound in the mixed phase is assumed negligible relative to the fluid velocity. More precise methods of calculating delay times are given later.

#### Lumped Capacitance and Inertial Effects in the Induced and Blocked Flow Conditions

One can surmise that the effect of the mass and compressibility of the fluid actually contained in the VJP will be small simply by observing that the volume contained in connecting lines will be much greater. However, in the case of choked flow some of the volume contained will be a mixed phase with relatively large compressibility.

Delaying the consideration of the choked condition for a moment consider the VJP in the blocked and induced flow regions. We will consider the effect of the diffuser volume and neglect the effects in the region immediately upstream which is a much smaller volume. The volume trapped between the check valve and the mixing region travels at low velocity and hence has only secondary inertial effect but may have capacitance effect in the blocked flow region when its pressure will vary with variations in  $P_L$ .

In order to determine the inertial effect, consider a control volume in the shape of the diffuser with incompressible flow.



$$\text{Geometry: } A = \text{Area} = \pi r^2 = \pi \left( \frac{r_2 - r_1}{l} \right)^2 x^2 = sx^2$$

$$\text{where: } s \equiv \pi \left( \frac{r_2 - r_1}{l} \right)^2 \quad 2.5$$

$$\text{Continuity: } V = Q/A \quad 2.6$$

First law: Assuming isentropic, incompressible flow:

$$Q \left[ \left( p_1 - \rho \frac{V_1^2}{2} \right) - \left( p_2 + \rho \frac{V_2^2}{2} \right) \right] = Q [\bar{p}_1 - \bar{p}_2] =$$

$$\frac{d}{dt} (\text{stored energy}) = \frac{dE}{dt} \quad 2.7$$

for our purposes:

$$E = \int_{x_1}^{x_2} \rho \frac{V^2}{2} dx \quad 2.8$$

$$\text{where: } V = \frac{Q}{sx}, \quad dx = \frac{dx}{sx} = \frac{dx}{sx^2}$$

solving Eq. 2.7 gives:

$$\bar{p}_1 - \bar{p}_2 = \frac{\rho}{s} [x_1^{-1} - x_2^{-1}] \frac{dQ}{dt} = \frac{\rho l}{\pi r_1 r_2} \frac{dQ}{dt} \quad 2.9$$

$$\text{Thus, the inertia is given by: } I = \frac{\rho l}{\pi r_1 r_2} \quad 2.10$$

This reduces to the usual lumped inertia equation for a transmission line when  $r_1 = r_2$ . Applying the standard VJP geometry of Fig. 1.1

we get:

$$I = \frac{\rho (8D)}{\pi \left(\frac{D}{2}\right) D} = \frac{16\rho}{\pi D} \quad 2.11$$

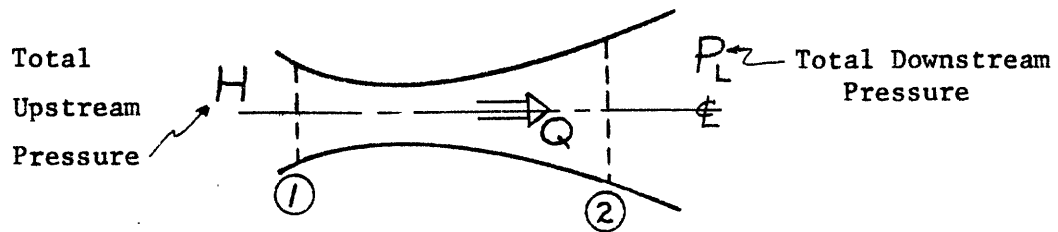
To obtain the capacitance effect, consider the entire volume to be lumped at the outlet--a very conservative assumption. For operation in the region of induced flow the volume affected is approximately  $5\pi D^3$ . If the operation is in blocked flow region approximately  $25\pi D^3$  is affected. This gives a capacitance of:

$$\begin{aligned} C &= \frac{v}{\beta} = \frac{5\pi D^3}{\beta} \quad (\text{induced flow}) \\ &= \frac{25 D^3}{\beta} \quad (\text{blocked flow}) \end{aligned} \quad 2.12$$

### The Choked Flow Condition

Next, we turn to a more thorough discussion of the flow in the choked condition. What follows is a speculative theory of choked flow as it occurs in the VJP. It is based on the assumptions of Murdock but extends his analysis to the conditions encountered in expected VJP applications. It is consistent with the observation of Cunningham, and Murdock and the experimental results of this thesis. However, no direct experimental verification has been attempted. The ultimate purpose is to estimate the compressibility, inertial, and time delay effects in the choked condition. However, it also serves to illuminate the mechanism of choking and the character of the flow situation in the choked condition.

Consider a one-dimensional oil flow in a diverging, converging circular section as shown:



The oil initially contains dissolved gases of vapor pressure  $p_o$ . Assume the process is isentropic except at the "shock" at 2. Mixed flow exists between some sections of 1 and 2. Where at 1 the static pressure is  $p_o$  and at 2 there is an irreversible shock from mixed flow to liquid flow. For this to be so, the stagnation pressures  $H$  and  $P_L$  are such that:

$$P_L < H \quad 2.13$$

For the mixed flow region the following equations apply.

First law:

$$u + pv + \frac{v^2}{2} = \text{constant} \quad 2.14$$

Assuming that there is no internal energy change when the gas dissolves or separates this becomes:

$$\frac{p}{\alpha} + \frac{v_l^2}{2} \rho_l = H \quad 2.15$$

where:

$$\alpha \equiv \frac{a_l}{a_g + a_l} = \frac{\text{area of liquid}}{\text{total area at any cross section}}$$

and where the velocity contribution of the gas is neglected because of its very small density. Assuming that Henry's Law applies to the gas evolution:

$$X = \frac{K(p_o - p)}{p} \quad \text{where} \quad X \equiv \frac{V_g}{V_L} \quad \frac{a_g}{a_l} \equiv (\text{SR}) \cdot \frac{a_g}{a_l} \quad 2.16$$

(SR) is the "slip ratio" used by Murdock: then

$$\frac{1}{\alpha} = 1 + \frac{a_g}{a_l} = 1 + \frac{X}{\text{SR}} = 1 + \frac{K(p_o - p)}{(\text{SR}) p} \quad 2.17$$

Continuity requires that:

$$A \alpha V_l = \text{const.} = Q \quad \text{or} \quad V_l = \frac{Q}{A\alpha} \quad 2.18$$

where again the contribution of the gas is neglected. Thus, Eq. 2.15 becomes:

$$p + \frac{K}{\text{SR}} \cdot (p_o - p) + \frac{\rho l}{2} \left(\frac{Q}{A}\right)^2 \cdot \left(1 + \frac{K}{\text{SR}} \cdot \frac{p_o - p}{p}\right)^2 = H \quad 2.19$$

or

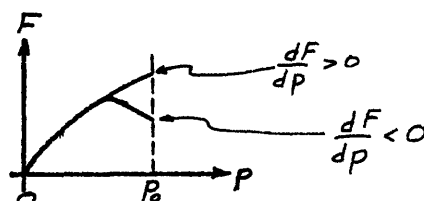
$$p + \kappa (p_o - p) + F \left(1 + \kappa \frac{p_o - p}{p}\right)^2 = H \quad 2.20$$

where  $\kappa \equiv \frac{K}{\text{SR}}$ ,  $F \equiv \frac{\rho l}{2} \cdot \left(\frac{Q}{A}\right)^2$

$$F = \frac{H - p - \kappa(p_o - p)}{\left(1 + \kappa \frac{p_o - p}{p}\right)^2} \sim \frac{1}{A^2} \quad 2.21$$

In order to see if a choking condition could exist in the mixed region we must see if  $F$  has a maximum (A minimum) in the region  $p_0 \geq p > 0$ .

Clearly as  $p \rightarrow 0$   $F \rightarrow 0$ .



For a maximum to exist  $\left. \frac{dF}{dp} \right|_{p=p_0} < 0$

or

$$\frac{2H\kappa}{p_0} - 1 - \kappa < 0 \quad 2.22$$

A question now arises. Does the model of a converging-diverging circular section with a single stream apply to the VJP where two streams are mixing? Probably not in the mixing region. However, the flow up to the throat can be considered two separate converging sections with separate streams. In fact, this was the assumption in the derivation of choked condition flow. Thus, Eq. 2.22 should apply to the two streams separately. Similarly downstream (in the diffuser) where the shock back to all liquid flow takes place mixing is assumed to have been completed and the single stream model should apply.

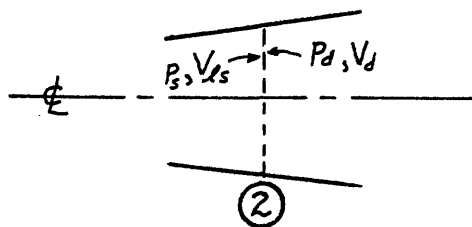
The requirement for  $p = p_0$  at the throat is that Eq. 2.22 not apply. The value of  $H$  for the exhaust stream is  $p_0 - P_{\text{vap}}$ . Thus, the requirement for  $p = p_0$  at the throat is:

$$1 - \kappa + \frac{2P_{\text{vap}}\kappa}{p_0} < 0 \quad 2.22a$$

Since  $H$  for the supply flow stream is greater, one needs to satisfy 2.22a only.

Does the inequality hold for "normal" VJP application? Since this depends on  $\kappa$  it is difficult to give a universal answer. However, it is probable that  $\kappa \geq .05^*$  in which case Eq. 2.22a always holds for the normal operating conditions given earlier. This means that section 1 is at the throat. Thus, the flow is choked by a minimum pressure at the throat--namely-- $p_o$  even though the fluid is traveling below the local speed of sound.

In order to locate the position of 2 we apply momentum conservation across 2. The subscript "s" is used to denote conditions at the shock.



Momentum:

$$p_s - p_d = \frac{Q}{A_s} \rho_l (v_d - v_{ls}) \quad 2.23$$

Energy:

$$p_d + \frac{\rho_l v_d^2}{2} = p_L \quad (\text{right side}) \quad 2.24$$

$$p_s + \kappa(p_o - p_s) + F_s \left(1 + \kappa \frac{p_o - p_s}{p_s}\right)^2 = H \quad (\text{left side}) \quad 2.25$$

\* Murdock found  $\frac{K}{SR} \equiv \kappa = .0519$  for J-43 at 100°F. Minimum  $H$  is 200 psia and  $p_o$  is 15 psia.

Continuity:

$$V_d = \frac{Q}{A_s} \quad 2.26$$

$$V_{\ell s} = \frac{Q}{A_s} \cdot \left(1 + \kappa \frac{p_o - p_s}{p_s}\right) \quad 2.27$$

Using 2.24, 2.26, 2.27 in 2.23 yields:

$$P_s - P_L = \frac{-\rho_{\ell}}{2} \cdot \left(\frac{Q}{A_s}\right)^2 \left(1 + 2\kappa \frac{p_o - p_s}{p_s}\right) \quad 2.28$$

Noting that  $\frac{\rho_{\ell}}{2} \cdot \left(\frac{Q}{A_s}\right)^2 = F_s$  Equation 2.28 gives:

$$F_s = \frac{P_L - p_s}{1 + 2\kappa \frac{p_o - p_s}{p_s}} \quad 2.29$$

Eq. 2.25 gives:

$$F_s = \frac{H - p_s - \kappa(p_o - p)}{(1 + \kappa \left(\frac{p_o - p}{p}\right))} \quad 2.30$$

by equating Eq. 2.29 and 2.30 the values of  $p$  and  $F$  can be found at section 2. Mathematically there may be more than one real value solution; however, the ones of interest are in the region  $0 < p_s \leq p_o$ . From the values of  $p_s$  and  $F_s$  other parameters of interest may be calculated.  $K$  and  $p_o$  are constants so that  $F_s$  and  $p_s$  and all other parameters of interest should be considered functions of  $H$  and  $P_L$ .

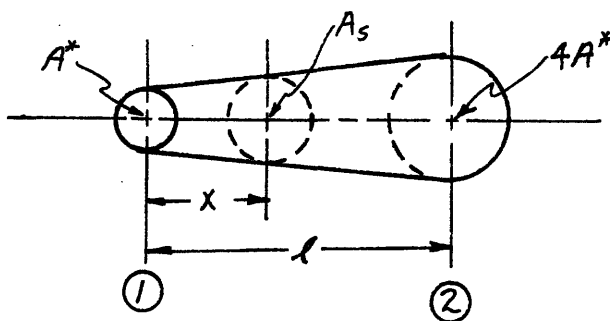
$$\frac{A_s}{A^*} = \frac{F_{\max}}{F_s} = \frac{\text{area at 2}}{\text{throat area}} \quad 2.31$$

where the inequality of Eq. 2.22a does apply--as is the expected usual case in VJP applications--then  $F_{\max}$  is found by substituting  $p = p_0$  in Eq. 2.21.

From Eq. 2.17 one gets the liquid fraction immediately before 2 to be:

$$\alpha_s = \left[ 1 + \kappa \frac{p_0 - p_s}{p_s} \right]^{-1} \quad 2.32$$

Of particular interest here is the effect of the mixed phase flow on the apparent lumped capacitance and inertia of the system. To calculate this lumped capacitance consider a diffuser shown below.  $x$  is the position of the shock.



Now from geometry:

$$x = l \left( \sqrt{\frac{A_s}{A^*}} - 1 \right), \quad A = A^* \left( \frac{x + l}{l} \right)^2 \quad 2.33$$



The total volume of gas in the diffusor is  $v_g$  and is given by:

$$v_g = \int_0^x [1 - \alpha] A d\xi \quad 2.34$$

for constant  $H$  the apparent compressibility is given by:

$$\frac{\partial v_g}{\partial P_L} = \int_0^x A \frac{\partial}{\partial P_L} (1 - \alpha) d\xi + [1 - \alpha_s] A_s \frac{\partial x}{\partial P_L} \quad 2.35$$

The first term is zero because  $\alpha$  is not a function of  $P_L$  ( $\alpha_s$  is, of course). Any change of volume of liquid phase has been ignored because it will be negligible compared to the change in the gaseous phase.

$$\frac{\partial v_g}{\partial P_L} = (1 - \alpha_s) A_s \frac{\partial x}{\partial P_L} \quad 2.36$$

For constant  $P_L$  the apparent compressibility is given by:

$$\frac{\partial v_g}{\partial H} = \int_0^x A \frac{\partial}{\partial H} (1 - \alpha) d\xi + (1 - \alpha_s) A_s \frac{\partial x}{\partial H} \quad 2.37$$

In order to evaluate equations 2.36 and 2.37 some simplifying but rather precise assumptions can be made. Recalling Eq. 2.21:

$$\frac{H - p - K(p_o - p)}{(1 + \kappa \frac{p_o - p}{p})^2} \sim \frac{1}{A^2} \quad 2.38$$

and using the fact that under expected conditions  $p < p_o$ ,  $p_o \ll H$ , and  $K$  of the order of 0.1.

$$\frac{H - p - K(p_o - p)}{(1 + \kappa \frac{p_o - p}{p})^2} \approx H\alpha^2 \sim \frac{1}{A^2} \quad 2.39$$

Therefore, because in our normalized model  $\alpha = 1$  when  $A = A^*$  provided the inequality of Eq. 2.22a holds:

$$\alpha \approx \frac{A^*}{A} \quad 2.40$$

referring to Eq. 2.18 then:

$$V_l \approx \text{const.} = (V_l \text{ at } A^*) = \frac{Q}{A^*} \quad 2.41$$

We wish to be able to get approximate analytic expressions of the conditions at the shock. Equating Eq. 2.29 to 2.30:

$$\frac{P_L - p_s}{1 + 2\kappa \frac{p_o - p_s}{p_s}} = \frac{H - p_s - \kappa(p_o - p_s)}{(1 + \kappa \frac{p_o - p_s}{p_s})^2} \quad 2.42$$

and using the fact that  $p_s < p_o$ ,  $p_o \ll H$ ,  $\kappa$  of the order of .1.

$$\frac{P_L}{1 + 2\kappa \frac{p_o - p_s}{p_s}} \approx \frac{H}{(1 + \kappa \frac{p_o - p_s}{p_s})^2} \quad 2.43$$

dividing by  $H$  and using Eq. 2.32 this simplifies to

$$\alpha_s = 1 - \sqrt{1 - \frac{P_L}{H}} \quad 2.44$$

using Eq. 2.40

$$A_s = A^* / \alpha_s \quad 2.45$$

From Eq. 2.33

$$x = \ell \left( \frac{1}{\sqrt{\alpha_s}} - 1 \right) \quad 2.46$$

Evaluation of Eq. 2.36 gives:

$$\frac{\partial v_g}{\partial P_L} = -\frac{1}{4} \cdot \frac{A^* \ell}{H} \cdot \left[ 1 - \sqrt{1 - \frac{P_L}{H}} \right]^{-5/2} \quad 2.47$$

Noting that  $\alpha$  is not a function of  $H$  (Eq. 2.40) the first term in Eq. 2.37 is zero, then:

$$\frac{\partial v_g}{\partial H} = \frac{\partial v_g}{\partial P_L} \cdot \frac{P_L}{H} = \frac{1}{4} \frac{A^* \ell P_L}{H^2} \left[ 1 - \sqrt{1 - \frac{P_L}{H}} \right]^{-5/2} \quad 2.48$$

The "exact" solution of Eq. 2.24 through 2.36 was carried out on a digital computer for  $p_0 = 15$ ,  $150 \leq H \leq 1500$ ,  $.25H \leq P_L \leq H$ , and  $.05 \leq \kappa \leq .15$ . Fig. 2.2 shows the excellent agreement with Eq. 2.44 through 2.48. The variations over the range of  $\kappa$  are too small to show on the graph. If the standard geometry of Fig. 1.1 is used then  $A^* = \frac{\pi D^2}{4}$  and  $\ell = 8D$ .

Before writing down the final formulas for the apparent capacitances of the VJP in the choked condition it is important to note that as  $P_L \rightarrow 0$ ,

$\alpha_s \rightarrow 0$ ,  $A_s \rightarrow \infty$ . However, in a real VJP the diffusor is presumed to end after 8 throat diameters (or when the area is four times the throat area). If the diffusor then merged smoothly into a tube it is possible for the mixed flow to extend down into the tube at low values of  $P_L$  because the shock back to an all liquid phase has not occurred. Since this is very undesirable it is probably wise to have a sudden expansion at the outlet of the diffusor to force the shock to occur at that point. If this is done then Eq. 30 - 34 apply only for  $A_s/A^* \leq 4$  which means for  $P_L/H > .44$ . Presumably for  $P_L/H < .44$  both of the apparent capacitances would be zero. However, in no case can  $P_L$  go below  $p_0$  without mixed phase filling all of the volume in the lines at  $P_L$ .

Thus, the final approximate equations for capacitance in the choked equation are:

$$\frac{\partial v_g}{\partial P_L} = -\frac{1}{2} \frac{\pi D^3}{H} \left[ 1 - \sqrt{1 - \frac{P_L}{H}} \right]^{-5/2} \quad \text{if } \frac{P_L}{H} > .44 \quad 2.49$$

$$= 0 \quad \text{otherwise}$$

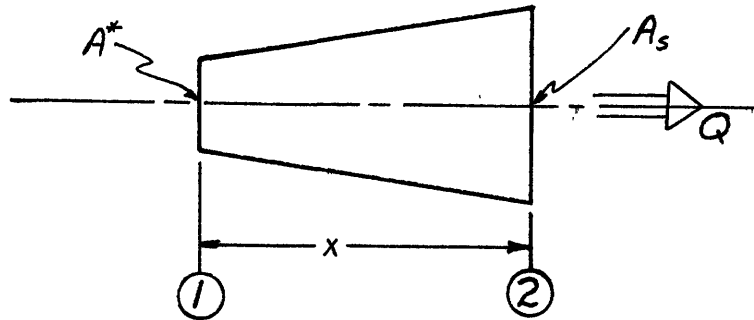
$$\frac{\partial v_g}{\partial H} = -\frac{\partial v_g}{\partial P_L} \frac{P_L}{H} \quad 2.50$$

Note that the maximum value of both with respect to  $P_L/H$  are:

$$\left. \frac{\partial v_g}{\partial P_L} \right|_{\max} = 16 \frac{\pi D^3}{H} \quad \left( \text{i.e., } \frac{P_L}{H} = .44 \right) \quad 2.51$$

$$\left. \frac{\partial v_g}{\partial H} \right|_{\max} = 7 \frac{\pi D^3}{H}$$

The lumped inertia of the mixed phase in the diffusor is easily calculated using the method that was previously used to calculate the inertia of the pure liquid phase. Consider a control volume just enclosing the mixed phase so that the pure liquid phase is all that crosses the boundaries:



First law:

$$Q[h_1 - h_2] = \frac{dE_{cv}}{dt} \quad 2.52$$

for our purposes:

$$E = \int_0^x \rho \frac{v^2}{2} dv_\ell \quad 2.53$$

where only the K.E. of the liquid phase is considered. Eq. 2.40 and 2.41 imply that

$$v_\ell = \frac{Q}{A^*} \quad \text{and} \quad dv_\ell = A^* d\xi \quad 2.54$$

hence

$$E = \frac{\rho}{2A^*} Q^2 x \quad 2.55$$

then:

$$Q \cdot [h_1 - h_2] = \frac{\rho Q x}{A^*} \cdot \frac{dQ}{dt} \quad 2.56$$

and  $I = \frac{\rho x}{A^*}$  which in terms of  $D$  is 2.57

$$I = \frac{4\rho}{\pi D^2} x \quad 2.58$$

Eq. 2.57 implies that the diffusing mixed phase has the same inertia as a pure phase traveling in a straight tube of length  $x$  and area  $A^*$ .

At most,  $x = \ell = 8D$ , in which case Eq. 2.58 becomes:

$$I_{\max} = \frac{32\rho}{\pi D^2} \quad 2.59$$

Comparing this with Eq. 2.11 shows that the mixed phase may have twice the inertia of the pure phase in the same diffusor.

Let us now return to consideration of the signal delay time in the mixed flow region. The signal will propagate at the velocity of the fluid plus the velocity of sound. The velocity of the fluid is given by Eq. 2.41 and is approximately constant. The velocity of sound is given at least approximately by:

$$C^2 = \frac{\beta}{\rho} = \frac{\text{bulk modulus}}{\text{density}} \quad 2.60$$

Since:

$$\beta \equiv \frac{-v}{dv/dp} \quad v \equiv \text{specific volume} \quad 2.61$$

It follows from Eq. 2.17 and  $v = \frac{v_l}{\alpha}$  that:

$$\beta = \frac{1}{\alpha} \frac{p^2}{\kappa p_o} \quad 2.62$$

Because  $\rho = \rho_l \alpha$

$$C^2 = \frac{1}{\alpha^2 \rho_l} \frac{p^2}{\kappa p_o} \quad 2.63$$

From Bernoulli's Equation and Eq. 2.41:

$$V_l^2 = \frac{2(H - p_o)}{\rho_l} \quad 2.64$$

$$\text{Thus, } \frac{V_l}{C} = \frac{\alpha}{p} \sqrt{2(H - p_o) \kappa p_o} \quad 2.65$$

Using Eq. 2.17 to eliminate p gives:

$$\frac{V_l}{C} = [1 + \kappa\alpha - \alpha] \sqrt{\frac{2(H - p_o)}{\kappa p_o}} \quad 2.66$$

Since the signal propagation velocity is  $V_l$  plus C an examination of the order of magnitude of the right-hand side of the equation may

allow us to neglect one of the terms. According to the typical VJP operating conditions put forth earlier  $H > 200$  psia,  $p_o \approx 15$  psia, and  $K$  is of the order of 0.05 at least for J-43 oil. This leads to the following (see Eq. 2.40):

$$\begin{aligned} \frac{V_\ell}{C} > 1.1 & \quad \text{at } \alpha = 1 \\ & \quad \text{(i.e., entrance to diffuser)} \\ > 8.7 & \quad \text{at } \alpha = .640 \\ & \quad \text{(i.e., 1/4 down diffuser)} & \quad 2.67 \\ > 12.8 & \quad \text{at } \alpha = .445 \\ & \quad \text{(i.e., half way down diffuser)} \\ > 16.9 & \quad \text{at } \alpha = .250 \\ & \quad \text{(i.e., at the downstream end of diffuser)} \end{aligned}$$

Since one is normally interested in transmission delay times when a large percentage of the diffuser is filled with mixed phase, the above inequalities suggest that neglecting  $C$  will be justified. A good approximation of the delay time is simply:

$$T = x/V_\ell \quad 2.68$$

where  $x$  is to the length of mixed phase given by Eq. 2.46 and 2.44.

$V_\ell$  can be expressed as  $V_\ell = \frac{Q}{A^*}$ .

### Interpretation of Results

The prime purpose here has been to make estimations of dynamic effects of the VJP. The table below illustrates the order of magnitude of these effects in terms of equivalent lengths of pipe of I.D. 3D.\*

---

\* For this pipe  $I = \frac{\rho \ell}{\pi 2.25D^2}$ ,  $C = \frac{2.25D^2 \ell \pi}{\beta}$ , Delay =  $\ell / 3.56 \times 10^4$



## LENGTH OF TUBE

<u>Condition of VJP</u>	<u>Capacitance</u>	<u>Inertia</u>	<u>Signal Propagation Delay</u>
blocked	11 D	36 D	8 D
induced	2.2 D	36 D	8 D
choked*	downstream $\frac{7.1 \times 10^5}{H} D$		
	upstream $\frac{-3.1 \times 10^5}{H} D$	72 D	$\frac{2.26 \times 10^3}{-P_{\text{vap}}} D$

It is apparent that the only factors which are likely to be significant are capacitance and delay in the choked condition.

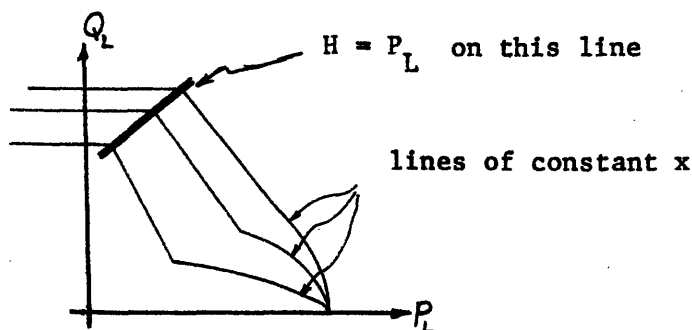
Note that the upstream capacitance on the choked condition is negative. This is because an increase in driving pressure  $H$  expands the mixed flow region resulting in a temporary increase in flow. Throughout the development  $H$  has been used as the upstream stagnation pressure of the oil entering the diffuser. This stagnation pressure must be related to the VJP characteristics. Eq. 2.13 states that under the assumption of an isotropic diffuser flow that for cavitation to exist  $P_L < H$ . Thus,  $H$  must equal  $P_L$  at the onset of cavitation.\*\* The line along which cavitation begins is the boundary between the induced and choked flow regions.

---

\*  $\beta = 10^5$  psi,  $\rho = 7.8 \times 10^{-5} \frac{\text{lb. sec}^2}{\text{in}^4}$  assumed for pure oil phase.

In every case the figures given for the choked flow are based on the worst case, i.e., the downstream pressure  $P_L$  is just sufficiently low to fill the diffuser with mixed flow.

\*\* Actually in the real VJP the diffuser flow is not isotropic but for the approximate calculations here this is a satisfactory assumption.



Clearly the boundary is given by some function  $H = H(x)$ , ( $x$  is cone position). Also, in the choked condition the steady state output flow is only a function of  $x$ . This is given by  $Q_L = F_1(x)$ .

The complete lumped parameter description of the flow in the choked condition neglecting inertial effects but including compressibility and delay are:

$$Q_L(t) = F_1(x_{[t-T]}) + \frac{\partial v_g}{\partial H} \cdot \frac{dH}{dt} \cdot \frac{dx}{dt} \Big|_{t-T} + \frac{\partial v_g}{\partial P_L} \frac{dP_L}{dt} \quad 2.69$$

where  $T$  is the delay time needed for signals to propagate through the mixed flow regions.

#### The Effect of the Check Valve

A generalized treatment of the dynamic effects of the check valve in the VJP appears to be very difficult. However, some considerations are presented below which indicate that the contribution may be made small.

Consider a simple check valve consisting of a disk, a seat for the disk, and a cage to retain the disk, as shown in Fig. 2.15. The time needed to switch from one state (i.e., fully closed or open) to the other is given by:

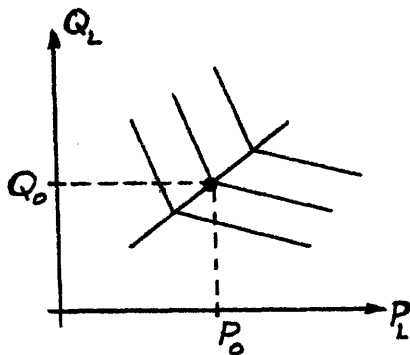
$$T = \sqrt{\frac{2\ell hp}{\bar{p}}} \quad 2.70$$

where the force on the disk per unit area is considered constant and equal to  $\bar{p}$ .  $\bar{p}$ , of course, is unknown and would vary with a great many factors determined by the VJP design and the check valve design and the particular operating conditions. As an indication of the order of magnitude of T the check valves used in the dynamic VJP of this chapter used an aluminum disk with  $\ell = .012$ ,  $h = .100$  which gives the following values of T.

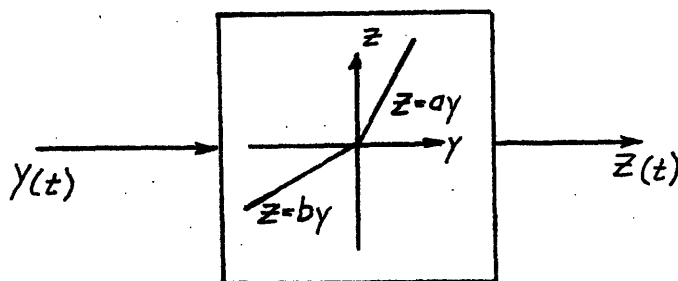
$\bar{p}$	$T$	"angular delay" at 100 cps $\frac{T}{100}$ (360)
1 psi	.00077 sec	27.7°
4 psi	.00038 sec	13.8°
16 psi	.00019 sec	6.9°

Various methods may be used to decrease T. First, a more restrictive check valve will increase  $\bar{p}$  but degrade VJP efficiency slightly. Secondly, it turns out that the flow capacity is proportional to  $(\ell h)$ , (because the diameter of the disk is proportional to h due to structural consideration) while T is proportional to  $\sqrt{\ell h}$ . Thus, it is possible to increase T by using a number of smaller disks in parallel.

The "angular" delay given in the table does not give a true picture of the actual phase shift and attenuations caused by the check valve in the VJP. To get an indication of this consider a linearized VJP characteristic in the neighborhood of the boundary between induced and blocked flow, (i.e., where the check valve nominally operates).



Suppose that there is a sinusoidal variation of  $Q_L$  or  $x$  about the nominal operating point  $(Q_0, P_0, x_0)$ . Then for either case the following block diagram applies.



$$y = x - x_0$$

or

$$y = -(Q_L - Q_0)$$

$$z = P_L - P_0$$

The desired variation of  $z$  for  $y = \sin t$  is

$$\begin{aligned} z_d &= a \sin t & 2\pi n \leq t < 2\pi n + \pi \\ &= b \sin t & 2\pi n + \pi \leq t < 2\pi n + 2\pi \end{aligned} \quad 2.71$$

If there is an angular delay  $\Delta$  then the actual variation of  $z$  is

$$\begin{aligned} z_a &= a \sin t & 2\pi n + \Delta \leq t < 2\pi n + \pi + \Delta \\ &= b \sin t & 2\pi n + \pi + \Delta \leq t < 2\pi n + 2\pi + \Delta \end{aligned} \quad 2.72$$

Using a modified describing function technique where:

$$z_d(t) = A_d + B_d \sin(t) + C_d \cos(t) + \dots \quad 2.73$$

$$z_a(t) = A_a + B_a \sin(t) + C_a \cos(t) + \dots$$

It turns out that:

$$\begin{aligned} A_d &= \frac{a-b}{\pi} & , & \quad B_d = \frac{a+b}{2} & , & \quad C_d = 0 \\ A_a &= \frac{a-b}{\pi} \cos \Delta & , & \quad B_a = \frac{a+b}{2} & , & \quad C_a = 0 \end{aligned} \quad 2.74$$

which means that in the sense of describing functions the check valve changes the d.c. value by

$$\frac{a-b}{\pi} (1 - \cos \Delta) \quad 2.75$$

and does not result in any phase shift or attenuations of the primary frequency component. Notice that the d.c. shift is small for even "large" values of  $\Delta$ . For instance, if  $\Delta = 32.5^\circ$  the shift is only  $(a - b) (.05)$ .

In actual practice, if the check is not spring loaded, the apparent opening time will likely be much faster than closing because a half open valve will give VJP output characteristics more similar to the open valve characteristics than the closed valve characteristics. Therefore, considering the case where:

$$\begin{aligned} z_a &= a \sin t & 2\pi n \leq t < 2\pi n + \pi + \Delta \\ &= b \sin t & 2\pi n + \pi + \Delta \leq t < 2\pi n + 2\pi \end{aligned} \quad 2.76$$

This results in:

$$\begin{aligned} A_a &= \frac{a-b}{2\pi} (1 + \cos \Delta) & B_a &= \frac{a+B}{2} + \frac{a-b}{2\pi} (\Delta - 1/2 \sin 2\Delta) \\ C_a &= \frac{a-b}{2\pi} \sin^2 \Delta \end{aligned} \quad 2.77$$

Hence, the d.c. shift is one-half that of the former case. Using approximate formulas for small  $\Delta$  :

$$\text{magnitude attenuation} = \frac{\sqrt{B_a^2 + C_a^2}}{B_d} \approx 1 + \frac{a-b}{(a+b)\pi} \Delta^3 \quad 2.78$$

$$\text{phase shift} = \tan^{-1} \left( \frac{C_a}{B_a} \right) \approx \frac{a-b}{\pi(a+B)} \Delta^2 \quad 2.79$$

which gives for  $\Delta = 20^\circ = .35_{\text{rad}}$

$$\text{phase shift} = \frac{a-b}{a+b} (2.24)^\circ \quad 2.80$$

$$\text{magnitude attenuation} = 1 + \frac{a-b}{a+b} (.014)$$

By the convention of this development if the phase shift is positive the actual output leads the desired output.

In any case, it is seen that sizable delays in check valva operations lead to only small changes in phase and amplitude. Further, since it appears possible to construct extremely fast check valves, the dynamics of the check valve should not be a problem.

#### Experimental Purpose

An experimental testing of the VJP was felt necessary to verify that the dynamic response of the VJP was not affected by transient changes in the flow regimes and to observe the effect of the check valve. Most of the dynamic effects predicted by the previous section are not significant enough to be observed in the experimental program. However, this supports the general conclusion that the dynamic contributions of the VJP are negligible.

#### Method of Attack

A small VJP capable of being driven by a torque motor was constructed. The output flow of the VJP was passed through a valve which could be varied to give a wide range of load conditioning. Both dynamic strain gage type pressure gages and static dial gages were attached to the 3 ports of the VJP and to the volume between the mixing region and the check valve. The position of the cone in the variable

nozzle is measured by means of a Linearsyn, a high dynamic response electromechanical position transducer. Response was measured by oscillating the cone at various frequencies and observing the pressures, particularly the output pressure, under various load conditions.

Because the load, a valve, is well known to have negligible dynamic effects in the "low" frequencies of interest, the output pressure and the flow of the VJP should reflect only the dynamics of the VJP and the connecting volumes (pipes, etc.). Since the downstream pressure on the valve is approximately one atmosphere, the flow and pressure through the valve are related by  $Q \sim \sqrt{P}$  where  $Q$  is flow, and  $P$  is the upstream gage pressure relative to the atmosphere. Therefore, it is only necessary to measure the dynamic variations of  $P$  to infer both  $P$  and  $Q$ . Hopefully, the dynamics of the volumes in the test apparatus will be negligible, and therefore if the dynamics of the VJP are indeed small as predicted by the previous analysis the output pressure of the VJP should have a one to one correspondence with the input slider position for a given load valve setting, supply pressure and exhaust pressure. Thus, the simple test of supplying various input wave forms of  $x$  to the VJP and comparing them with the output wave forms of  $P$  illustrates the dynamic effects of the VJP.

#### Experimental Apparatus

Mechanical drawings of the VJP used in the dynamic tests are given in Fig. 2.3. Photographs of the unit assembled and disassembled are given in Fig. 2.4 and 2.5. An interesting feature of this unit is the balancing piston needed to minimize force feedback to the torque motor.



The decision to locate the small hole in the cone face at  $\frac{1}{\sqrt{2}}$  of the radius of the cone was based on qualitative experiments described in Chapter 1. It would probably not be necessary to balance cone forces in a well designed 2 stage valve. I.e., where the cone itself is driven by a spring loaded hydraulic piston.

A mechanical layout of the test apparatus is shown in Fig. 2.6. The dial pressure gages were calibrated by dead-weight pressure calibrators. The dynamic pressure gages are Dynisco strain gage pressure transducers with natural frequencies in excess of 10,000 cps. The Lynearsyn was excited at 20,000 cps. The output was rectified and filtered with a 2,000 cps. filter. Two torque motors\* were employed, both of which allowed oscillation of the cone up to 200 cps. Although it was desired to be able to generate sine wave oscillations of the cone--usually somewhat truncated sine waves were achieved due primarily to friction in the VJP. This, of course, introduces harmonic frequency components in the input. The supply pressure  $P_s$  is regulated by a Vickers pressure relief valve located in the pump room and a 1 gal. capacity accumulator located immediately adjacent to the VJP. The exhaust pressure  $P_e$  is regulated by a Rivett pressure relief valve and a 1 gallon capacity accumulator, both located immediately adjacent to the VJP.

A dial gage, graduated to .0001 inch was used to calibrate the Lynearsyn. Photographs of the mechanical apparatus are shown in Fig. 2.7.

---

\* A model #11F Midwestern torque motor and a modified model #104 American Measurement and Control torque motor. The AM&C torque motor had no spring and thus was outfitted with an external spring.

A schematic of the electrical apparatus is given in Fig. 2.8. The essential components are, (1) 2-6 v. batteries, (2) an 20,000 cps. oscillator to drive the linearsyn, (3) a rectifier and 2,000 cps. filter for the Linearsyn, (4) a dual beam type 502 Tektronix oscilloscope, (5) a Hewit-Packard Model #202A function generator, (6) an AM&C Model #652 servo-amplifier, and (7) a VTVM for calibration purposes.

A Polaroid camera was available to fit the oscilloscope screen.

### Experimental Results

The results were largely as expected except in the region of blocked flow where a good deal of phase shift and amplitude attenuation was experienced. Since in this region the check valve is closed, the VJP operates as a variable orifice (or ordinary valve). It was hard to believe the apparent dynamics could be attributed to the VJP. It was finally determined that the compressibility effect of the fluid volume in the test apparatus did have a substantial dynamic effect under certain conditions. These conditions occur when the VJP is in the blocked state.

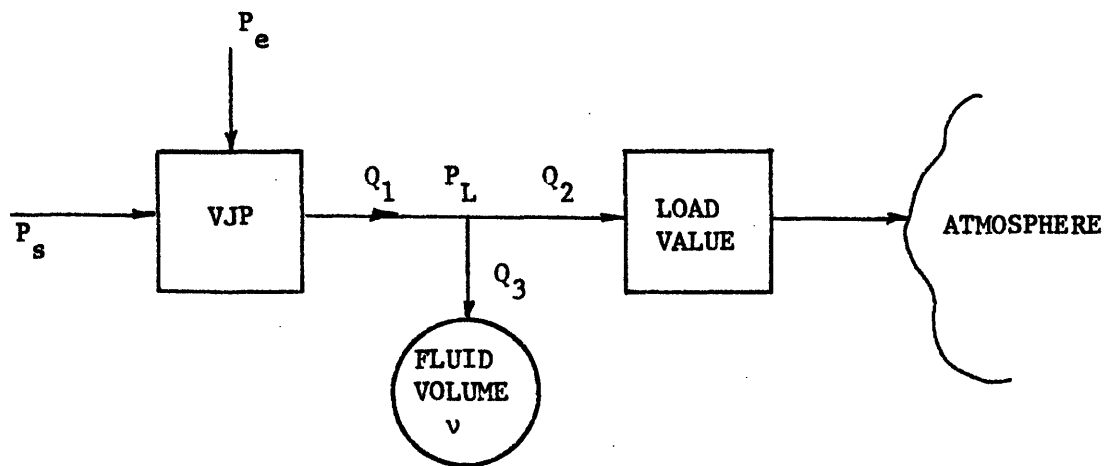
It was found that the output pressure followed the input position very well up to at least 200 cps. in the induced and choked condition. Representative photographs of input and output wave forms as well as Lissajous figures of the same are shown in Fig. 2.8 and 2.9. The mean operating conditions are given beside the photographs. Note that the input wave forms are not sine waves and hence contain higher frequency components than the basic frequency. The output generally preserves this wave form.

In the choked condition a good deal of "noise" appears in the output pressure. This is believed to be due to turbulence. It is much more pronounced in the photographs of the choked condition because (1) the total pressure fluctuations are much smaller (the gain of the pressure measuring circuit is 5 times that used in the induced region); (2) the flow rate is much greater. The turbulent pressure fluctuations in the photographs are of the order of 5 psi or 0.5% of  $P_s$ .

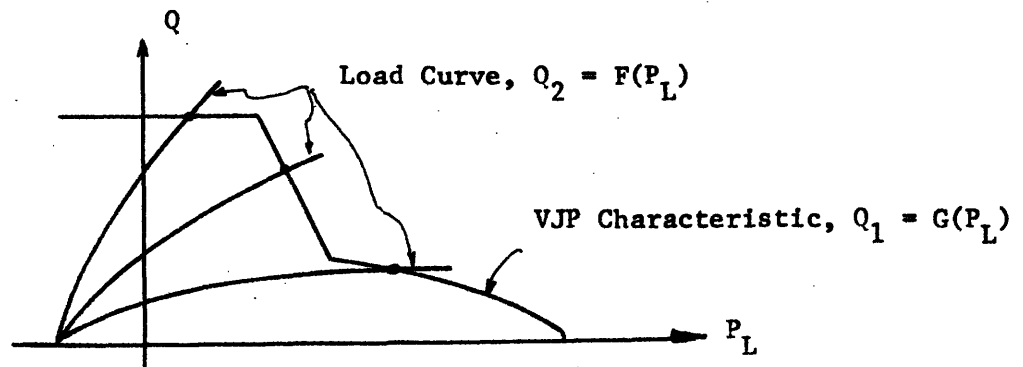
Actually, the photographs of VJP response in the choked region are made using a first order RC filter with a break frequency of 2,000 cps. If this filter is removed, the resultant wave form is shown in Fig. 2.10. The extremely high frequency variations occur only in the choked condition and are characteristic of it. When expanded on the scope face, it appears that the oscillations are irregular with about 25,000 peaks per second and under certain conditions contains peaks of up to  $\pm 100$  psi (with supply pressure of 1200 psi). This is believed to be caused by the violent collapse of the mixed phase.

In the blocked flow region considerable phase shift and amplitude attenuation was noted at higher frequencies. Explanations considered as possible causes of this phenomena include, (1) improper seating of the check valve, (2) changes in the physical dimensions around the nozzle, especially deflection of the nozzle plate, (3) transient flow regimes, (4) instrumentation dynamics, (5) hysteresis in the load valve, and (6) dynamics associated with the fluid in the test apparatus. By replacing the check valve with a plug the first hypothesis was eliminated. With regard to (2), deflection of the nozzle plate would logically result in lead, not a lag and would be a very rapid phenomena which would not show

up in the testing of other VJP conditions. By replacing the load valve with a fixed orifice the chances of hysteresis in the load was minimized. Further, when the VJP was replaced by an ordinary spool valve the same general low frequency attenuations were noted. The following considerations led to the conclusion that the compressibility of the fluid in the test apparatus between the check valve at one end and the load valve at the other led to the observed dynamics.



Consider the previous schematic of the test apparatus. For any given cone position of the VJP the equilibrium value of  $P_L$  is given by the intersection of the pressure-flow characteristics of the VJP and the load value.



The two preceding figures and conservation of mass give:

$$Q_1 = Q_2 + Q_3$$

$$G(P_L) = F(P_L) + \frac{v}{\beta} \frac{dP_L}{dt} \quad 2.81$$

Linearizing the equation about an equilibrium point  $P_o$  where:

$$G(P_o) = F(P_o)$$

$$\left. \frac{dG}{dP_L} \right|_{P_L=P_o} (\Delta P) = \left. \frac{dF}{dP_L} \right|_{P_L=P_o} (\Delta P) + \frac{v}{\beta} \frac{d}{dt} (\Delta P) \quad 2.82$$

where:  $\Delta P = P_L - P_o$

This is a first order linear differential equation with a decaying exponential solution with time constant.

$$T = \frac{v}{\beta} / \left( \left. \frac{dF}{dP_L} - \frac{dG}{dP_L} \right) \right|_{P_L = P_o} \quad 2.83$$

Note that under the conditions of the test:

$$\left( \left. \frac{dF}{dP_L} - \frac{dG}{dP_L} \right) > 0 \quad 2.84$$

but that its value is considerably smaller in the blocked flow condition.

To verify that this was the probable cause of output attenuation, a number of different volumes were attached between the VJP and the load valve and the output-input relation observed at different frequencies.

The volumes used are listed in the table:

<u>Trial #</u>	<u>Estimated Volume</u>	<u>Construction</u>
1	1.2 in <sup>3</sup>	plug in check valve part, close nipple connecting pressure gage to load valve
2	2.0 in <sup>3</sup>	Fig. 2.6 construction
3	4.6 in <sup>3</sup>	27 in. of .4" I.D. steel tubing connecting pressure gage to load valve
4	3.4 in <sup>3*</sup>	20" of Aeroquip #8 hose between pressure gage and load valve
5	8.5 in <sup>3*</sup>	66" of Aeroquip #8 hose between pressure gage and load valve

Trials with the above volumes were run under two blocked flow conditions. First with  $P_s = 1240$  psig,  $\bar{P}_L = 500$  psig, and  $\bar{Q}_L = 0.66$  gpm (the  $\bar{\quad}$  indicates average value). Second with  $P_s = 1240$  psig,  $\bar{P}_L = 365$  psig and  $\bar{Q}_L = 0.3$  gpm. Photographs of the Lissajous figures of input cone positions versus output pressures are shown in Fig. 2.11 and 2.12 for  $\bar{Q}_L = 0.66$  gpm and  $\bar{Q}_L = 0.3$  gpm respectively. The increase in attenuations as volume increases can be markedly seen. As expected with the higher flow rate the attenuation is also less.

A computation of expected break frequencies follows. At  $\bar{Q}_L = .66$  gpm = 2.54 in<sup>3</sup>/sec,  $\bar{P}_L = 500$  psig, and  $P_s = 1240$  psig.

---

\* This uses Aeroquip hose as capacitance. Since the hose itself is elastic, an apparent volume greater than listed is to be expected.

$$\frac{dF}{dP_L} - \frac{dG}{dP_L} = \frac{2.54}{2 \cdot 500} + \frac{2.54}{2(1240-500)} * = .00425 \frac{\text{in}^5}{\text{lb. sec.}} \quad 2.85$$

If  $\beta$  is assumed to be  $10^5$  psi then Eq. 2.86 writes:

$$T = v(2.35 \times 10^{-3}) \text{ sec} \quad 2.86$$

Similarly for:  $\bar{Q}_L = 0.3 \text{ gpm} = 1.16 \text{ in}^3/\text{sec}$ ,  $\bar{P}_L = 365 \text{ psig}$ ,  $P_s = 1340 \text{ psig}$

$$T = v(4.44 \times 10^{-3}) \text{ sec} \quad 2.87$$

When crude Bode plots are constructed from the photographs of Fig. 2.11 and 2.12, Eq. 2.86 and 2.87 predict rather well the break points (within a factor of 2, except the hoses lead to much higher apparent volumes,  $v$ ). Fig. 2.13 and 2.14 show these Bode plots with the predicted and experimental break points.

---

\* It is not obvious that this expression gives  $\frac{dF}{dP_L} - \frac{dG}{dP_L}$  but it does follow from the geometric relationship of the load characteristics  $F$  and the VJP characteristic  $G$  since they are both parabolas.

## Chapter 3

### CONTROL SYSTEM CONSIDERATIONS IN VJPV DESIGN

#### Introduction

This chapter deals with the construction of a 4-way variable jet pump valve, VJPV, for constant supply pressure use. Particular emphasis is placed on how the various dimensional parameters affect the pressure-flow characteristics of the valve. A state space analysis of a simple class of control systems is worked out. Because of the pronounced non-linearity of the VJPV no general analytical technique for achieving an "optimal" or even stable control system can be presented.

There are a great number of possible types of control valves that could be constructed using VJP's. The two and three-way constant pressure valves are special cases of the four-way and follow immediately from this chapter. The constant-flow valves are somewhat different in construction. A brief discussion of these other applications of VJP's to high pressure hydraulic control are given in Chapter 6.

Numerical calculations of the relative efficiency of VJPV's is relegated to Chapter 4.

#### Mechanical Arrangement

The elements of a VJPV (unless specified otherwise this will be taken to mean a 4-way VJPV for constant supply pressure use) are two VJP's and two variable orifices and possibly two fixed orifices. These are mechanically coupled as shown in Fig. 3.1. There are 7 basic parameters which are variable in this arrangement:



1. The over or under-lap of the variable orifices,  $x_{\text{orifice}}$
2. The over or under-lap of the VJP cones,  $x_{\text{VJP}}$
3. The diameter of the cones,  $d$
4. The diameter of the VJP throat,  $D$
5. The effective circumference of the variable orifices,  $\ell$
6. The area of the fixed orifices,  $A_f$
7. The effective flow area of the check valve when fully open,  $A_c$

Besides these there are some generally minor parameters which arise because of manufacturing limitations such as the clearance of the cones and spool when the nozzles and orifices are "closed." It is convenient to introduce some non-dimensional parameters that are combinations of the above. Namely:

$$1. \quad \frac{d}{D}$$

$$2. \quad \frac{x_{\text{orifice}}}{d/2} \equiv x_{\text{orifice}}$$

$$3. \quad \frac{x_{\text{VJP}}}{d/2} \equiv x_{\text{VJP}}$$

3.1

$$4. \quad \frac{C_d A_c}{\pi D^2/4} \equiv K_c$$

where  $C_d$  discharge coefficient  
for check valve

$$5. \quad \frac{C_d \ell (d/2)}{\pi D^2/4} \equiv K_o$$

where  $C_d$  discharge coefficient  
for variable orifice

$$6. \quad \frac{C_d A_f}{\pi D^2/4} \equiv K_f$$

where  $C_d$  discharge coefficient  
for fixed orifices

The displacement of the entire spool from its equilibrium position will be given by:

$$x \equiv \frac{x}{d/2} \quad 3.2$$

If all the orifices are sharp edged,  $C_d$  can be assumed to be about .6\* VJP parameters.

Besides the mechanical parameters there are a number of parameters which are needed to describe the flow characteristics of the VJP. These have been developed in Chapter 1 and are reviewed here.

<u>Symbol</u>	<u>Name</u>	<u>Range of Values</u>
$\eta$	"diffusor" efficiency	$.54 \leq \eta \leq .61$
$C_v$	nozzle velocity coefficient	.97
$\psi$	exhaust flow momentum coefficient	.84
$q_{eo}$	linearizing "average" exhaust flow	.35
$q_{no}$	leakage flow	—
$\rho_{vap}$	normalized vapor pressure of dissolved gases	negative
$c_v$	nozzle saturation coefficient of velocity	.99
$k_v$	exhaust saturation coefficient of velocity	.93
$C_d$	nozzle coefficient of discharge	$.63 \leq C_d \leq .65$

---

\* See Blackburn et. al. p. 181-184 for a discussion of discharge coefficients.

### Limiting the Number of Parameters

Clearly the number of parameters that can vary is too large to deal with in calculating numerical examples of pressure-flow characteristics. Fortunately, some vary over only a narrow range and an average value will give good representative results. On this score we can make  $\eta = .57$ , and  $C_d = .64$ . The leakage flow should be made as small as possible and is limited by manufacturing techniques. It will not affect the pressure-flow characteristics greatly. For numerical examples it is taken such that  $(d/D)^2 q_{no} = .005$  which is quite easy to obtain in practice since in terms of machining tolerance it means that the diametral clearance of the cone shaft in the nozzle hole is approximately 0.5% of the diameter.

The normalized vapor pressure,  $P_{vap}$ , should be made as large as possible (in the absolute sense--by the conventions  $P_{vap}$  is negative) in order to delay cavitation and thereby increase flow gain and efficiency. However, to do so increases the absolute pressure in all of the hydraulic lines of the system. Increasing  $|P_{vap}|$  beyond 0.20 or 0.25 gains little in efficiency. Under most circumstances we will take  $P_{vap} = -.235$  in numerical examples.

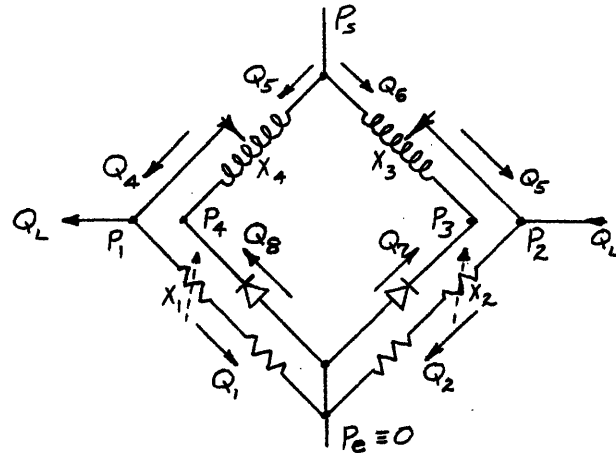
The parameter  $(d/D)$  might vary between 0.8 and 0.9 according to Fig. 1.1 and may, of course, be varied over an even wider range to achieve special characteristics. Here in numerical examples,  $(d/D) = .9$ .

### A Schematic Representation of the 4-Way VJPV

A suggested schematic representation of the 4-way VJPV is given in Fig. 3.2. The VJP is represented as a variable transformer. The check valve as a diode. A comparison with Fig. 3.1 may help clarify the schematic.

Analytic Description of the VJPV Pressure-Flow Characteristics

Consider the VJPV described schematically below.



The  $x_i$  dimensions are the total opening of the various orifices and VJP nozzles. For clarification:



The  $Q_i$  are flows in various branches. The  $P_i$ , the pressures at various nodes.  $Q_L$  is the load flow,  $P_L = P_1 - P_2$  or

$$p_L = p_1 - p_2$$

3.3

gives the load pressure of the valve.

From geometry (and a convention regarding  $x$ )

$$\begin{aligned}
 x_1 &= x_{\text{orifice}} - x & X_1 &= X_{\text{orifice}} - X \\
 x_2 &= x_{\text{orifice}} + x & X_2 &= X_{\text{orifice}} + X \\
 & & \text{or} & \\
 x_3 &= x_{\text{VJP}} - x & X_3 &= X_{\text{VJP}} - X \\
 x_4 &= x_{\text{VJP}} + x & X_4 &= X_{\text{VJP}} + X
 \end{aligned}
 \tag{3.3a}$$

where  $x$  is the position of the spool. Conservation of mass requires that (assuming incompressible flow) :

$$\begin{aligned}
 Q_L &= Q_4 - Q_1 = Q_2 - Q_3 & q_L &= q_4 - q_1 = q_2 - q_3 \\
 Q_8 &= Q_4 - Q_5 & q_8 &= q_4 - q_5 \\
 & & \text{or} & \\
 Q_7 &= Q_3 - Q_6 & q_7 &= q_3 - q_6
 \end{aligned}
 \tag{3.4}$$

The orifice equation gives the flow through the variable orifices as

$$\begin{aligned}
 Q_i &= C_d x_i \frac{P_i}{|P_i|} \sqrt{\frac{2|P_i|}{\rho}} & i = 1, 2 & \quad x_i > 0 \\
 & & & \\
 &= 0 & & \quad x_i \leq 0
 \end{aligned}
 \tag{3.5}$$

or recalling that the normalized flow is given by  $\frac{\pi D^2}{4} \sqrt{\frac{2P_s}{\rho}}$  :

$$\begin{aligned}
 q_i &= K_o x_i \frac{\rho_i}{|\rho_i|} \sqrt{|\rho_i|} & i = 1, 2 & \quad x_i > 0 \\
 & & & \\
 &= 0 & & \quad x_i \leq 0
 \end{aligned}
 \tag{3.6}$$

If there are fixed orifices of area  $A_f$  in series with the variable orifices then it is not hard to show that:

$$q_i = K_o K_f x_i \frac{p_i}{|p_i|} \sqrt{\frac{|p_i|}{K_f^2 + K_o^2 x_i^2}} \quad \begin{array}{l} x_i > 0 \\ \\ x_i \leq 0 \end{array} \quad 3.7$$

$$= 0$$

In Chapter 1 the characteristics of a VJP were presented. There it was assumed that a loss-less check valve was attached to the exhaust port of the VJP. In other words, the pressure at the exhaust port was held at a constant pressure  $P_e \equiv 0$  psig when the VJP is in the choked or induced flow condition. In an actual valve there will be a finite pressure drop across the check valve. In particular:

$$Q_i = C_d A_c \sqrt{\frac{-2P_{i-4}}{\rho}} \quad (i = 7, 8) \quad \begin{array}{l} P_{i-4} < 0 \\ \\ P_{i-4} \geq 0 \end{array} \quad 3.8$$

$$= 0$$

or

$$q_i = K_c \sqrt{-P_{i-4}} \quad \begin{array}{l} i-4 < 0 \\ \\ i-4 \geq 0 \end{array}$$

$$= 0$$

Now the maximum value of  $q_7$  or  $q_8$  is given by (see Eq. 1.43)

$$q_{imax} = k_v \sqrt{-P_{vap}} \quad i = 7, 8 \quad 3.9$$

therefore:

$$-\mathcal{P}_{i-4} < -\mathcal{P}_{\text{vap}} \left(\frac{k_v}{K_c}\right)^2 \quad 3.10$$

It is not difficult to make  $(k_v/K_c) < 1/4$  and  $-\mathcal{P}_{\text{vap}}$  is usually of the order .25. Therefore, the maximum value of  $-\mathcal{P}_{i-4}$  is of the order of .015. In this case, the maximum error introduced by assuming:

$$\mathcal{P}_3 = \mathcal{P}_4 = 0 \quad 3.11$$

is about 3%.<sup>\*</sup> The author urges anyone making calculations of VJPV characteristics to make this assumption if the small errors can be tolerated. If this assumption is made the equations of Chapter 1 apply directly. Namely:

$$\begin{aligned} \text{Defining: } g(\chi_4) &\equiv \left(\frac{d}{D}\right)^2 (C_d f(\chi_4) + q_{\text{no}}) & \text{where } f(\chi) &\equiv 2\chi - \chi^2 & (\chi > 0) \\ & & f(\chi) &\equiv 0 & (\chi \leq 0) \end{aligned} \quad 3.12$$

If  $\mathcal{P}_1 \leq 2C_v \cdot g(\chi_4) - (2 - \eta) \cdot g^2(\chi_4)$  then the VJP is not in the blocked condition and:

$$q_5 = g(\chi_4) \text{ and } q_8 \text{ is the least of}$$

$$q_8 = \frac{2C_v q_5 - (2 - \eta) q_5^2 - \mathcal{P}_1}{2(2 - \eta) q_5 + (2 - \eta - \psi) q_{e0}} \quad (\text{induced flow region}) \quad 3.13$$

or

$$q_8 = \left[1 - \frac{q_5}{c_v} \sqrt{(1 - \mathcal{P}_{\text{vap}})^{-1}}\right] \cdot k_v \cdot \sqrt{-\mathcal{P}_{\text{vap}}} \quad (\text{choked flow condition}) \quad 3.13$$

<sup>\*</sup>This is the error introduced in calculating the choked flow at maximum  $q_e$ . See Eq. 1.45.

If  $\mathcal{P}_1 > 2C_v g(\chi_4) - (2 - \eta) \cdot g^2(\chi_4)$  then the VJP is in the blocked condition and:

$$q_8 = 0$$

$$q_5 = \sqrt{\frac{1 - \mathcal{P}_1}{2 - \eta - (2C_v g^{-1}(\chi_4) + g^{-2}(\chi_4))}} \quad 3.14$$

A set of Equations identical to Eq. 3.12 through 3.14 applies to the other VJP where  $\chi_4$  is replaced by  $\chi_3$ ,  $\mathcal{P}_1$  by  $\mathcal{P}_2$ ,  $q_5$  by  $q_6$ , and  $q_8$  by  $q_7$ .

Eq. 3.3, 3.4, 3.6 or 3.12, 3.13, and 3.14 completely specify the pressure flow characteristics of a VJPV under the assumption of Eq. 3.11. Although a machine solution is preferable it turns out that a piece-wise analytic solution can be easily obtained if  $P_L$  is calculated as a function of  $q_L$  and  $x$ ;  $g_{no}$  is neglected; and the valve is line-to-line or underlapped (i.e., there is flow in only 2 branches for any value of  $x$ ).

The solution for the pressure flow relationships can be expressed at least graphically as:

$$G_1(\mathcal{P}_L, \chi, q_L) = 0$$

$$G_2(\mathcal{P}_L, \chi, q_s) = 0$$

$$G_3(\mathcal{P}_L, q_L, q_s) = 0 \quad 3.14a$$

These correspond to the  $F_1$ ,  $F_2$ , and  $F_3$  functions for the individual VJP. If one does not make the assumption of Eq. 3.11 the equations specifying  $G_1$ ,  $G_2$ , and  $G_3$  are changed slightly for the worse. These are given in Appendix 3.



### Effects of Parameters on VJPV Characteristics

The major parameter that can be manipulated by the control systems designer are  $x_{\text{orifice}}$ ,  $x_{\text{VJP}}$ ,  $K_c$ ,  $K_o$ ,  $K_f$ , and  $P_{\text{vap}}$ , as well as the normalizing parameters  $d$ ,  $D$ , and  $P_s$ . The normalizing factors are generally determined by the size of the job to be done. In other words on the basis of the maximum flow, power, and/or pressure needed. The other factors are not so obvious and the determination of these requires good judgment and a knowledge of the effects of their variation (and probably considerable experience). The principal factors involved in such a judgment in the case of a VJPV are, (1) power efficiency considerations, (2) dynamic control considerations, and (3) system cost and weight considerations.

Two general statements apply with regard to power efficiency and dynamic control on VJPV's. First, from the standpoint of efficiency, orifices should be used for directional control only and the VJP's should handle the actual power modulation. Second, attempts to use the above principal will lead to some "undesirable" side effect. The "undesirable" effects are increased nonlinear or in the case of check valves decreased switching time.

With regard to  $x_{\text{orifice}}$  and  $x_{\text{VJP}}$ , the most natural situation and one that has many advantages is the "line-to-line" arrangement where  $x_{\text{VJP}} \approx x_{\text{orifice}} \approx 0$ . In this configuration the VJPV (like the ordinary 4-way orifice valve) is very stiff in the neighborhood of  $Q_L = 0$ , i.e.,  $\left. \frac{dP_L}{dx} \right|_{Q_L = 0}$  is very large. This is very desirable when one wishes to

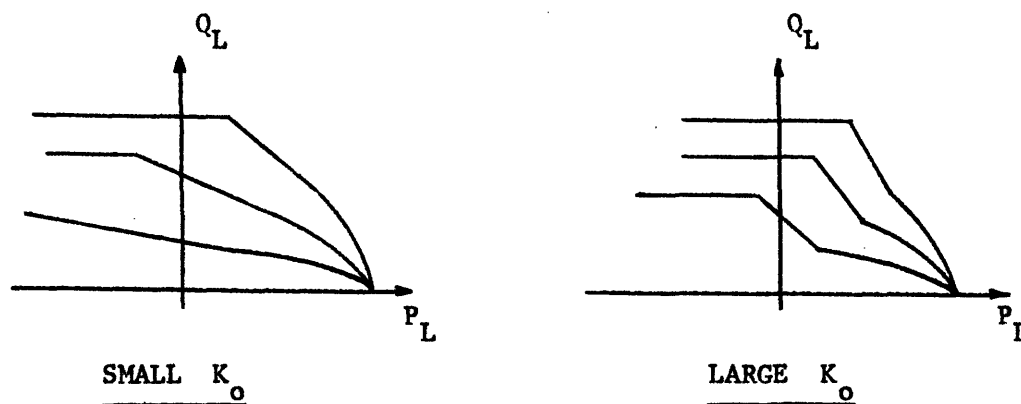
regulate a position. Also in the line-to-line situation there is no steady-state power drain except for leakage. If  $x_{\text{orifice}}$  or  $x_{\text{VJP}}$  are negative then the VJPV is overlapped and there will be range of  $x$  (deadband) for which the output characteristics will not vary appreciably at least for small values of  $Q$ . There are three possible reasons to use overlap, however. First, if  $x_{\text{VJP}} = x_{\text{orifice}} < 0$  then leakage may be reduced. Second, the deadband may have a stabilizing affect by decreasing the effect gain (both pressure and flow) in the neighborhood of  $x = 0$ , and  $Q_L = 0$ . Although a hunting or limit cycle operation is another likely consequence in this case. Third, if  $x_{\text{VJP}} < 0$ ,  $x_{\text{orifice}} = 0$  then an improvement in efficiency will result. This type of valve might be very satisfactory where a reactive\* load is in continuous oscillatory motion. There appears to be little reason for underlapping a VJPV in view of the fact that an increase in efficiency is the primary reason for using a VJPV and underlapping either the orifices or the VJP's leads to a great decrease in efficiency.

With regard to  $K_c$ , the normalized flow area of the check valve, and  $K_o$ , the normalized circumference of the variable orifice, the general rule is to make them as large as possible for high efficiency. As pointed out earlier, increasing  $K_c$  beyond  $4k_v$  (see Eq. 3.10) has little effect on the flow characteristics. In as much as the check valve dynamics

---

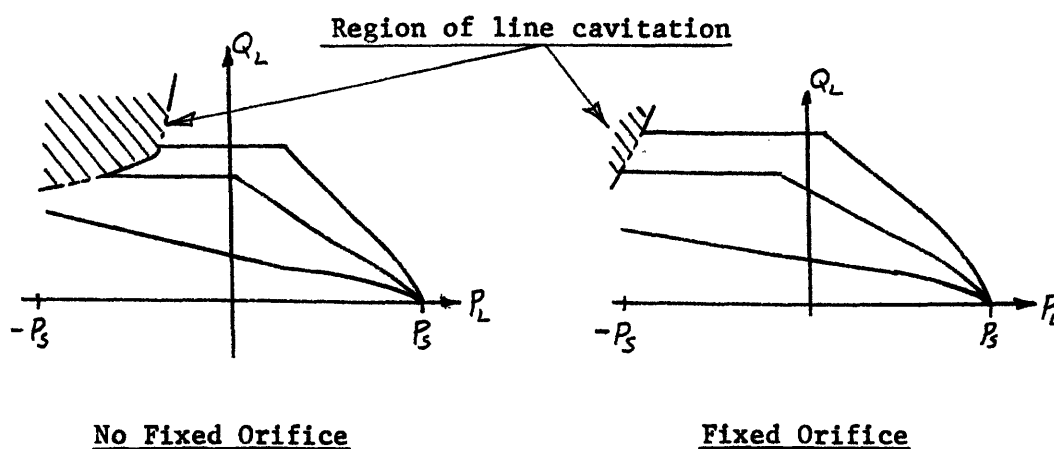
\*The flow and pressure are considerably out of phase such as driving a spring or mass.

are not likely to be a problem  $K_c$  in the order of 4 - 6 is expected to be quite satisfactory.  $K_o$  on the other hand has a marked effect on the linearity of the VJPV characteristics. A large  $K_o$ , desirable for efficiency, increases the non-linearity as sketched below.

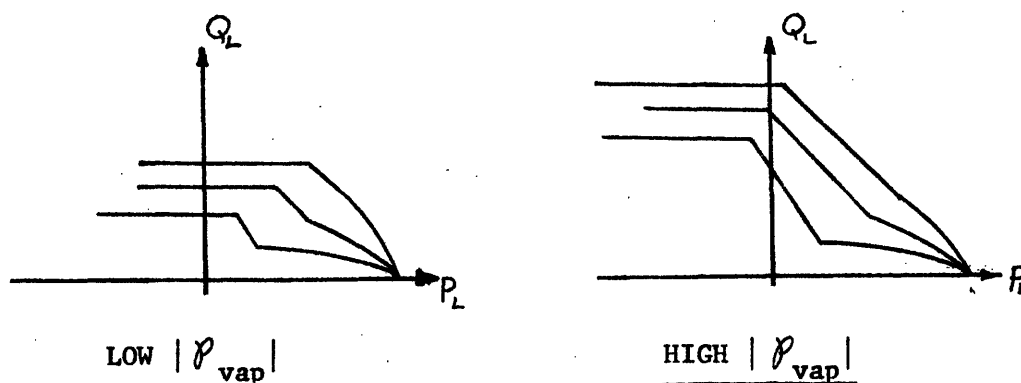


FOR LINE-TO-LINE VJPV

$K_f$  is the normalized area of a fixed orifice in series with the variable orifice. This fixed orifice may be dispensed with altogether. Its purpose—if used—would be to delay the onset of the choked flow condition and increase the available operating range of the VJPV by preventing outright cavitation of the entire low-pressure line in cases where  $Q_L$  is large,  $P_L$  is large and  $P_L$  and  $Q_L$  are opposite signs. In other words, under certain rather unusual load conditions it may be possible for the absolute pressure in one of the load lines to fall below the vapor pressure of the dissolved gases. The fixed orifice retards this effect but also has a tendency to reduce efficiency.



The last of the parameters is  $\mathcal{P}_{\text{vap}}$  which is a measure of the difference between the exhaust pressure and the vapor pressure of dissolved gases in the fluid. By decreasing  $\mathcal{P}_{\text{vap}}$  (increasing  $|\mathcal{P}_{\text{vap}}|$ ) the same desirable effects are achieved as by adding the fixed orifice without the same side effects. Decreasing  $\mathcal{P}_{\text{vap}}$  retards choking, increases the available operating range of the VJPV and increases efficiency. The disadvantage of decreasing  $\mathcal{P}_{\text{vap}}$  is that a decrease of  $\mathcal{P}_{\text{vap}}$  is tantamount to increasing all pressures in the system since the absolute pressures of  $P_e$  and  $P_s$  are both increased for the same  $P_s - P_e$ . This may lead to increased cost and weight. But since a completely pressurized exhaust system is needed in any case it might be better to raise  $|\mathcal{P}_{\text{vap}}|$  than to add the fixed orifices.



### Examples of VJPV Characteristics

To obtain a better feel for effect of parameter variations of VJPV characteristics, a number of particular characteristics were generated. The computations were carried out on an electronic computer so that no simplifying assumptions were necessary. The table below gives the parameters used.

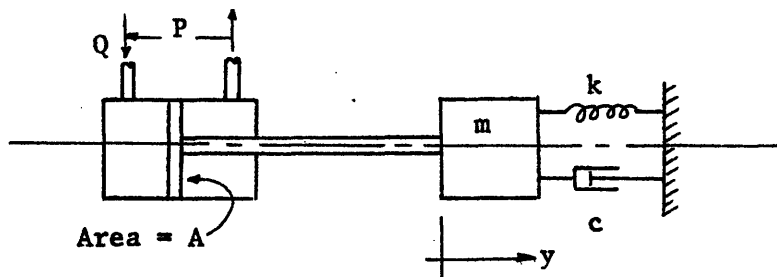
Figure	$K_c$	$K_o$	$K_f$	VJP	$P_{vap}$
3.3a	3.98	2.98	--	0	-.235
3.3b	5	10	--	0	-.235
3.3c	5	10	1	0	-.235
3.3d	5	5	--	-.15	-.235
3.3e	5	5	1	-.1	-.235
3.3f	5	10	--	0	-.47
3.3g	2	10	--	0	-.235

In each case the parameter of the VJP (i.e.,  $\eta$ ,  $C_v$ ,  $k_v$ ,  $c_v$ ,  $\psi$ ,  $q_{no}$ ,  $q_{eo}$ ) are taken as mentioned earlier in the section on limitation of parameters. In every case  $\chi_{orifice}$  was taken as .001. This value was picked to simulate a line-to-line orifice characteristic and is not zero to account for the inevitable leakage. As discussed earlier taking  $\chi_{orifice}$  less than zero results in a deadband which does not change the form of the characteristics--it only means the line on the characteristics where  $\chi = 0$ , now includes all values of in the range  $-\chi_{orifice} \geq \chi \geq \chi_{orifice}$ .  $\chi_{orifice}$  was not taken greater than zero because this has generally undesirable effects from the efficiency standpoint.

The particular values used in Fig. 3.3a are chosen to simulate a breadboard VJPV described in Chapter 5. Fig. 3.3b is a basic configuration that can be compared with Fig. 3.3a, c, f, and g, to show the effects of varying  $K_o$ ,  $K_f$ ,  $P_{vap}$ , and  $K_c$  respectively. Note that the effect of varying  $K_c$  is very small (compare Fig. 3.1b with g), therefore, Fig. 3.3a differs from 3.3b almost entirely because of a change in  $K_o$ . The effects on efficiency of some of these parameters variations are illustrated in Chapter 4.

#### State Space Analysis of a Simple Control System

Consider a VJPV regulating the position of a piston. Attached to the piston is a mass spring and dashpot.



Newton:

$$PA = \rho P_s A = ky + c\dot{y} + m\ddot{y} \quad 3.15$$

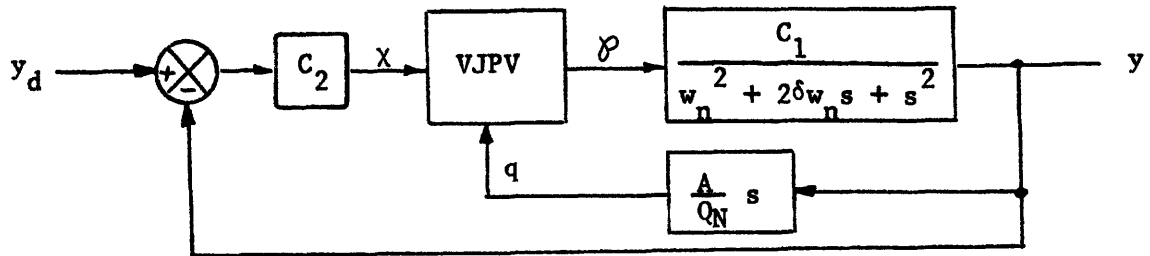
continuity:

$$Q = qQ_N = A\dot{y} \quad 3.16$$

$$y = \left[ \frac{AP_s}{k + cs + ms^2} \right] \rho = \left[ \frac{P_s A/m}{\frac{k}{m} + \frac{c}{m}s + s^2} \right] \rho \equiv \left[ \frac{C_1}{w_n^2 + 2\delta w_n s + s^2} \right] \rho \quad 3.17$$

$$q = \left[ \frac{A}{Q_N} s \right] y \quad 3.18$$

Let the control system be given by:



If we denote the VJPV characteristics by  $\mathcal{P} = G_1(x, q)$ , then the dynamic equations of the system are:

$$\ddot{y} + 2\delta w_n \dot{y} + w_n^2 y = C_1 \mathcal{P} \quad 3.19$$

$$q = A \dot{y} \quad \text{where} \quad A \equiv \frac{A}{Q_N} \quad 3.20$$

$$\mathcal{P} = G_1(x, q) \quad 3.21$$

$$x = C_2(y_d - y) \quad y = y_d - \frac{x}{C_2} \quad 3.22$$

If  $x$  and  $q$  are taken as state variables the above becomes:

$$\dot{q} = A C_1 G_1(x, q) - 2\delta w_n q - A w_n^2 \left( y_d - \frac{x}{C_2} \right) \quad 3.23$$

$$\dot{x} = -\frac{C_2}{A} q \quad 3.24$$

from which

$$\frac{dq}{dx} = - \frac{A^2 C_1}{C_2} \cdot \frac{G_1(x, q)}{q} + \frac{2w_n \delta A}{C_2} + \frac{A^2 w_n^2}{C_2 q} \left( y_d - \frac{x}{C_2} \right) \quad 3.25$$

Eq. 3.25 describes the state space trajectories where, for reference:

$$A \equiv \frac{A}{Q_N}, \quad C_1 \equiv \frac{P_s A}{m}, \quad w_n \equiv \sqrt{\frac{k}{m}} \quad 2\delta w_n \equiv \frac{C_2}{m} \quad 3.26$$

Eq. 3.19 through 3.25 do not apply in the choked condition where  $q$  depends only on  $x$ . In this region the problem degenerates into a first order problem where if  $q = G_1(x)$  gives the relation between  $q$  and  $x$ , then,

$$\dot{x} = - \frac{C}{A} G_1(x) \quad 3.27$$

In order to illustrate a particular case, assume that the hardware is fixed; only the gain  $C_2$  is variable. Let:

$$A = \text{lin}^2, \quad Q_N = 100 \text{ in}^3/\text{sec}, \quad P_s = 1000 \text{ psi},$$

$$m = 100 \text{ lb.} = .26 \frac{\text{lb. sec.}^2}{\text{in.}}, \quad w_n = 0$$

This is the case of a pure mass. A particularly good example because it is a marginally stable plant and Eq. 3.25 greatly simplifies.

Namely,

$$C_2 \frac{dq}{dx} = -.384 \frac{G_1(x, q)}{q} \quad 3.29$$



Let  $G_1(x,q)$  be that given by Fig. 3.3b which is a particularly non-linear VJPV. Fig. 3.4 gives the state space plot for  $C_2 = 1$ . From Eq. 3.29 it is apparent that different values of  $C_2$  result in uniform changes in the slope of the state space trajectories in Fig. 3.4. In this very simple case one can prove stability for all values of  $C_2$ .

The characteristics of Fig. 3.3b are such that:

$$\begin{array}{ll} x > 0 & q > 0 \\ x < 0 & q < 0 \\ x = 0 & q = 0 \end{array} \quad 3.30$$

for all practical purposes.\* Then if one considers a Lyapunov function,

V:

$$\begin{array}{ll} V \equiv |x| & \text{(positive definite)} \\ \dot{V} = \frac{x}{|x|} \dot{x} = -\frac{C_2}{A} \frac{x}{|x|} q & \text{(negative definite)} \end{array} \quad 3.31$$

and thus all control systems described by Eq. 3.23, 3.24, and 3.30 are stable.

---

\*Strictly speaking one could argue with Eq. 3.30. It assumes that  $|\varphi| < 1$ , and leakage at  $x = 0$  is negligible.

## Chapter 4

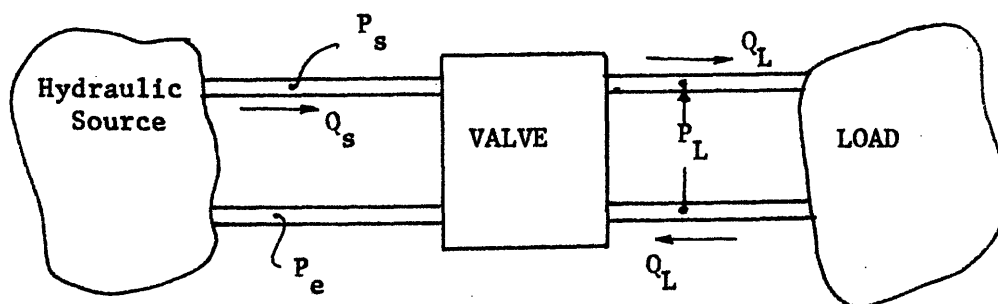
## RELATIVE POWER EFFICIENCY OF VJPV CONTROL SYSTEMS

Introduction

Chapter 4 deals with the relative power efficiency of the VJPV and the ordinary variable orifice valve. As in Chapter 3, discussion is limited to the 4-way constant-supply-pressure case. It is the increase in efficiency that is to justify the use of the VJPV.

Index of Relative Efficiency

It seems natural to define an index of relative efficiency as the ratio of the hydraulic power dissipated in a VJPV control system and an orifice valve control system. Both can be represented by the schematic below.



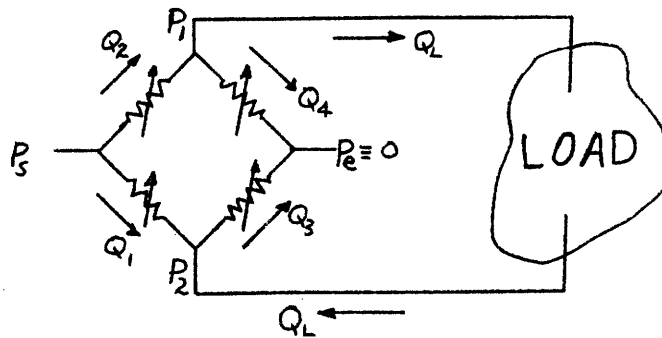
In each case there is a source of hydraulic power with constant supply pressure  $P_s$ . This supply power is modulated by a valve to drive a hydraulic load. Regardless of the type of valve used in a particular application it is desirable that the variation of  $Q_L$  and  $P_L$  with time be the same. However, the variation of  $Q_s$  will depend on the valve being

used. In an ideal (i.e., no leakage) line-to-line orifice valve  $Q_s = |Q_L|$ . It is suggested that this be taken as the reference valve for computing the index of relative efficiency,  $I$ , in the constant supply pressure case.  $I$  being defined by:

$$I \equiv \lim_{T \rightarrow \infty} \frac{\int_0^T P_{s_r} Q_{s_r} dt}{\int_0^T P_s Q_s dt} = \lim_{T \rightarrow \infty} \frac{\int_0^T Q_{s_r} dt}{\int_0^T Q_s dt} = \lim_{T \rightarrow \infty} \frac{\int_0^T |Q_L| dt}{\int_0^T Q_s dt} \quad 4.1$$

Where  $P_{s_r}$ ,  $Q_{s_r}$  are the values of  $P_s$  and  $Q_s$  that would occur using a line-to-line orifice valve. Clearly,  $I$  is a function of the time functions,  $Q_L$  and  $P_L$  as well as the valve. Provided this limit exists, it represents the relative average power demand of a given control system and a control system doing the same task using an ideal line-to-line orifice valve.

It is not hard to show that the ideal line-to-line orifice valve is the most efficient symmetric\* 4-way valve for constant-pressure applications.



\* It is possible to devise unsymmetric 4-way valves and 4-way valves using check valves, that are more efficient than the symmetric valve for certain load conditions even without using a VJP.

By definition:

$$P_L \equiv P_1 - P_2 \quad 4.2$$

By symmetry:

$$P_2 = \frac{P_s}{2} - \frac{P_L}{2}, \quad P_1 = \frac{P_s}{2} + \frac{P_L}{2} \quad 4.3$$

Noting that all such valves are built to operate in the range  $|P_L| < P_s$

then:

$$0 \leq P_1 \leq P_s, \quad 0 \leq P_2 \leq P_s \quad \text{and} \quad Q_i \geq 0, \quad i = 1, 2 \quad 4.4$$

To minimize  $Q_s = Q_1 + Q_2$  observe that

$$\text{Min } Q_s \geq \text{Min } Q_1 + \text{Min } Q_2 = 0 + Q_L = -Q_L + 0 = |Q_L| \quad 4.5$$

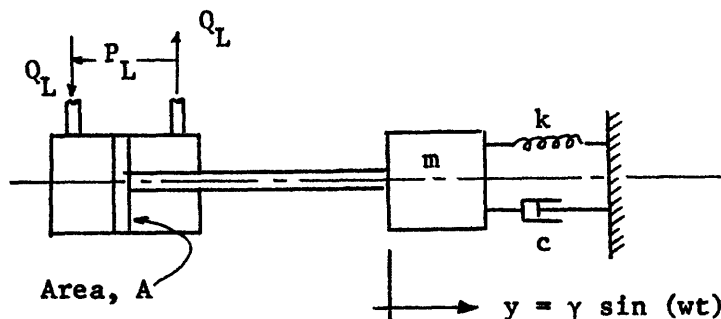
$$(\text{if } Q_L > 0) \quad (\text{if } Q_L < 0)$$

But in the ideal line-to-line case  $|Q_L| = Q_s$  and hence this is at least as efficient as any symmetric 4-way orifice valve. Thus, for any real symmetric 4-way valve  $I < 1$ . In fact many 4-way orifice valves are close to ideal so that  $I$  is close to 1.

In order to make any numerical calculations of  $I$ , some descriptions of  $Q_L(t)$  and  $P_L(t)$  must be known. In cases where the control system must manipulate the load in a cyclic fashion the functions  $Q_L(t)$  and  $P_L(t)$  need only be specified over one cycle. In other cases the best that can be done is to estimate a distribution function for the "random" variables  $(Q_L, P_L)$ . Either of these cases provide a direct evaluation of  $I$ .

### Simple Cyclic Examples

Consider a valve controlled piston driving a mass, spring and dashpot in a sinusoidal fashion.



The equation of motion is:

$$F = m\ddot{y} + c\dot{y} + ky = AP_L \quad 4.6$$

Conservation of mass gives:

$$Q_L = A\dot{y} \quad 4.7$$

After normalizing about  $Q_N = \frac{\pi D^2}{4} \sqrt{\frac{2P_s}{\rho}}$  and  $P_s$  these reduce to:

$$P_L = P_{\max} \sin(\omega t + \phi) \quad \text{where} \quad P_{\max} = \frac{\gamma}{AP_s} \sqrt{(-m\omega^2 + k)^2 + c^2\omega^2}$$

$$q_L = q_{\max} \cos(\omega t) \quad q_{\max} = \frac{\gamma A \omega}{Q_N} \quad 4.8$$

$$\phi = \tan^{-1} \left( \frac{c\omega}{-m\omega^2 + k} \right)$$

Eq. 4.8 describes what is sometimes called the load locus.\* Then from Eq. 4.1:

$$I = \lim_{T \rightarrow \infty} \frac{\int_0^T |Q_L| dt}{\int_0^T Q_S dt} = \frac{\int_0^{2\pi/w} |q_L| dt}{\int_0^{2\pi/w} q_S dt} \quad 4.9$$

where  $q_S$  is a function of  $q_L$  and  $P_L$  given by the VJPV characteristics. Since in any symmetric VJPV  $|q_L|$  and  $q_S$  are the same at  $(q_L, \mathcal{P}_L)$  and  $(-q_L, -\mathcal{P}_L)$  it is only necessary to integrate on a region of  $0 \leq t \leq \pi/w$ . Further substituting  $t' = tw$  the same value of  $I$  results if:

$$I = \frac{\int_0^\pi |q_L| dt'}{\int_0^\pi q_S dt'} \quad \text{where } q_S = G_3(q_L, \mathcal{P}_L) \quad 4.10$$

Thus, the parameters  $\mathcal{P}_{\max}$ ,  $q_{\max}$ , and  $\phi$  together with the VJPV characteristics are sufficient to determine  $I$ .

Although Eq. 4.8 indicates that  $0 \leq \phi \leq \pi$  is the complete range of  $\phi$  it is actually only necessary to consider the range  $0 \leq \phi \leq \pi/2$  because all other things being equal,  $I$  at  $\phi$  equal  $I$  at  $\pi - \phi$  which is demonstrated below.

Consider the denominator of Eq. 4.10:

---

\* See Blackburn<sup>1</sup> et. al., p. 148.

$$\int_0^{\pi} q_s dt' = \int_0^{\pi} G_3(q_L, \varphi_L) = \int_0^{\pi} G_3(q_{\max} \cos t', \varphi_{\max} \sin(t' + \phi))$$

4.11

substituting  $t' = \pi - t$  gives:

$$\int_0^{\pi} q_s dt' = \int_{\pi}^0 G_3(q_{\max} \cos(\pi - t), \varphi_{\max} \sin(\pi - t + \phi)) (-dt)$$

4.12

$$= \int_0^{\pi} G_3(-q_{\max} \cos t, -\varphi_{\max} \sin(\phi - t)) dt$$

because  $G_3$  is symmetric about the origin:

$$\int_0^{\pi} q_s dt' = \int_0^{\pi} G_3(q_{\max} \cos t, \varphi_{\max} \sin(\phi - t)) dt$$

4.13

$$= \int_0^{\pi} G_3(q_{\max} \cos t, \varphi_{\max} \sin(\pi - \phi + t)) dt$$

which when compared with 4.11 shows that substituting  $\pi - \phi$  for  $\phi$  does not change the denominator of I. Obviously the numerator is unchanged since it does not depend on  $\phi$ . Therefore, referring to Eq. 4.8 it is sufficient to examine I over the range  $0 \leq \phi \leq \frac{\pi}{2}$ .

The integration of the denominator of Eq. 4.10 requires graphical or numerical techniques. An electronic computer program was written to calculate the index I. This program was used to calculate the index I for the load situation described by Eq. 4.8 for the range:

$$0 < \rho_{\max} \leq .6, \quad 0 < q_{\max} \leq .6, \quad 0 \leq \phi \leq \pi/2 \quad 4.14$$

with 4 different VJPV characteristics given by Fig. 3.3a, b, c, and d. The results are given in Fig. 4.1a, b, c, and d respectively.

Two further simple cyclic loads are considered briefly here. First the case of a piston driving a friction type load where

$$F = F_{\max} \frac{\dot{y}}{|\dot{y}|} \quad 4.15$$

again assuming  $y = Y \sin \omega t$ . After normalizing as before, the load locus are given by:

$$q_L = q_{\max} \cos(\omega t) \quad \rho_{\max} = \frac{F_{\max}}{P A} \quad 4.16$$

$$\rho_L = \rho_{\max} \frac{q_L}{|q_L|} \quad \text{where} \quad q_{\max} = \frac{Y A \omega}{Q_N}$$

Again the calculations were carried out for  $0 < \rho_{\max} \leq .6$ ,  $0 < q_{\max} \leq .6$ , and VJPV characteristic given by Fig. 3.3d. The results are given in Fig. 4.2d.

Second consider the case of a piston driving a constant force load in a sinusoidal manner. Then

$$F = F_{\max}, \quad y = Y \sin \omega t \quad 4.17$$

and after normalizing:



$$\rho_L = \rho_{\max} \qquad \rho_L = \frac{F_{\max}}{P_s A}$$

where

$$q_L = q_{\max} \cos (wt) \qquad q_{\max} = \frac{YAw}{Q_N} \qquad 4.18$$

Again the calculations were carried out for:

$$0 \leq \rho_{\max} \leq .6, \quad 0 \leq q_{\max} \leq .6$$

and the VJPV characteristic given by Fig. 3.3b and d. The results are given in Fig. 4.3b and d respectively.

#### Interpretation of Numerical Examples

Fig. 4.1, b, c, and d show dramatically the effect of the fixed and variable downstream orifices on I, the index of relative efficiency. Comparing b with a illustrates the decrease in efficiency that results from changing  $K_o$  from 10 to 2.98. It is apparent that  $K_o$  should be made quite large for efficiency sake. The decrease in efficiency as a result of adding a fixed orifice is illustrated by comparing Fig. 4.1b with c.

The large increase in I that results from overlapping the VJP nozzles but not the variable orifice is shown by Fig. 4.1d. This, of course, results in a pronounced non-linearity of the VJP characteristics and would probably only be suitable for applications where static regulation of the position is not required.

These other conclusions can be drawn from the examples. An increase in  $q_{\max}$  (or one could say average flow rate) generally results in an increase in  $I$  which is quite desirable because at high flow rates it is most important to achieve efficiency. An increase in  $\mathcal{P}_{\max}$  generally results in a decrease in  $I$ . As  $\phi$  increases from  $0^\circ$  to  $90^\circ$  there is a decrease in  $I$ . Referring to Eq. 4.8 it is apparent that  $\phi$  is a measure of the amount of damping in a system. At  $\phi = 0$  there is no damping and in fact no net power supplied to the load. At any other  $\phi$  the average power supplied to the load is:

$$= \frac{1}{T} \int_0^T (\mathcal{P} P_s) (q Q_N) dt = \frac{\mathcal{P}_{\max} P_s q_{\max} Q_N}{2\pi} \int_0^{2\pi} \cos(t) \sin(t+\phi) dt$$

$$\frac{\mathcal{P}_{\max} P_s q_{\max} Q_N}{2} \sin \phi$$

This is very similar to the power factor used in electrical circuits. Thus, it is generally true that as the power factor increases the relative efficiency decreases, assuming  $\mathcal{P}_{\max}$  and  $q_{\max}$  are constant.

#### Other Efficiency Considerations

There is the possibility that in some applications a considerable indirect savings in total power consumption and initial system cost and weight will result from using the VJPV. This is a consequence of the flow multiplications in the VJPV at low output pressures. Where high flow is needed only at lower pressures the use of the VJPV may enable the use of a smaller flow capacity hydraulic power source. This property is displayed by a number of load situations. When driving a highly reactive load such as a spring or mass the highest flow is needed at zero

pressure. Machine tool spindles, tables, rams, etc., usually operate at highest speeds when under lowest loads and highest loads at lowest speeds.

To determine the maximum supply flow needed it is only necessary to construct the load locus on the VJPV characteristics and observe the maximum supply flow. The supply flow needed for any ordinary orifice valve is at least the maximum load flow. Thus, the two are readily compared. Fig. 4.4 illustrates this flow savings for several load loci using the VJPV characteristics of Fig. 3.3b.

### Conclusions

Under favorable load conditions it appears the VJPV will be of the order of twice as efficient as an orifice valve. Also the necessary flow capacity of the supply system may be reduced by a factor of the order of 50%. The most favorable load conditions are achieved when the valve is used a substantial amount of the time delivering high flows at low pressures.

In order to realize the savings that are possible it is important that the flow saved in the control system not be dissipated in the hydraulic supply system.

## Chapter 5

### EXPERIENCE WITH A 4-WAY VJPV

#### Introduction

A breadboard 4-way VJPV was constructed. The VJPV was incorporated in a feedback control system used to position a mass. Various tests were conducted to verify the feasibility of achieving dynamic control and improved efficiency with this valve.

#### Apparatus:

The complete apparatus consists of a hydraulic position control system with necessary instrumentation. The block diagram of the control system is indicated in Fig. 5.1. The mechanical arrangement of the VJPV and the load cylinder are given in Fig. 5.20. Photographs of the complete VJPV control system and close up photos of several of its details are given in Fig. 5.2b, c, d, and e. Clearly the construction is crude by commercial valve standards but is quite suitable for demonstration of the principal of the VJPV. The VJP's are of the same design used in Chapter 2 (Fig. 2.3). The 2 orifice spool valve is an adaptation of a commercial 4 orifice spool valve. It has a 1/4 inch bore with approximately 3/4 of the circumference machined out at the orifices. A special housing was made to hold the sleeve and provide the oil ports. Fig. 5.3 clarifies the orifice valve construction. All load line tubing is 3/8 O.D., 5/16 I.D. steel. The flexible connections attaching the torque motor to one VJP and the spool valve are made of .031 piano wire. Threaded connections are brazed on the ends of the wire to allow connection

to the individual components and adjustment of the relative positions of the spool and the two VJP nozzle cones. The same pressure control system was used as in the testing of single VJP dynamics.

The essential instrumentation consisted of position and velocity transducer (Bourns Co, Model No. 108, Sanborn Co. LYsyn-6LVA8 respectively), on the hydraulic cylinder, two static pressure gages to measure supply and exhaust pressure, a position transducer (Sanborn Co. Linearsyn 590-DT-.025) to measure the torque motor position and flow meters to measure flow returned to stand. The dynamic signals were displayed on a Tektronix dual beam oscilloscope (Model #502). Permanent records of the scope output were made using a scope mounted Polaroid camera.

The hydraulic cylinder has a one-inch bore and stroke. The central shaft is 0.375 in diameter giving a piston area of  $0.675 \text{ in}^2$ . To the cylinder could be attached a mass of up to 115 lb.

A Hewlett-Packard model #202A low frequency function generator was used to provide the desired position signal. An American Measurement and Control Model #652 servo-amp was used to sum the desired position and actual position signals and amplify these to drive the AM&C Model #104 servo motor.

Aligning the orifices on the spool valve and the nozzle cones on the VJP's was accomplished as follows. On the supply pressure port of each VJP and on the exhaust port of the spool valve provision was made to connect an air hose--after disconnecting the hydraulic line. Just as the orifice (or nozzle) opens a distinct change in sound results as

the air rushes through the opening. By using the very sensitive position transducer attached to the torque motor it was possible to observe at what torque motor position each orifice or nozzle opened. Through repeated trials it was possible to align the orifices and nozzles to approximately .0005 inch. The resulting VJPV is approximately line-to-line. Subsequent tests measuring valve output flow as a function of torque motor position indicated that the valve was slightly overlapped.

#### VJPV Parameters

The throat diameter on the VJP's is .070 in. which results in:

$$Q_N = \frac{\pi}{4} D^2 \sqrt{\frac{2}{\rho} P_s} = (126)^* (.070)^2 \sqrt{P_s} = 0.616 \sqrt{P_s} \text{ in}^3/\text{sec}$$

$$0.16 \sqrt{P_s} \text{ gpm}$$

5.1

The variable orifice constant is approximately:

$$K_o = \frac{C_d \ell d/2}{\pi D^2/4} = \frac{(0.0625) (\pi 0.25.75) (.03125)}{\pi (.070)^2/4} = 2.98 \quad 5.2$$

where  $d = .0625$ ,  $D = .070$ ,  $\ell$  = circumferential length of variable orifice is approximately equal to  $(3/4) \pi (.25)$ . The value of  $C_d = .0625$  is quite often taken as the discharge coefficient for sharp edge

---

\*  $\frac{\pi}{4} \sqrt{\frac{2}{\rho}} = 126$  see appendix 2.

orifices but various investigators have found slightly different values.

The check valve constant is given by:

$$K_c = \frac{C_d A_c}{\pi D^2/4} = \frac{(0.0625) (.650) \pi (.012)}{\pi (.07)^2/4} = 3.98 \quad 5.3$$

where  $A_c$  is the product of the check valve disk circumference, 0.625 in., and the travel of the disk, .012 in.

As much as possible  $x_{\text{orifice}}$ , and  $x_{\text{VJP}}$ , are zero.  $(d/D)$  is  $0.892 \approx .9$ . There is no fixed orifice so  $K_f$  does not apply.

### Efficiency

The index I for the case where the load consists of a mass driven sinusoidally was determined in the following manner. By introducing a sinusoidal input signal from the function generator, the piston and attached mass would move in an approximately sinusoidal fashion. By measuring the amplitude of the piston displacement and knowing the frequency of oscillation the average load flow was readily determined. The average supply flow was measured on a flow meter as the oil returned to the test stand. The ratio of these two (i.e., load flow/supplying flow) is clearly I. Assuming the motion is sinusoidal  $\mathcal{P}_{\text{max}}$  and  $q_{\text{max}}$  are determined by Eq. 4.8.

In this case  $\phi = 0$  (see Eq. 4.8). The index I should not depend on  $\mathcal{P}_{\text{max}}$  to any appreciable extent as indicated by Fig. 4.1a. Therefore, the experimental results can be compared with the theoretical prediction on a single graph of I versus  $q_{\text{max}}$ .

Fig. 5.4 is such a graph. The data is taken from a trial where  $P_s = 1240$  psig, and  $P_e = 237$  psig. Therefore,  $P_{vap} = -.236$ . Load weights of approximately 60 and 0 pounds were used at frequencies between 2.5 and 10 cps.

The experimental points lie slightly above the predicted values at all but the lowest values of  $q_{max}$  but retain the general shape of the curve. Possible causes of this slightly higher efficiency are: (1) the VJP cones are slightly overlapped with respect to the orifices (i.e.,  $x_{VJP} > x_{orifice}$ ); (2) the value of  $K_o$  is too low because  $C_d > 0.625$ .

#### Closed Loop Dynamic Response

The purpose here is to present the result of frequency and step response tests to demonstrate the feasibility of achieving stable, reasonably fast dynamic control. The breadboard system has several features which prevent the very best dynamic performance. Among these are somewhat flexible connections between components and long lines connecting the valve to the cylinder.

The frequency and step responses were taken under 2 load conditions-- 0 and 60 lb. load. In each case the gain was adjusted to give approximately the "best" dynamic performance. A bode plot for the 0 load and 60 lb. load are given in Fig. 5.5a and 5.5b. Very roughly these both appear to give underdamped systems with damping ratio:  $\delta = 0.5$ . The corresponding step responses are given in Fig. 5.6a and 5.6b. Figure 5.7 shows another step response for the 60 lb. load where the gain is one-third greater than in Fig. 5.6b. The step responses also indicate a considerable underdamped second-order system. Fig. 5.8 illustrates typical wave forms for input and output driving a 60 lb. load.



### Dynamic Spool Position-Flow Tests

It is common procedure in valve testing to measure the load flow at zero load pressure as a dynamic function of spool position. In the case at hand, the spool position is given by the output of the position transducer measuring the torque motor position. The flow is taken as being proportional to load cylinder velocity.

By supplying a sinusoidal input to the feedback loop with the loop gain set low, the torque motor position varies approximately sinusoidally. With all load removed the load pressure is approximately zero. The velocity of the load piston is proportional to the load flow which is now only a function of torque motor position. This is found to be experimentally true at low frequencies. Figure 5.10 is a photograph of two Lissajous figures taken at 5 cps. The central figure is torque motor position on the horizontal axis with load piston velocity on the vertical axis. The velocity is seen to correlate well with position. An apparent overlap of the valve is shown by the inflection of the curve at zero velocity. The outer or circular Lissajous in Fig. 5.8 is of the torque motor position on the horizontal axis with load piston position on the vertical axis. Since position is the integral of velocity it is expected that this Lissajous show a  $90^\circ$  phase shift. Figure 5.9 is a similar figure for 50 cps oscillation of the torque motor. Here the correspondence of torque motor position to load cylinder is poor. However, in terms of the principal frequency component there seems to be little phase shift or amplitude attenuation up to 50 cps in the torque motor position - load piston velocity relationship.

<u>Cps</u>	<u>Input</u> *	<u>Output</u> *	<u>Phase</u>
5	5	6.6	0
30	5	6.0	0
50	5	5.5	0

### Conclusion

The VJPV has been demonstrated to offer a means of improving power efficiency in hydraulic control systems. Indications are that the quality of control (dynamic response and stability) is similar to orifice valve control.

---

\*  
cm on scope face

## Chapter 6

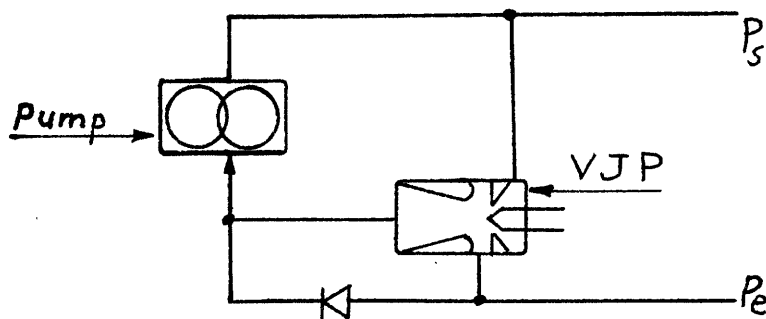
## OTHER APPLICATIONS AND SUGGESTED FUTURE RESEARCH

Examples of Other VJP Applications

A particular application of the VJP has been studied in detail in Chapter 3, 4, and 5--namely the 4-way VJPV for constant supply pressure. However, as a general principle the VJP may be applied in any situation where the flow of fluid is normally regulated by variable orifices. Some of these applications are qualitatively described here.

Pressure Control or Relief Valves\*

Frequently it is desirable to provide a pressure regulated supply of hydraulic fluid using a constant flow pump. In this case the excess of the pump flow over the flow demanded is throttled through a pressure control or a relief valve. This excess flow might better be used to increase the back pressure on the pump using a VJP as shown below.



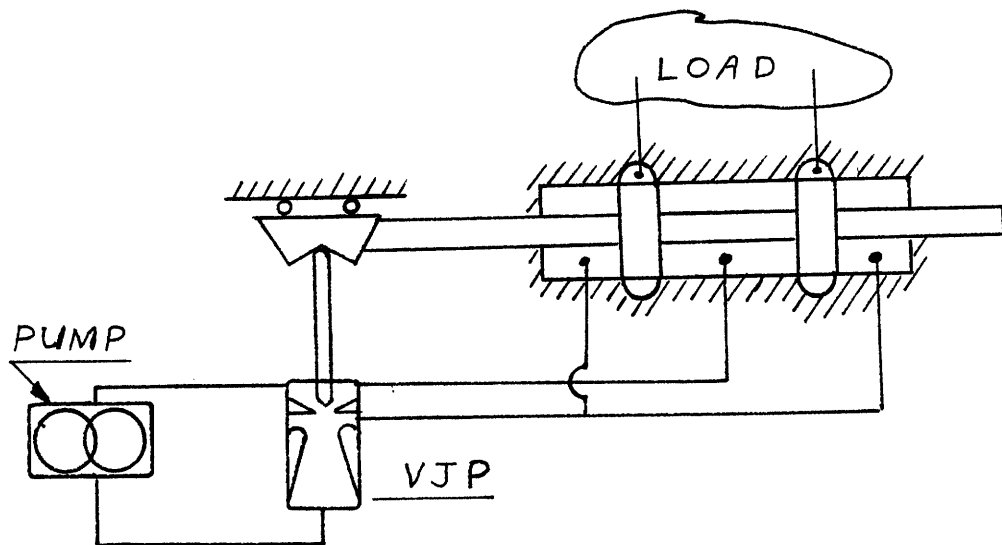
The spool position is manipulated to maintain the desired pressure difference  $P_s - P_e$ .

---

\*This application may be restricted by patent<sup>7</sup> no. 2,457,388.

### Constant Flow Valves

The 4-way constant-flow valve appears to have no simple construction as did the 4-way constant pressure valve. However, a valve for this application is conceptually possible. In this case it is desirable to use the excess flow to build up the back pressure on the pump. A schematic is shown below.



### 2 and 3-way Valve

These are obvious extensions of the 4-way valve. The VJP itself is a 2-way valve and in such applications as a one-directional speed control may have immediate application.

### Suggested Areas of Future Research

Many problems concerning actual mechanical design and manufacture of VJPV's need attention. Particular instances are, (1) the structural analysis of nozzle plate stresses, strains, and endurance; (2) check valve design for speed and reliability; and (3) "optimal" shape and arrangement of parts.

A nicely defined basic research work could be done in verifying, or modifying the two phase flow theory given in Chapter 2. In this regard the very rapid pressure fluctuations believed to be caused by the collapse of the 2 phase flow is of theoretical interest.

The increasing emphasis on no-moving-parts hydraulic and pneumatic equipment poses the question of whether a device with no moving parts could be devised to perform the function of the VJP.

Finally, one might ask, is there a possible need for pneumatic VJP's and if so can they be successfully built.

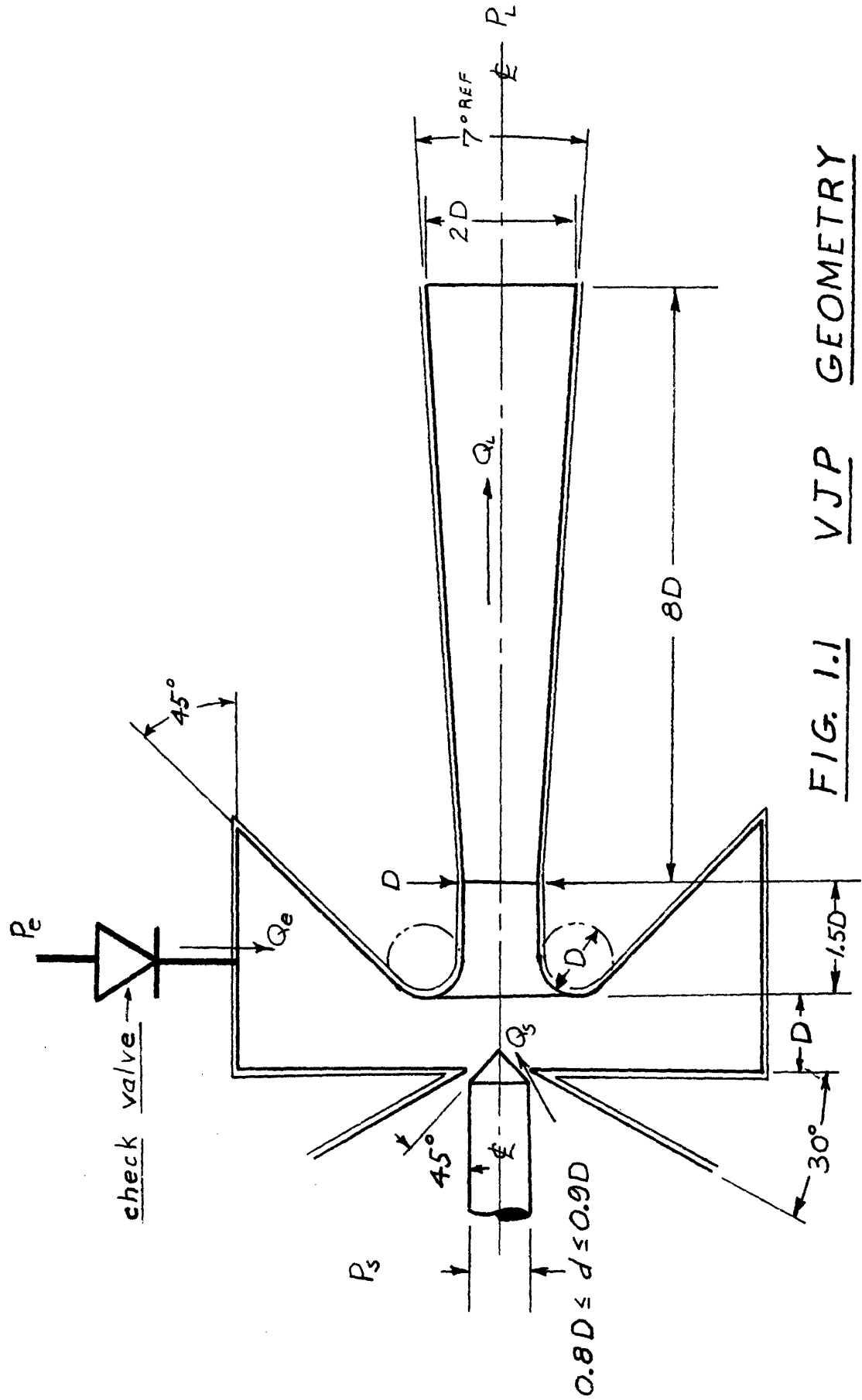


FIG. 1.1    VJP    GEOMETRY

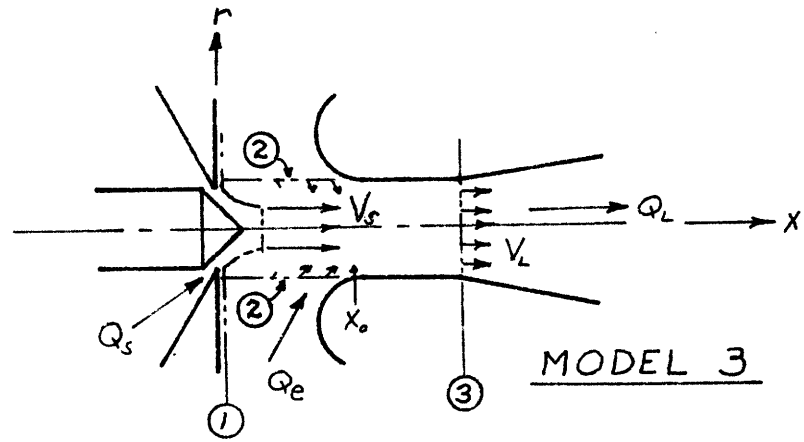
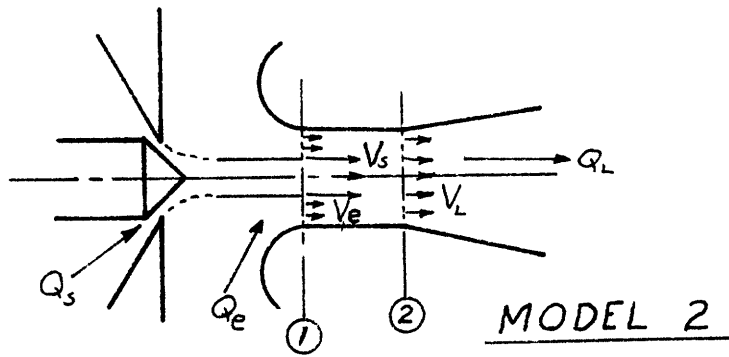
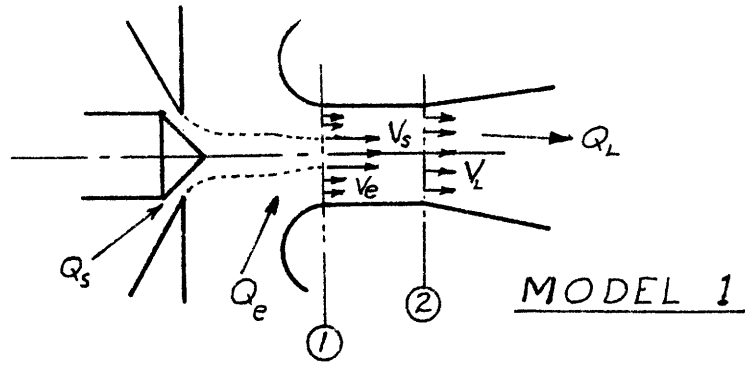


FIG. 1.2 Induced Flow  
Models

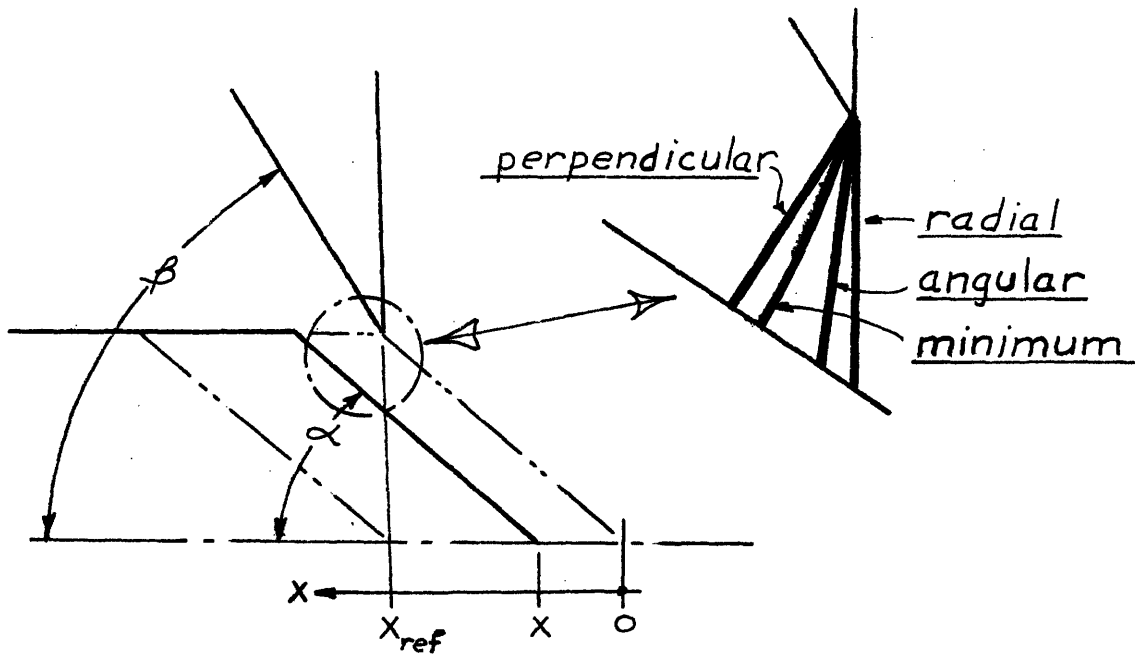
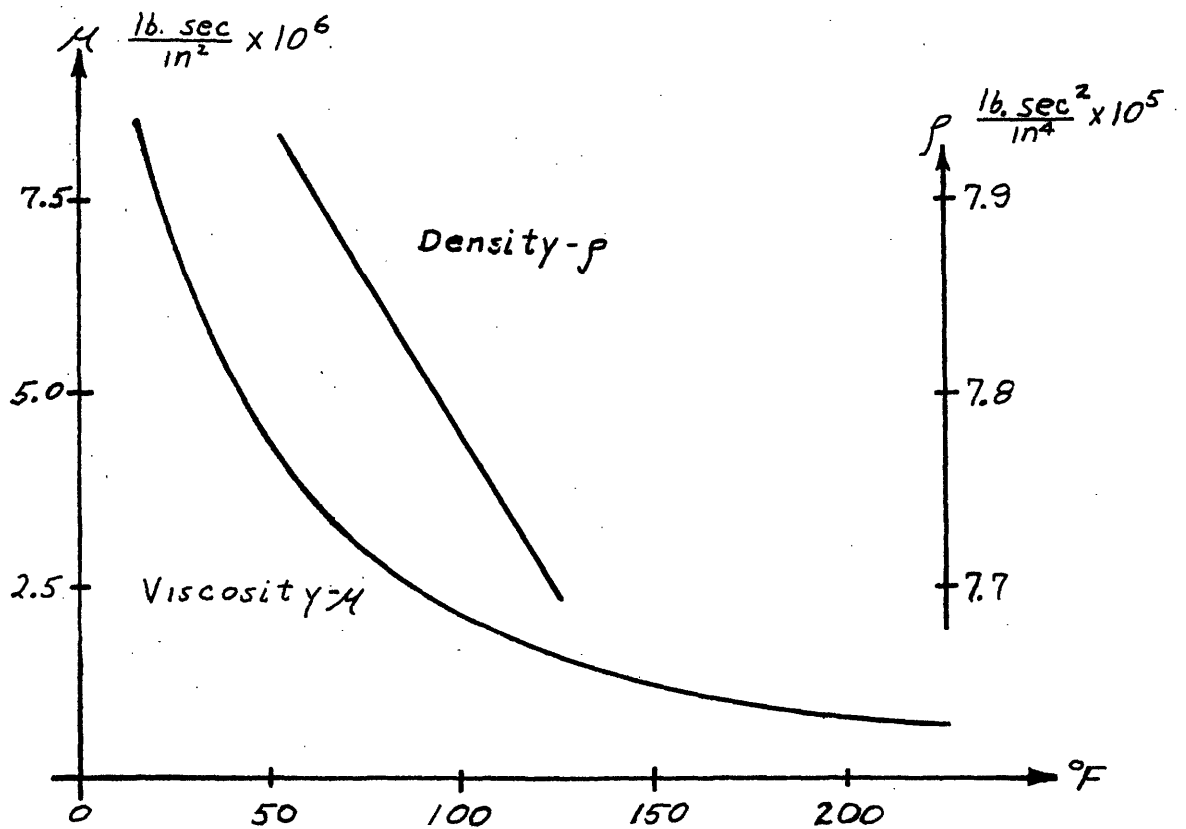
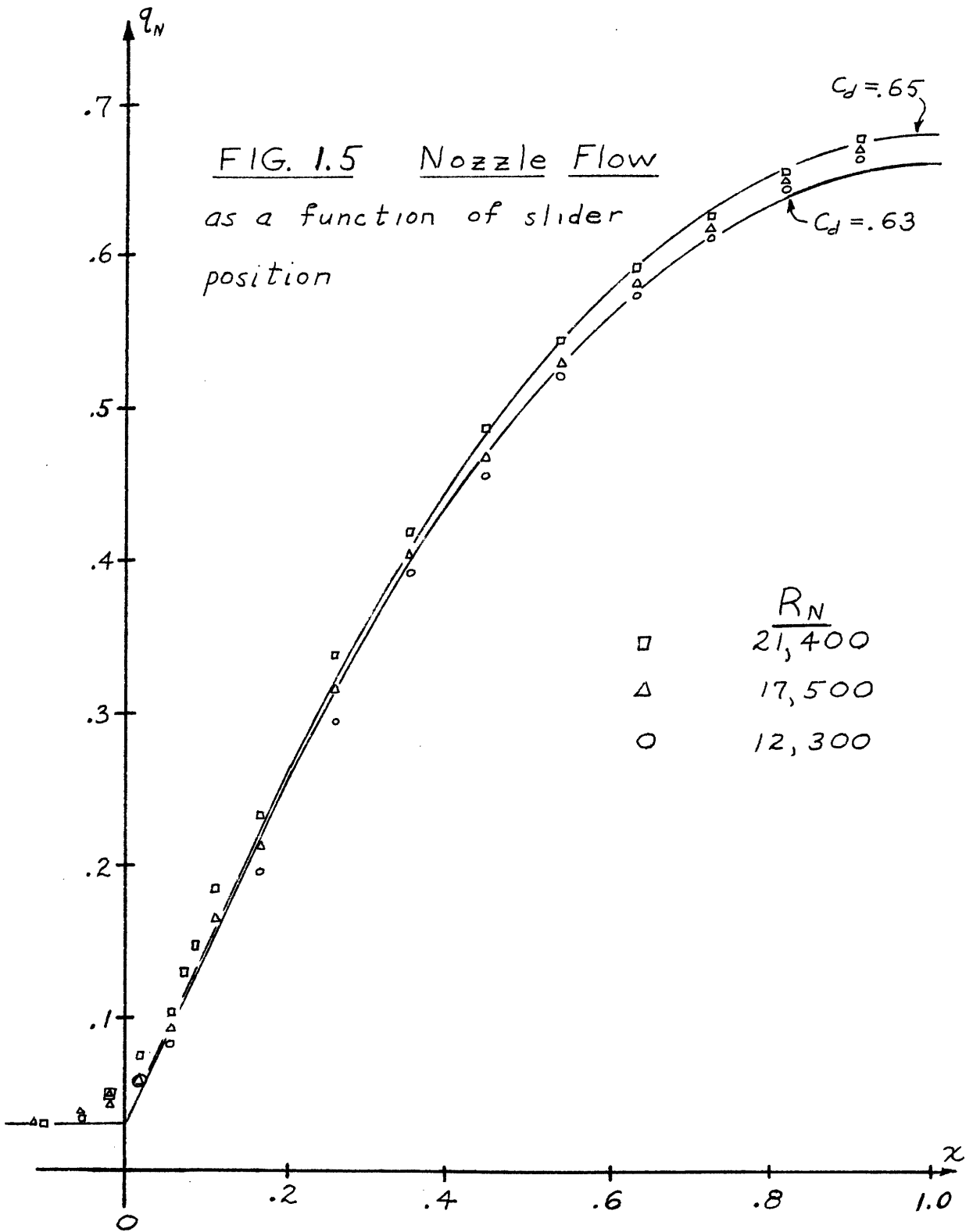


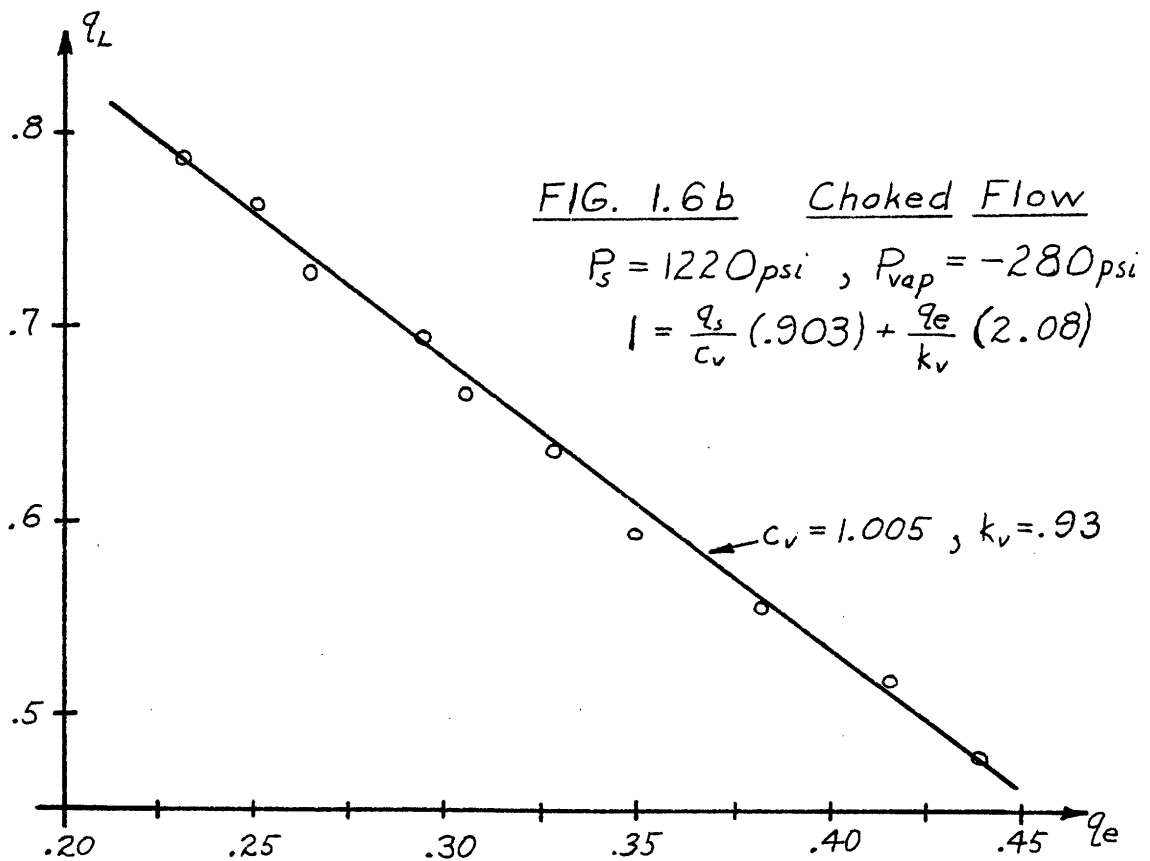
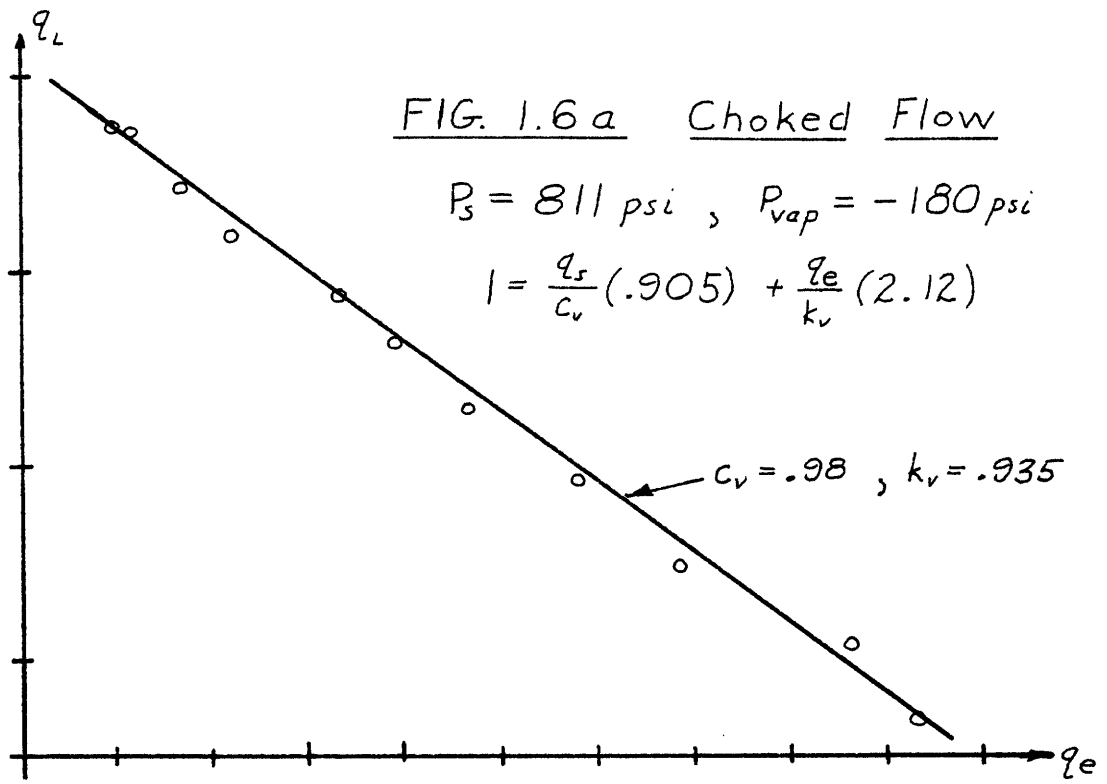
FIG. 1.3 Nozzle Nomenclature

FIG. 1.4 Viscosity and Density of J-43









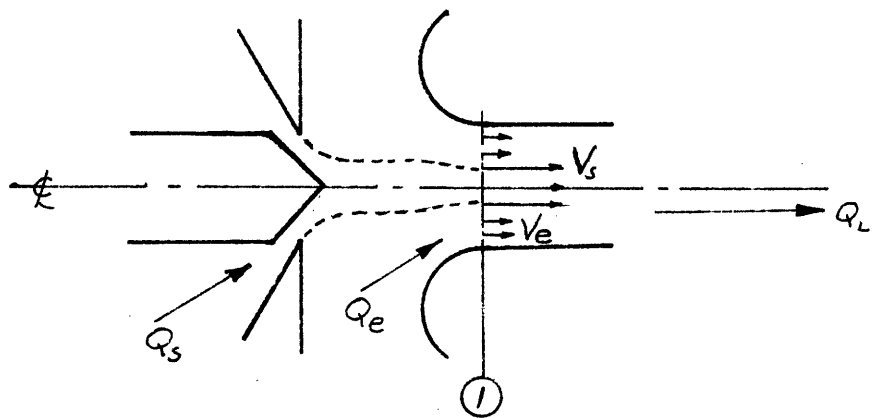
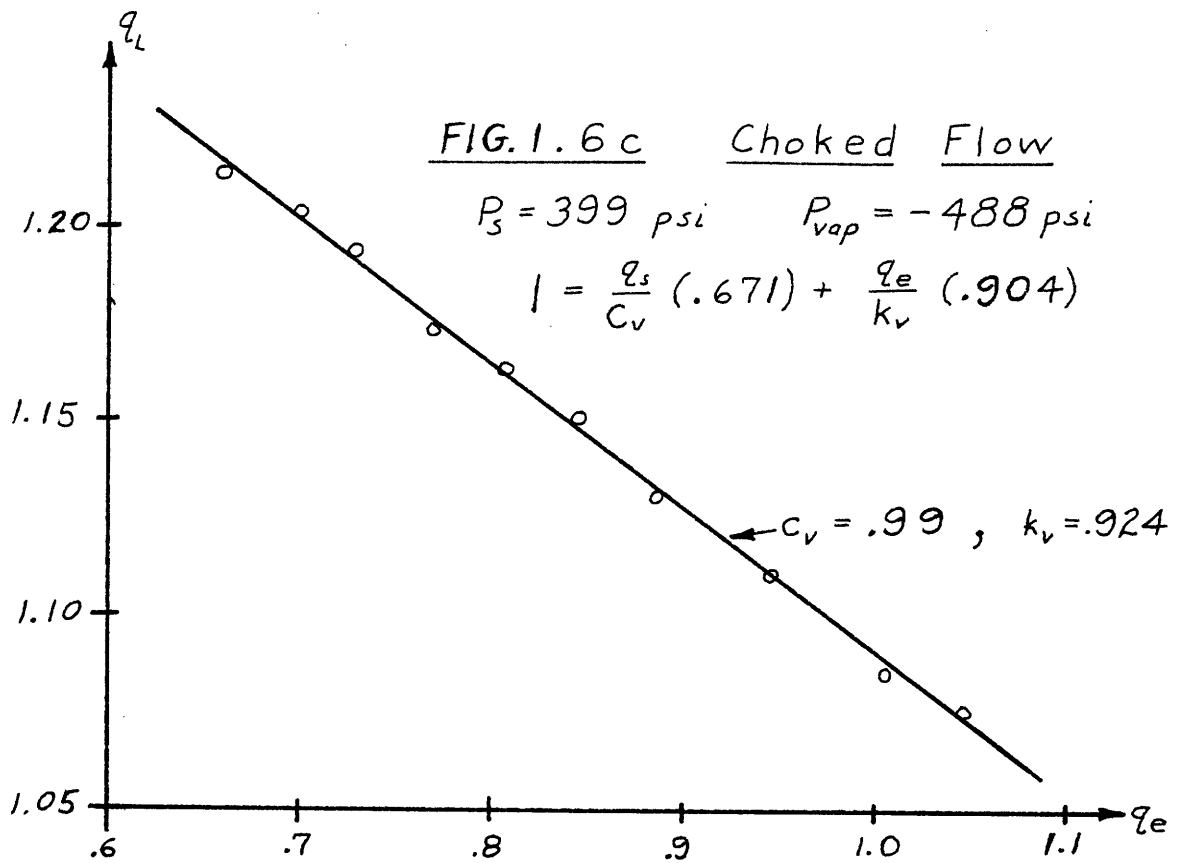


FIG. 1.6 d    Choking Model

FIG. 1.7a Induced Flow

$R_T = 25,000$

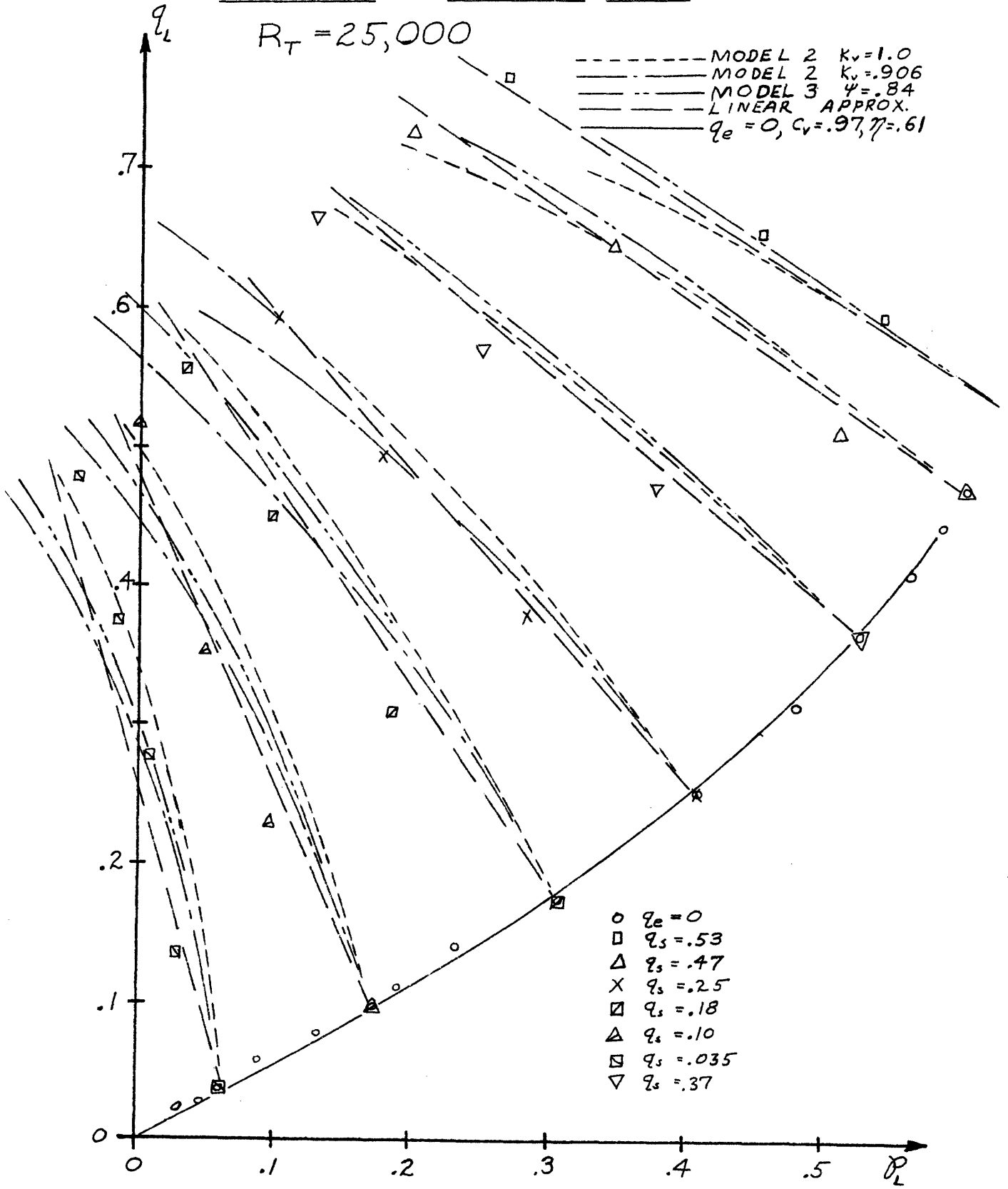


FIG. 1.7b Induced Flow

$R_T = 20,000$

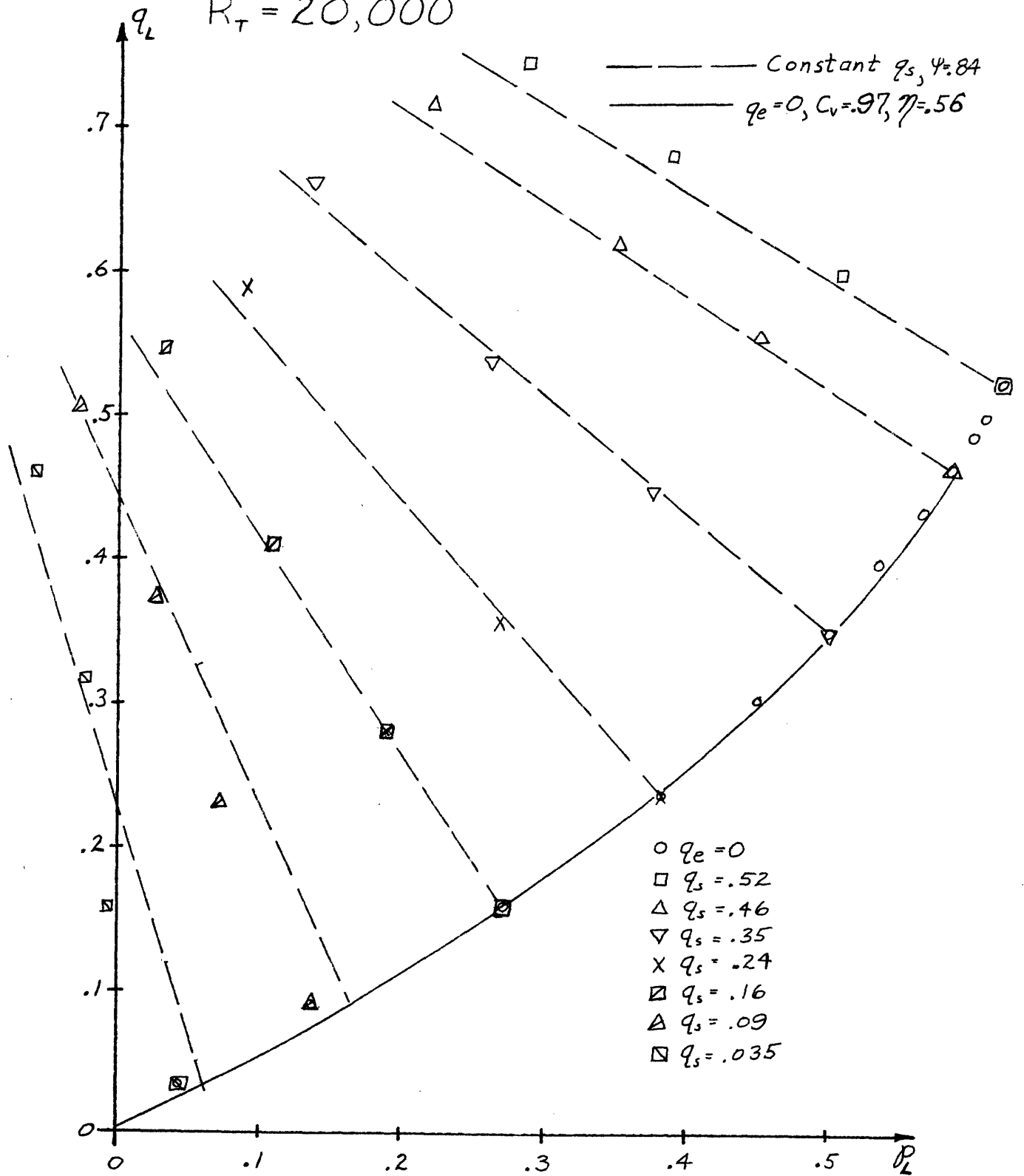
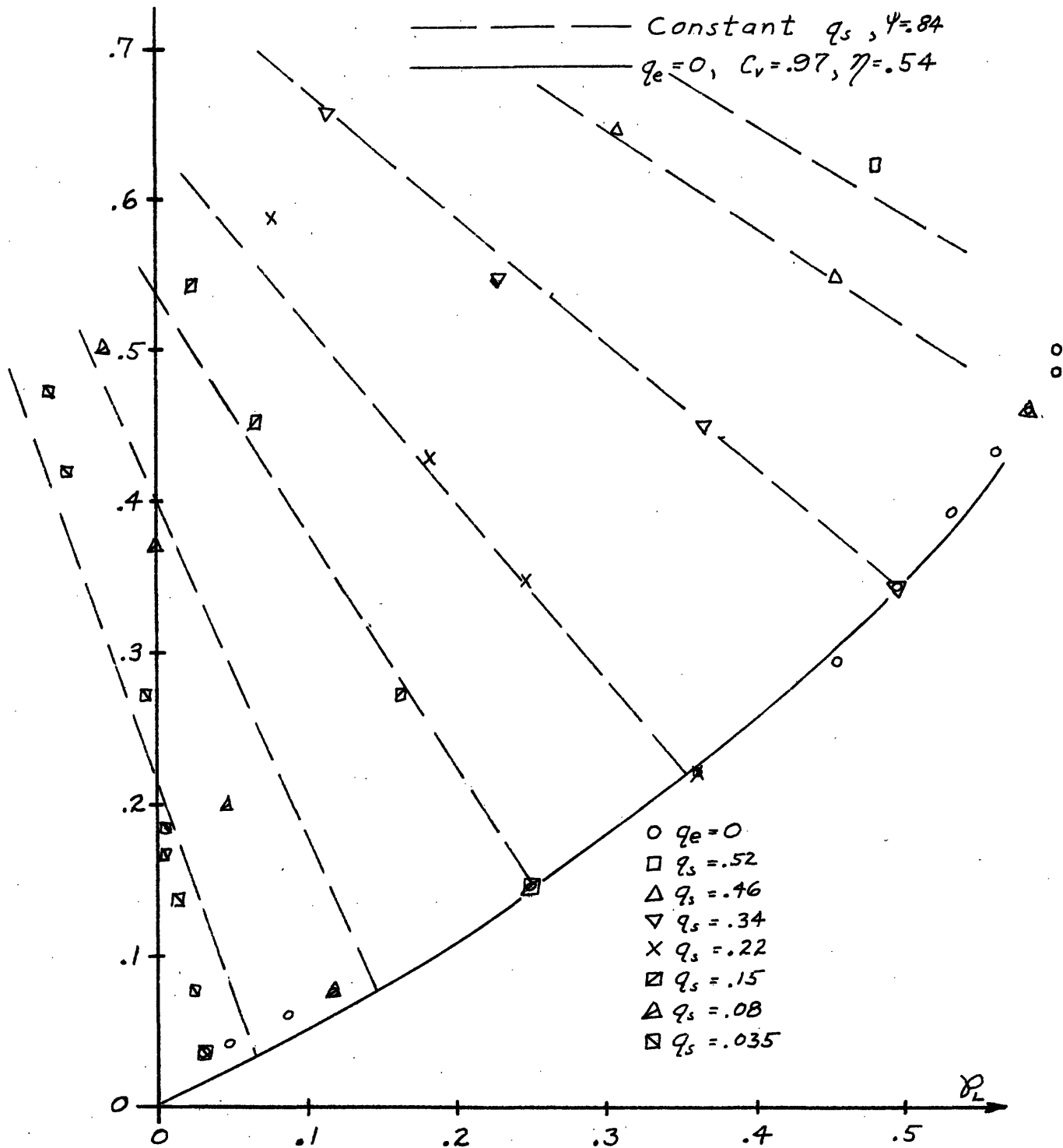
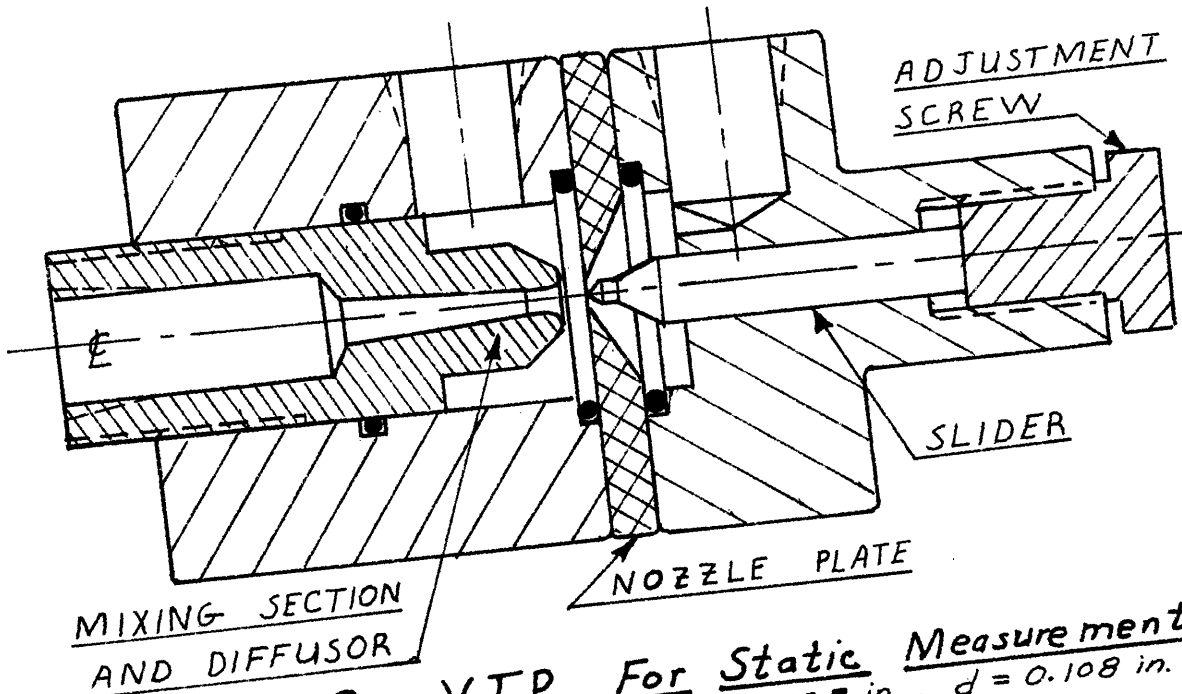


FIG. 1.7c Induced Flow

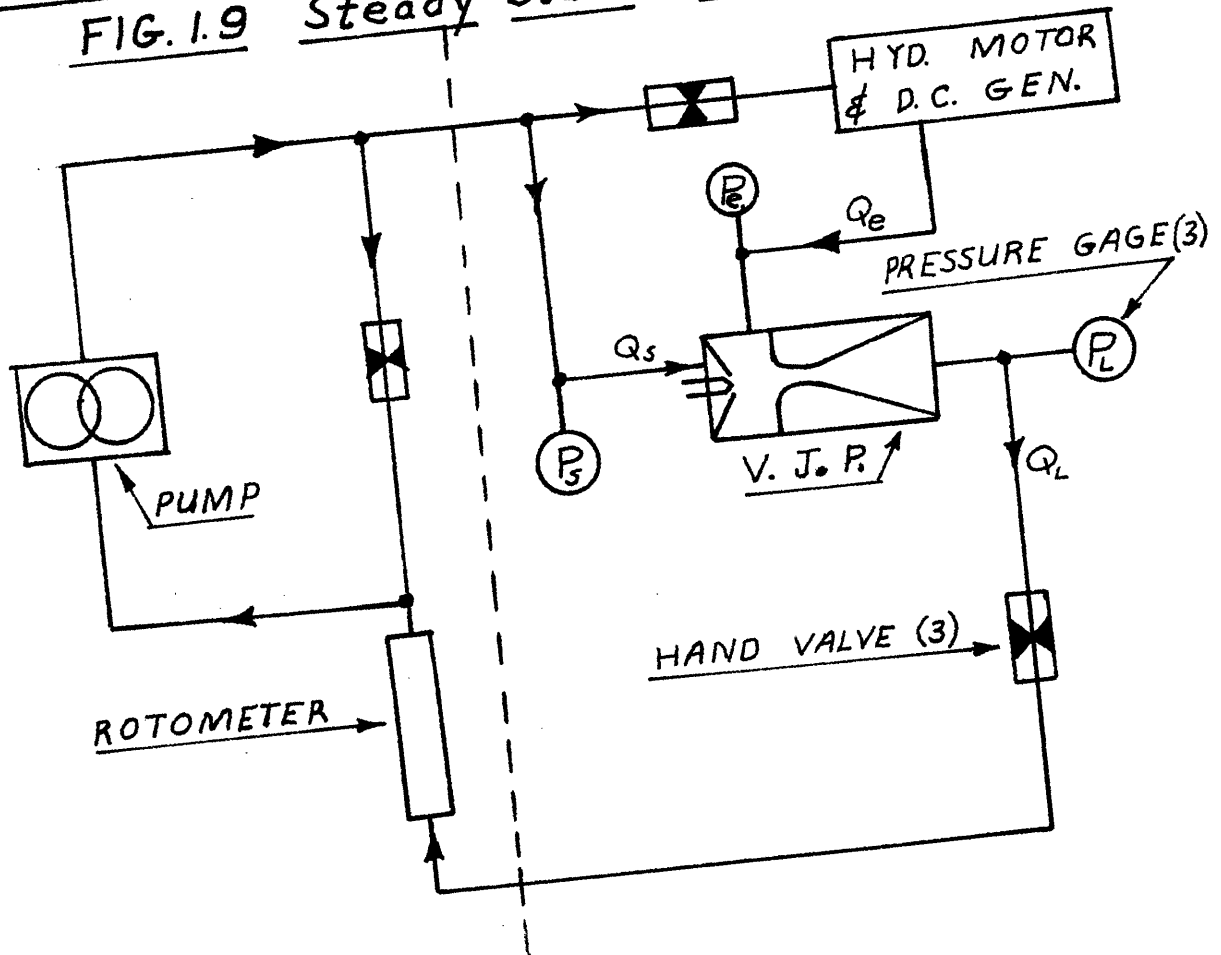
$R_T = 14,000$





**FIG. 1.8** VJP For Static Measurements  
APPROX. FULL SCALE  $D = 0.125$  in.,  $d = 0.108$  in.

**FIG. 1.9** Steady State VJP Apparatus



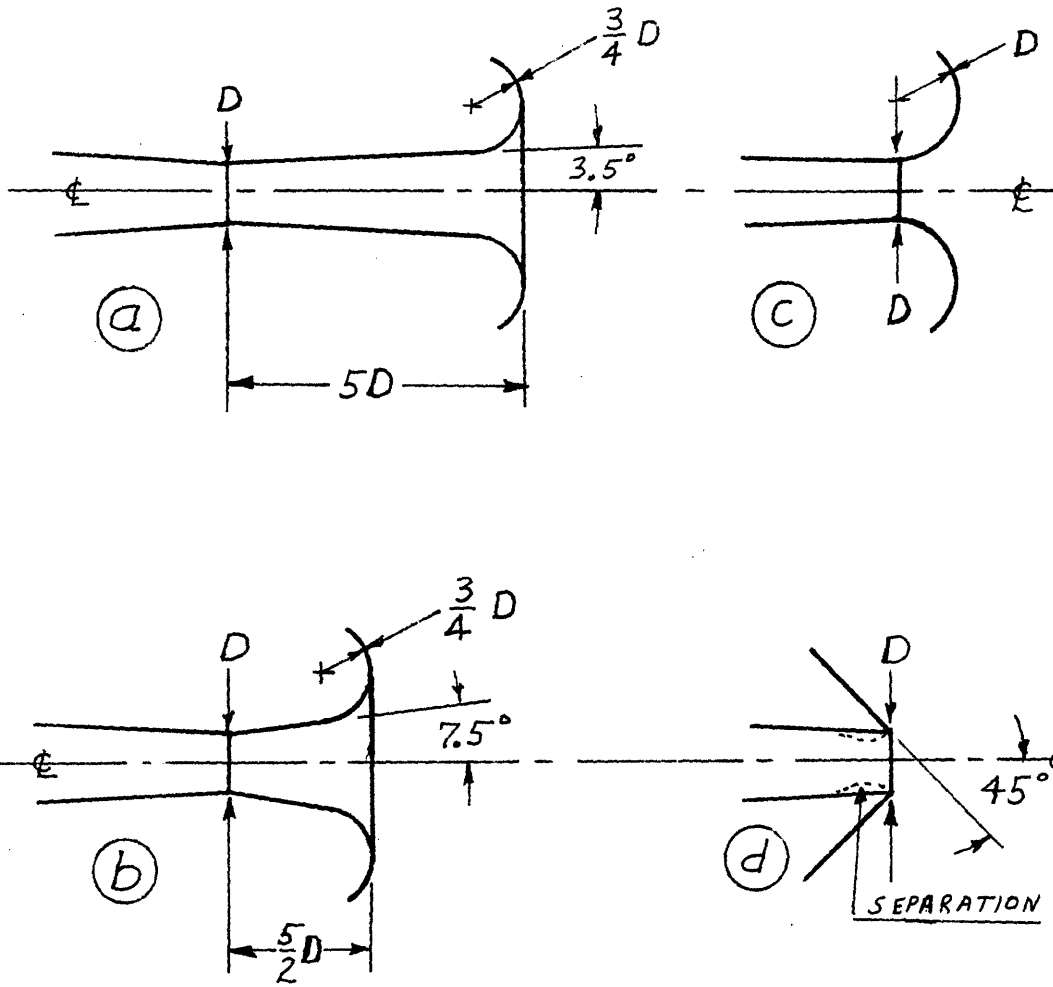


FIG. 1.10 Mixing Section Geometries

All Diffusers Have  $7^\circ$  Included Angle

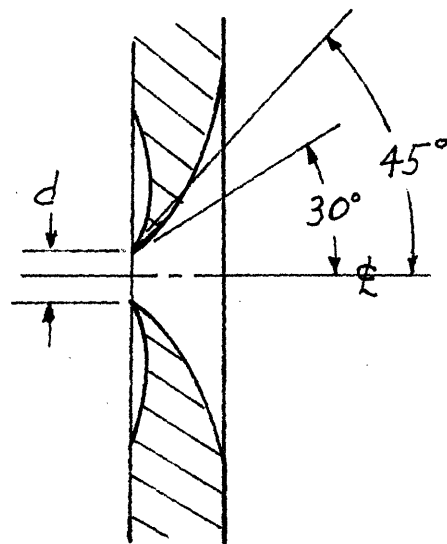
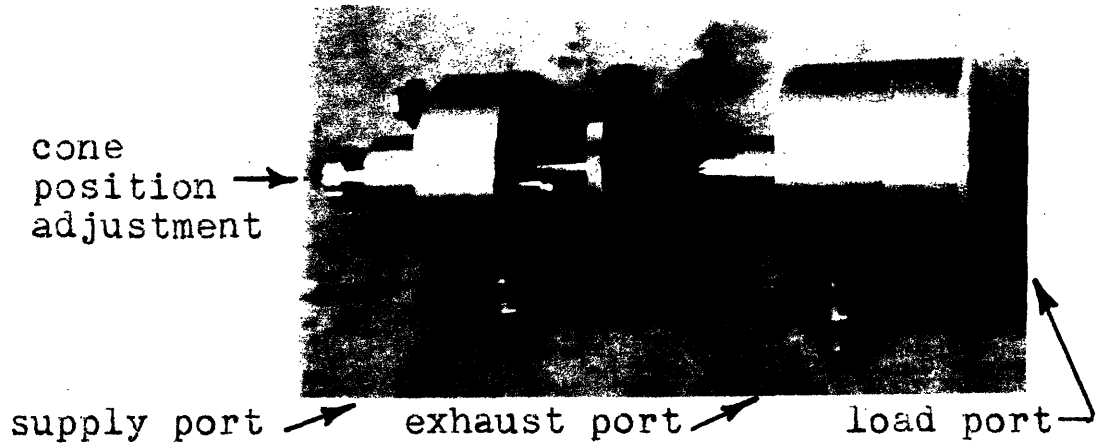


FIG. 1.11

Sculptured Nozzle Plate



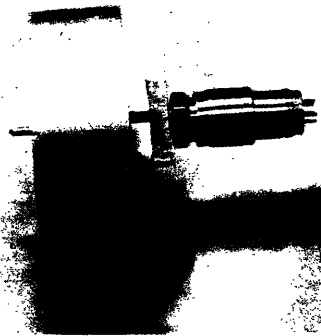
Fig. 1.13 Steady State VJP



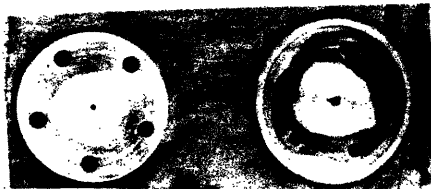
Disassembled VJP



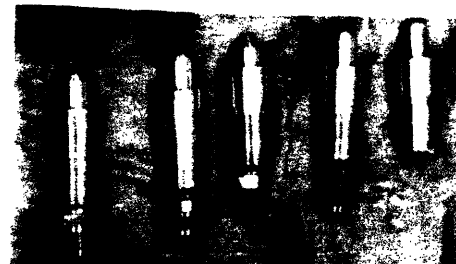
Assembled VJP



Adaptor for Cone Force Measurement



Nozzle Plates



Mixing Section and Diffuser Inserts

FIG. 1.14

Average Slider Pressure,  $P_N$ , vs.  
Nozzle Flow,  $q_N$

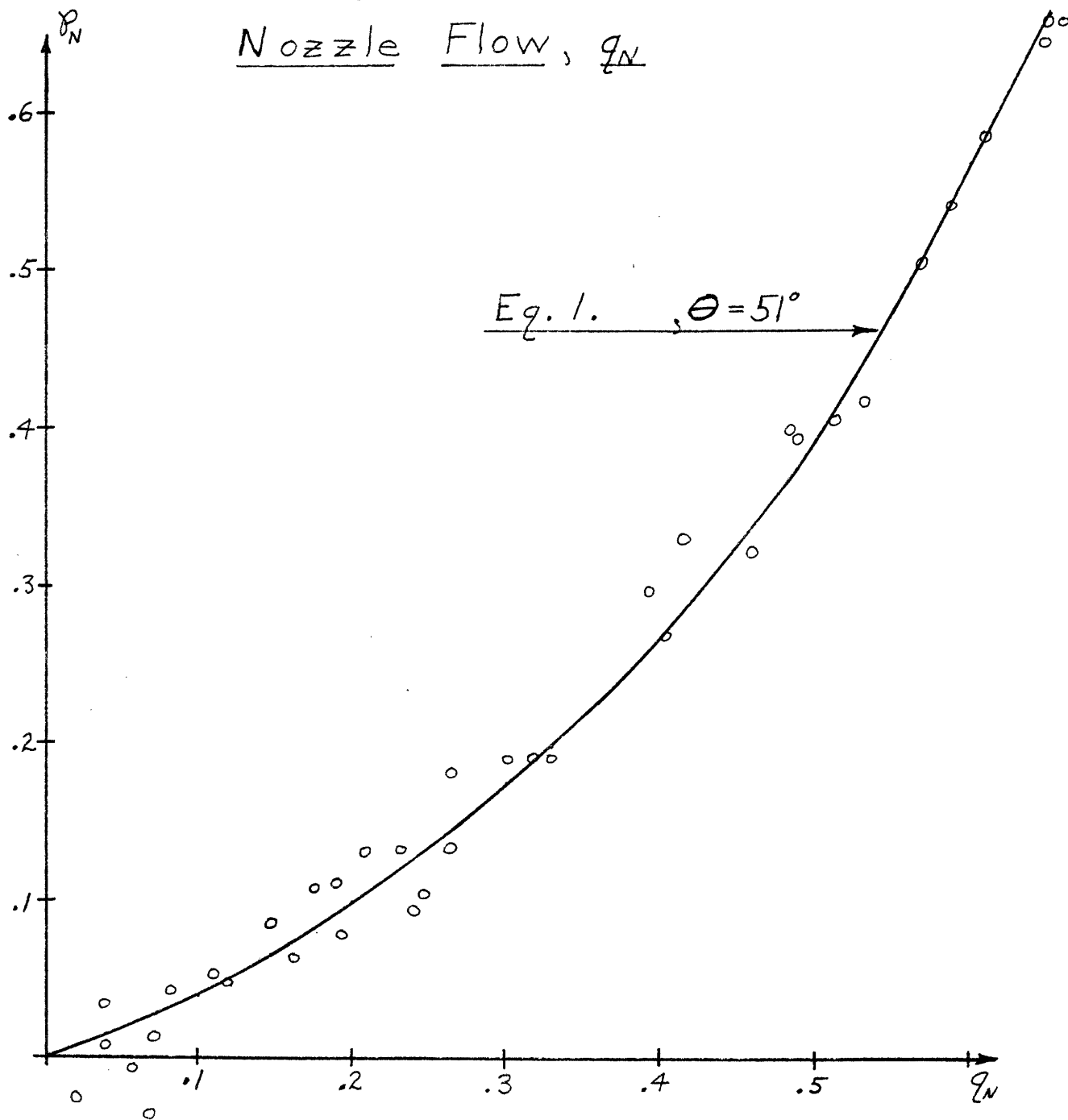


FIG. 1.15a Adapter for Cone Force Measurement

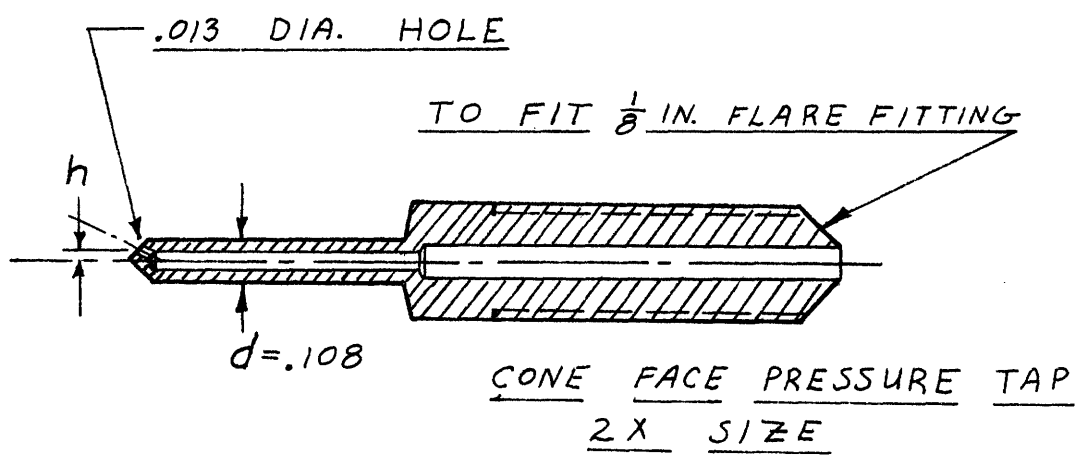
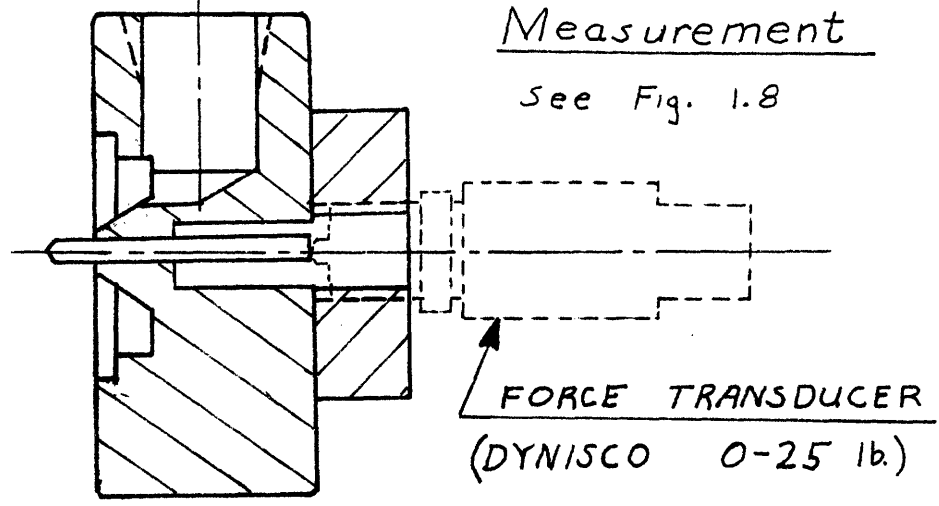
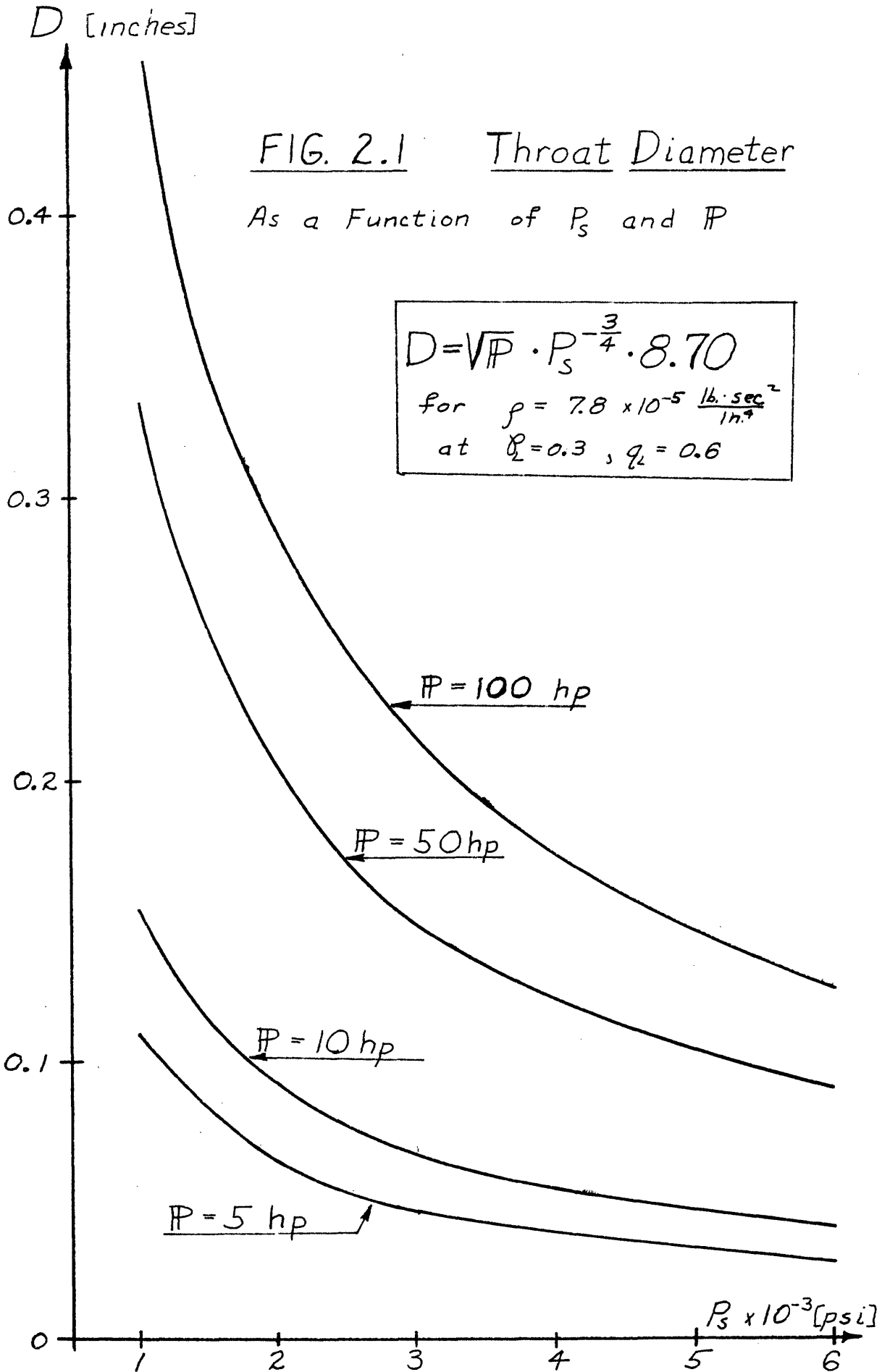
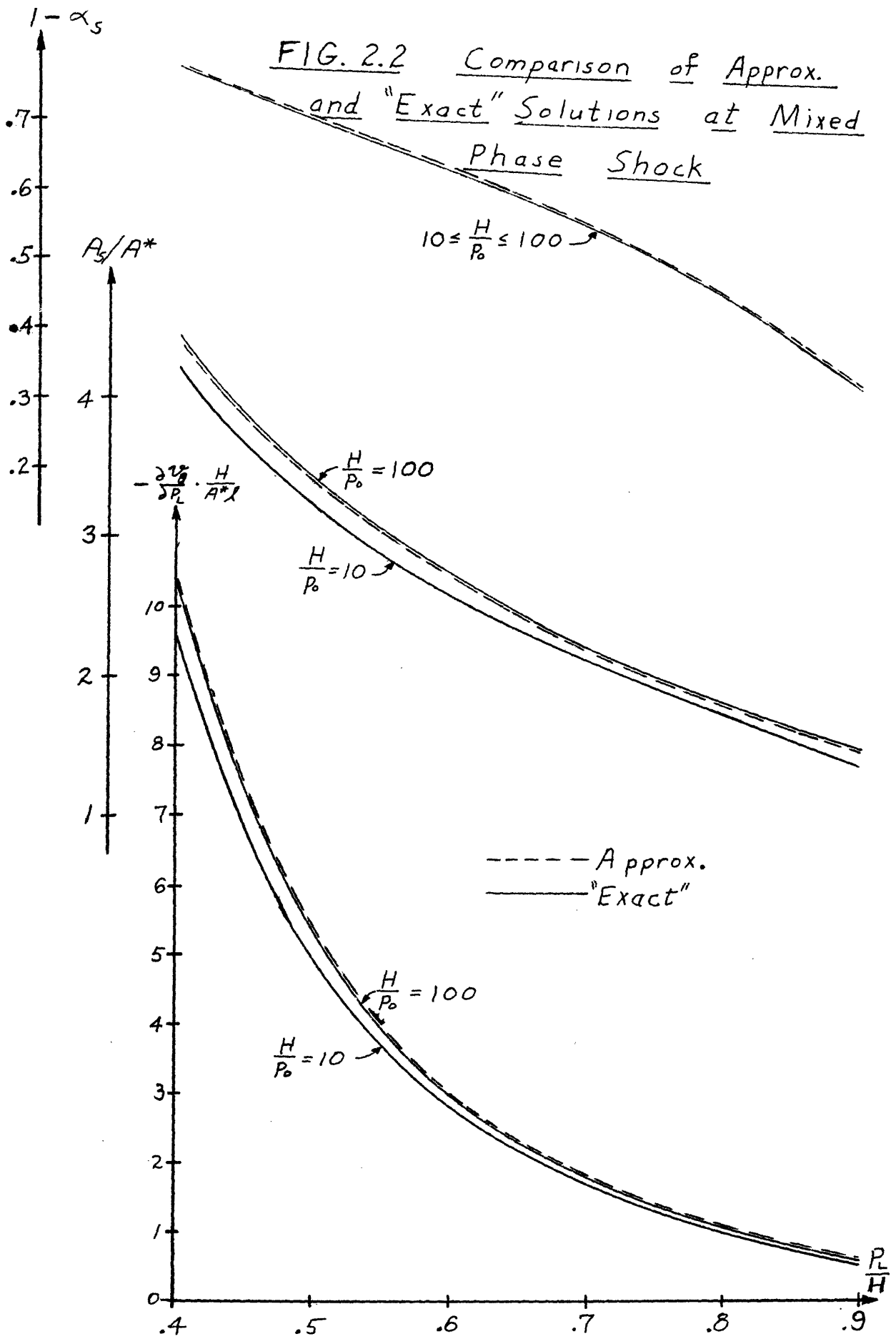
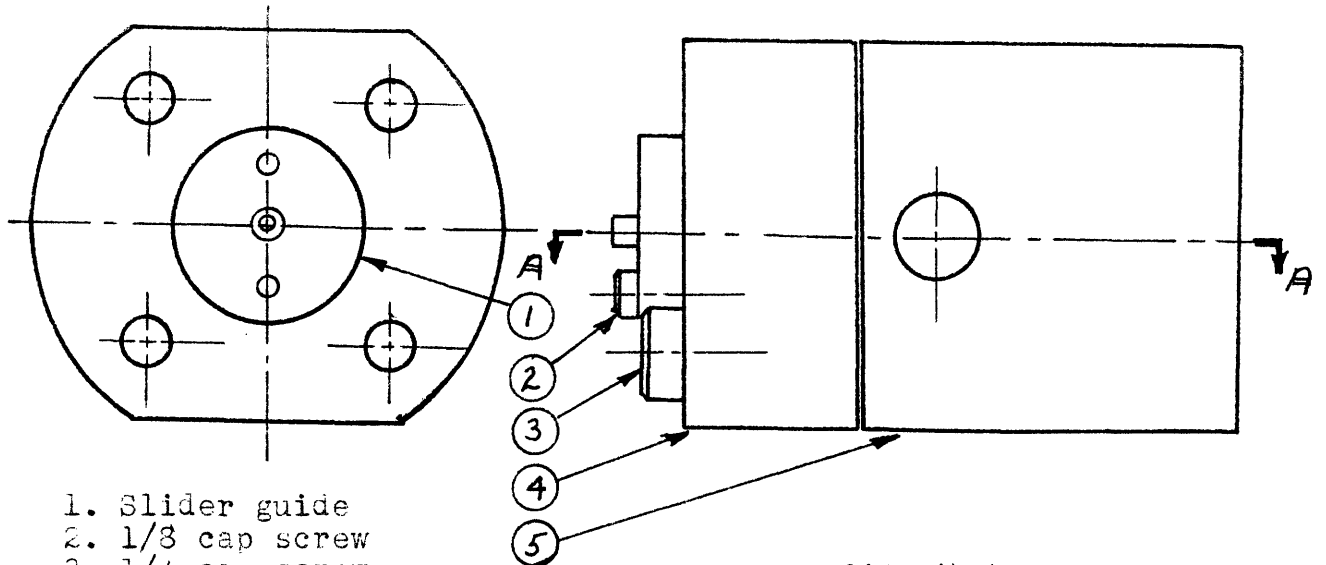


FIG. 1.15b Adaptor for Cone Pressure Measurement

(Used in above apparatus)







- 1. Slider guide
- 2. 1/8 cap screw
- 3. 1/4 cap screw
- 4. Slider housing
- 5. Diffuser housing
- 6. Piston retainer
- 7. Push rod
- 8. Piston
- 9. Slider
- 10. Nozzle Plate

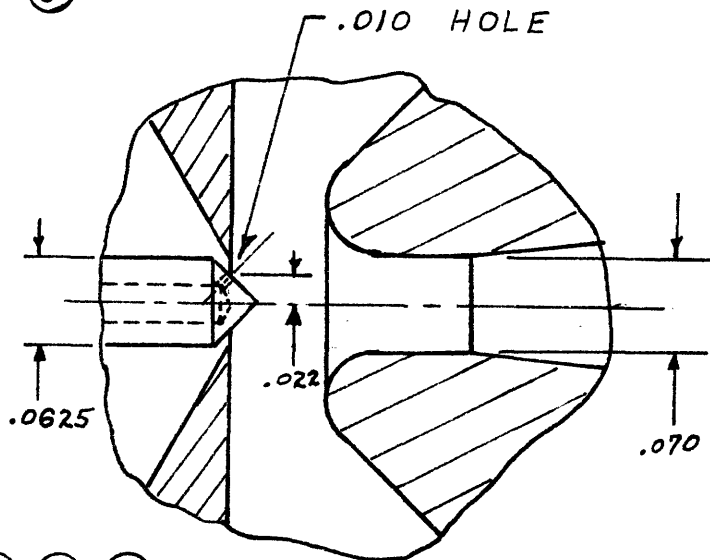
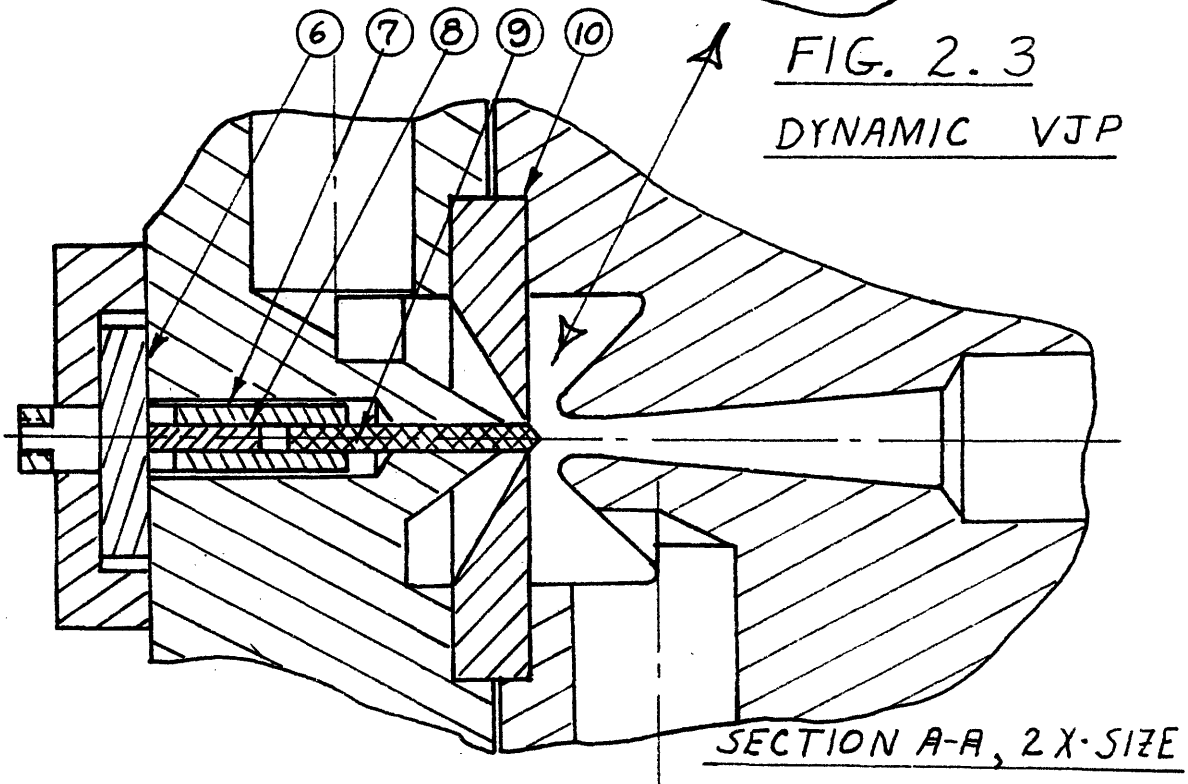


FIG. 2.3  
DYNAMIC VJP



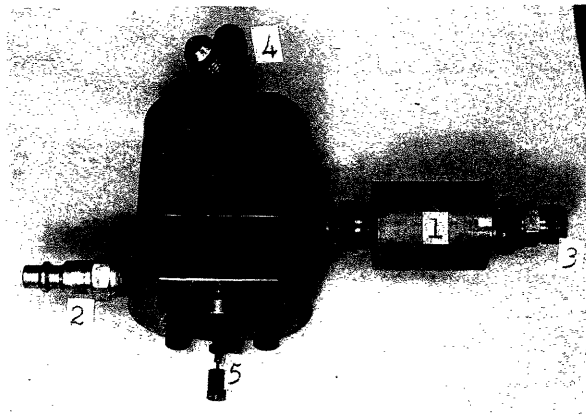


Fig. 2.4

Assembled Dynamic VJP

showing

- (1) check valve
- (2) supply port
- (3) exhaust port
- (4) load port
- (5) slider

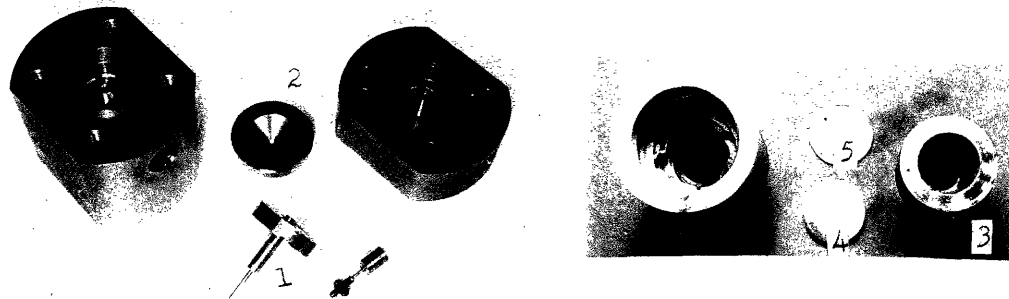


Fig. 2.5 Disassembled Dynamic VJP showing

- (1) nozzle plate
- (2) slider
- (3) check valve seat
- (4) check valve disk
- (5) dime

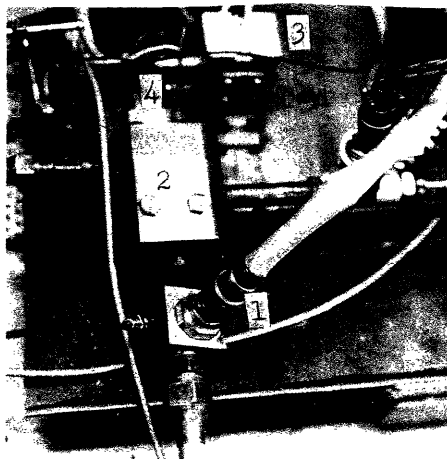


Fig. 2.7

Dynamic VJP Test Setup showing

- (1) dynamic load pressure transducer
- (2) VJP
- (3) torque motor
- (4) torque motor position transducer

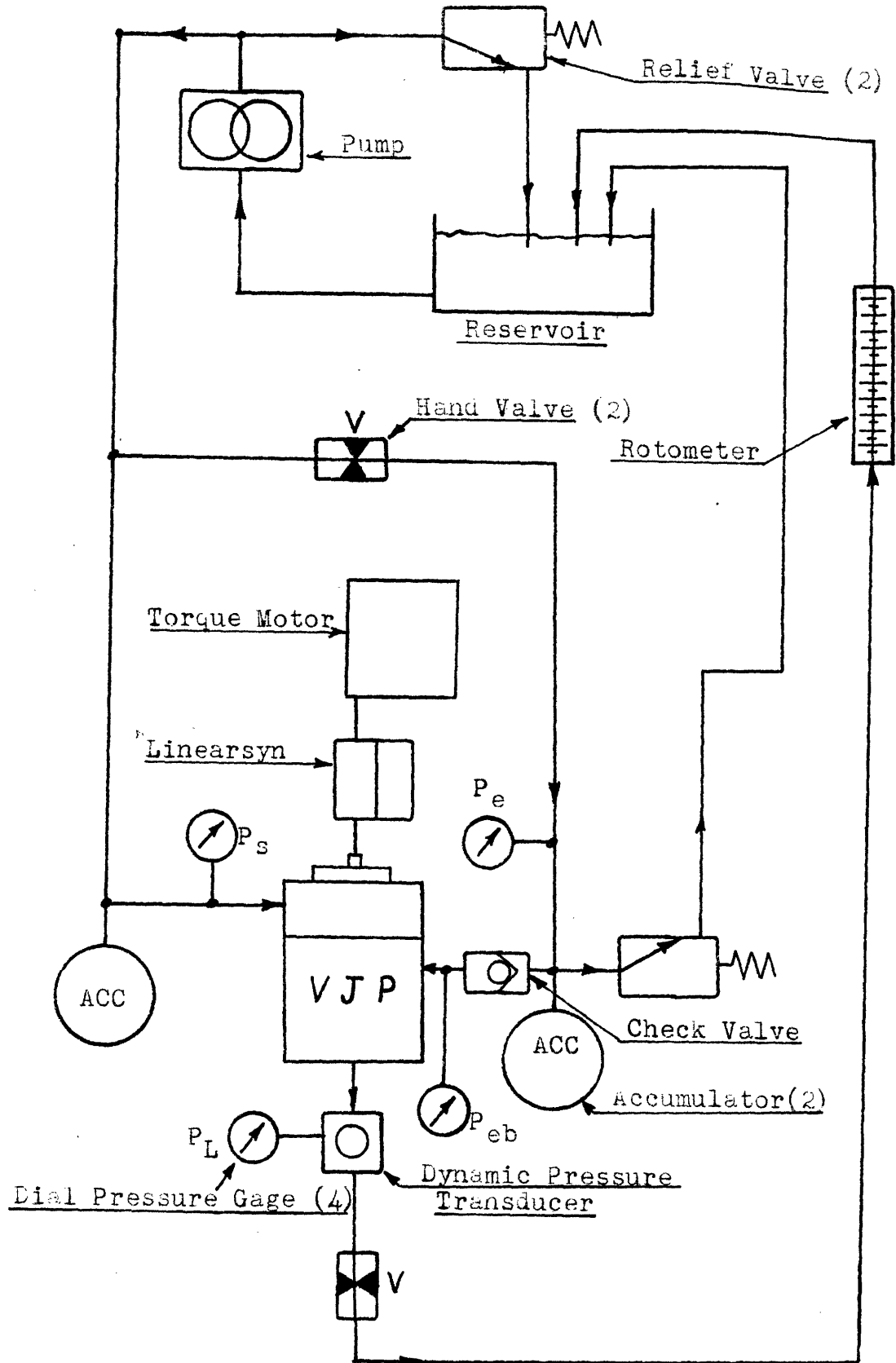


FIG. 2.6 Pictorial of VJP Dynamic Test Apparatus



DYNAMIC CORRELATION OF CONE POSITION (X) & OUTPUT PRESSURE (P<sub>e</sub>)

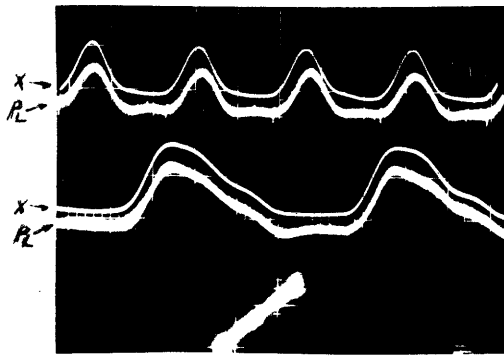


FIG. 2.8a Induced flow  
 $P_s = 1240 \text{ psig}$ ,  $P_e = 220 \text{ psig}$ ,  $\bar{P}_e = 290 \text{ psig}$   
 $\bar{Q}_s = .3 \text{ gpm}$ ,  $\bar{Q}_e = 1.2 \text{ gpm}$ , upper 200cps  
 middle 100cps, lower 30cps

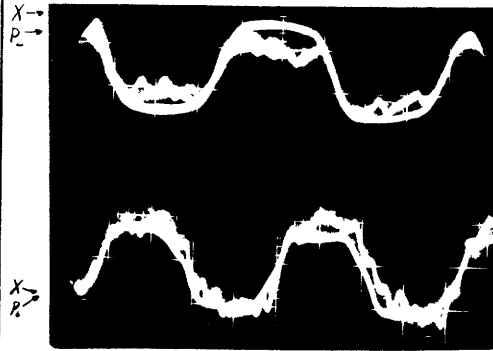


FIG. 2.9a Choked flow  
 $P_s = 1240 \text{ psig}$ ,  $P_e = 220 \text{ psig}$ ,  $\bar{P}_e = 220 \text{ psig}$   
 $\bar{Q}_s = .7 \text{ gpm}$   
 upper 50cps lower 100cps

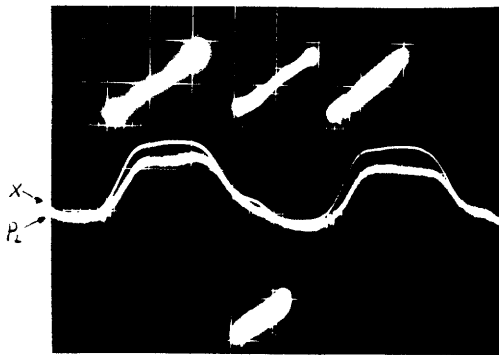


FIG. 2.8b Induced flow  
 $P_s = 1240 \text{ psig}$ ,  $P_e = 220 \text{ psig}$ ,  $\bar{P}_e = 320 \text{ psig}$   
 $\bar{Q}_s = .66 \text{ gpm}$ ,  $\bar{Q}_e = 1.4 \text{ gpm}$ , upper left 20cps  
 upper center 50cps, upper right 100cps  
 middle 100cps, lower 200cps

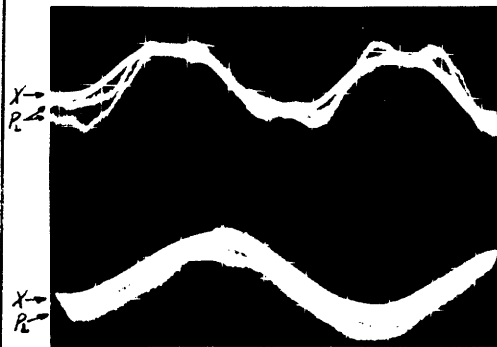


FIG. 2.9b Choked flow  
 $P_s = 1240 \text{ psig}$ ,  $P_e = 220 \text{ psig}$ ,  $\bar{P}_e = 220 \text{ psig}$   
 $\bar{Q}_s = .7 \text{ gpm}$   
 upper 200cps, lower 300cps



FIG. 2.8c Induced flow  
 $P_s = 1240 \text{ psig}$ ,  $P_e = 220 \text{ psig}$ ,  $\bar{P}_e = 455 \text{ psig}$   
 $\bar{Q}_s = 1.35 \text{ gpm}$ ,  $\bar{Q}_e = 2.2 \text{ gpm}$ , lower 200cps  
 middle 200cps, upper left 20cps  
 upper center 50cps, upper right 100cps

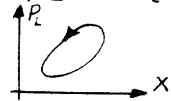


FIG. 2.10 Choked flow  
 $P_s = 1240 \text{ psig}$ ,  $P_e = 220 \text{ psig}$ ,  $\bar{P}_e = 220 \text{ psig}$   
 $\bar{Q}_s = .7 \text{ gpm}$  300cps without  
 filter on P<sub>e</sub> transducer.

DYNAMIC CORRELATION OF CONE POSITION (X) & OUTPUT PRESSURE (P<sub>L</sub>) IN BLOCKED FLOW CONDITION

FIG. 2.11

(LISSAJOU FIGURES



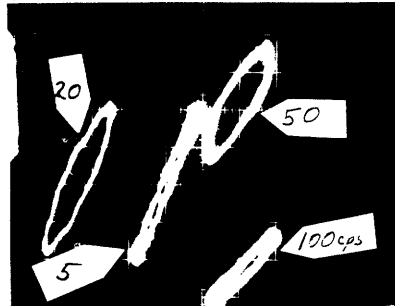
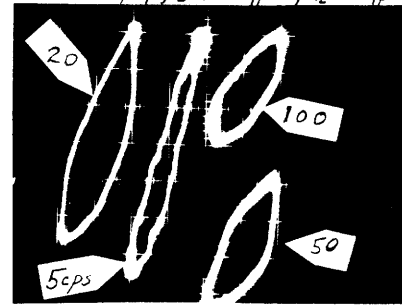
) FIG. 2.12

FIG. 2.11 • P<sub>s</sub> = 1240 psig, P<sub>L</sub> = 500 psig, Q̄ = 0.66 gpm

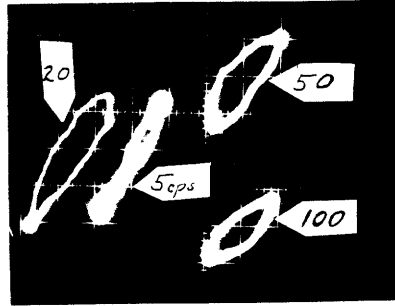
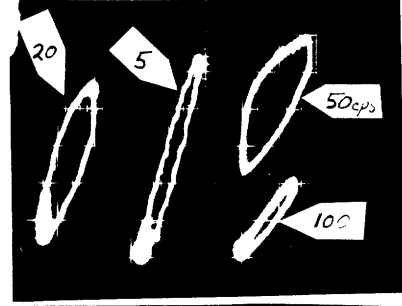
FIG. 2.12 • P<sub>s</sub> = 1240 psig, P<sub>L</sub> = 365 psig, Q̄ = 0.39 gpm



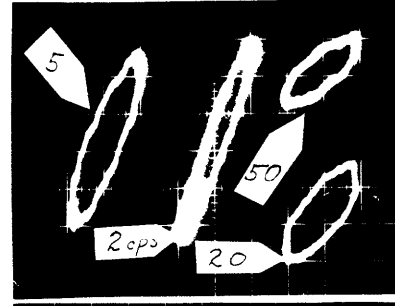
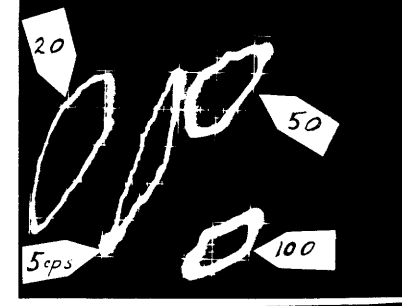
TRIAL #1  
1.2 in<sup>3</sup>



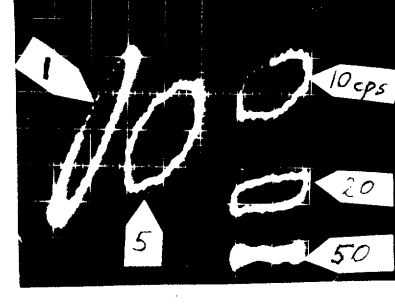
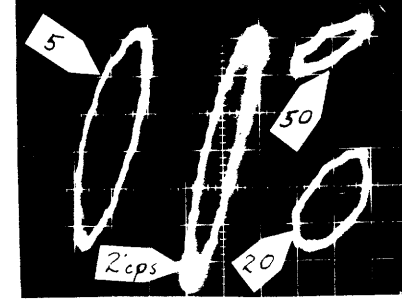
TRIAL #2  
2.0 in<sup>3</sup>



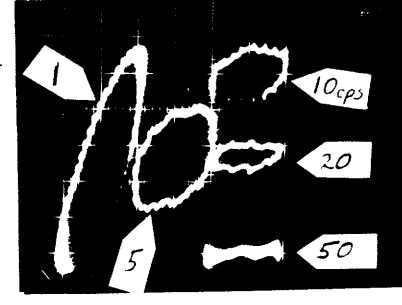
TRIAL #3  
4.6 in<sup>3</sup>

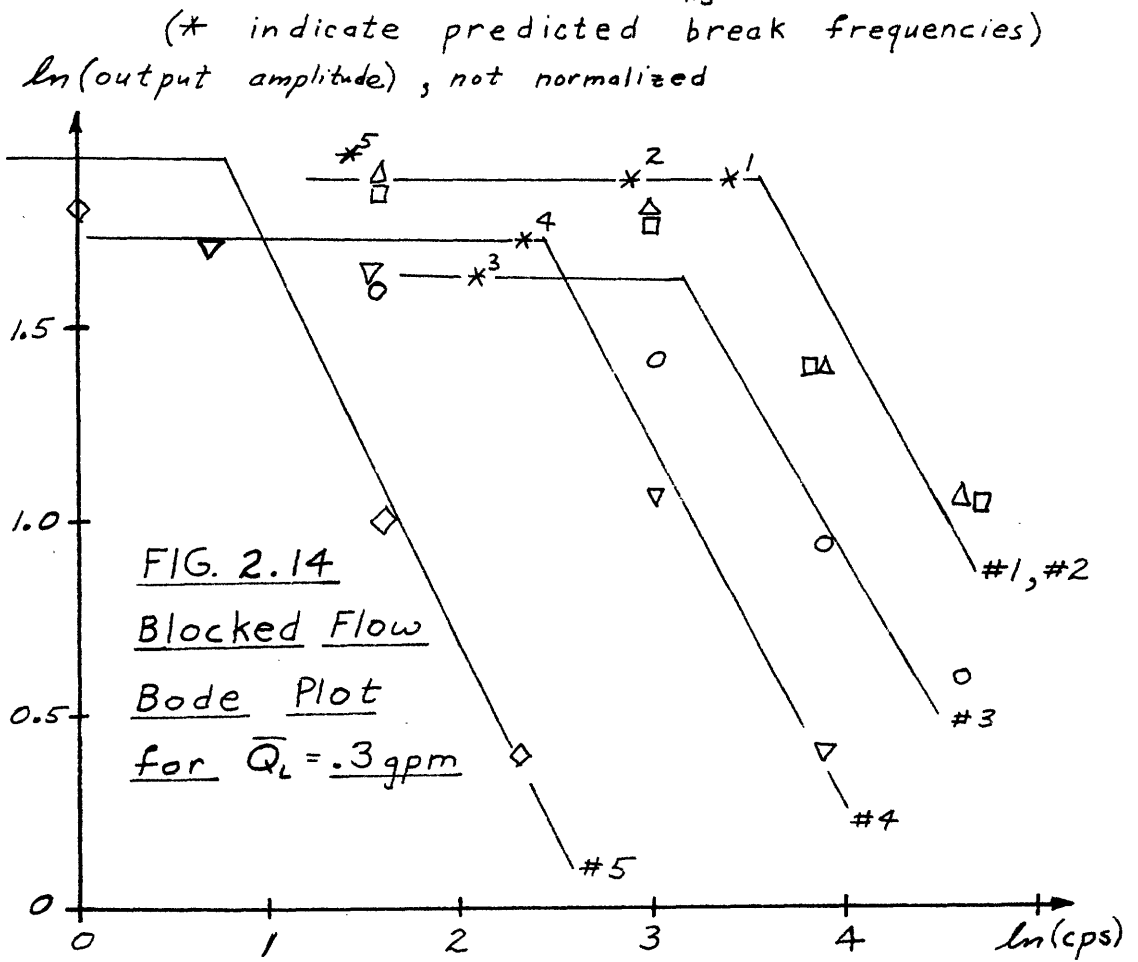
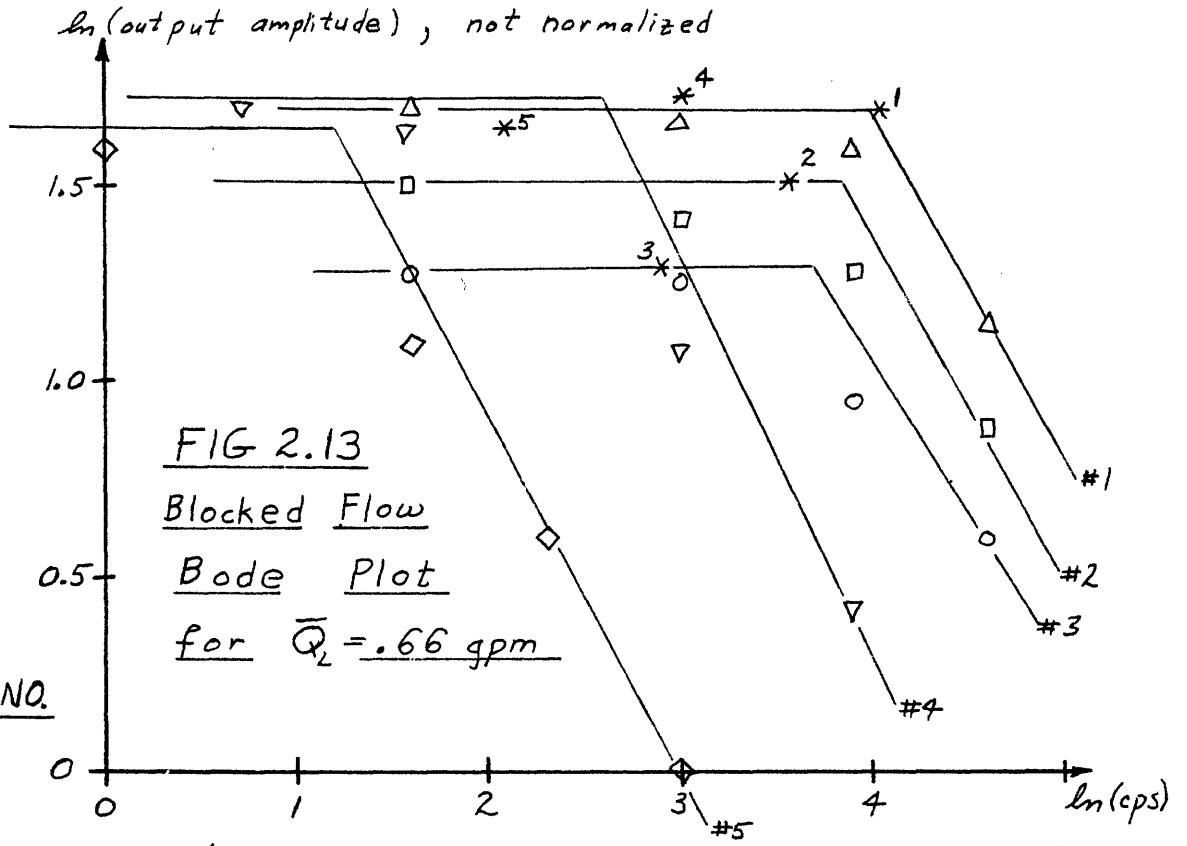


TRIAL #4  
3.4 in<sup>3</sup>  
(hose)



TRIAL #5  
8.5 in<sup>3</sup>  
(hose)





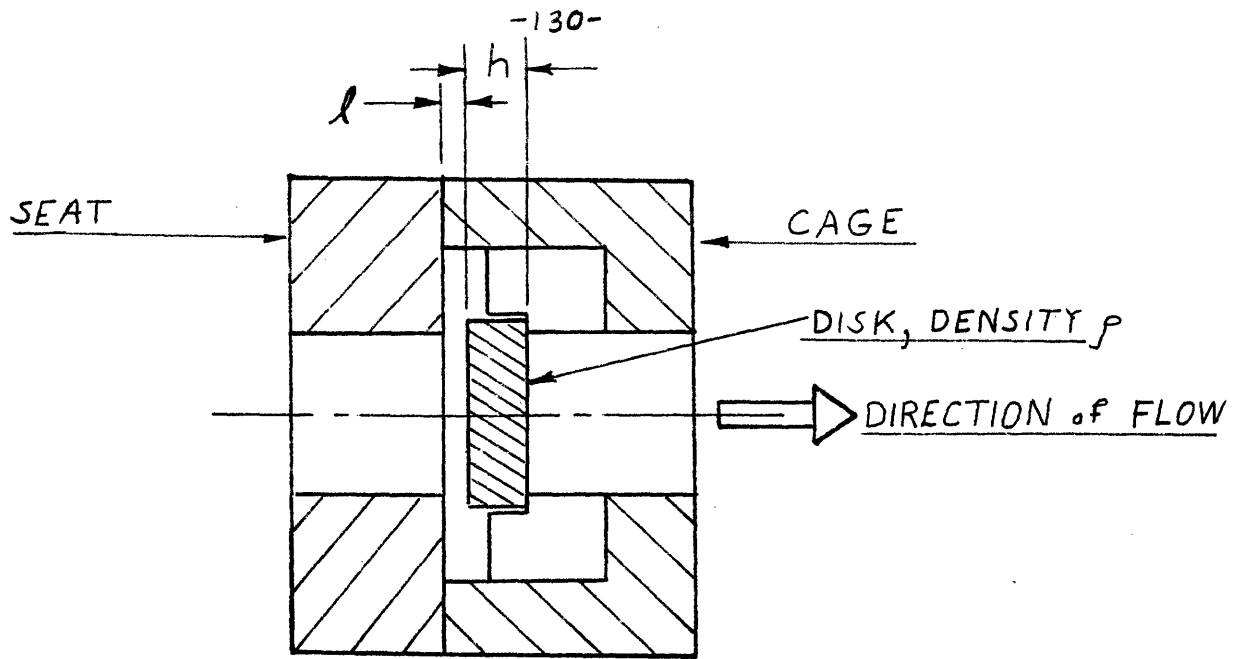


FIG. 2.15 Simplified Check Valve

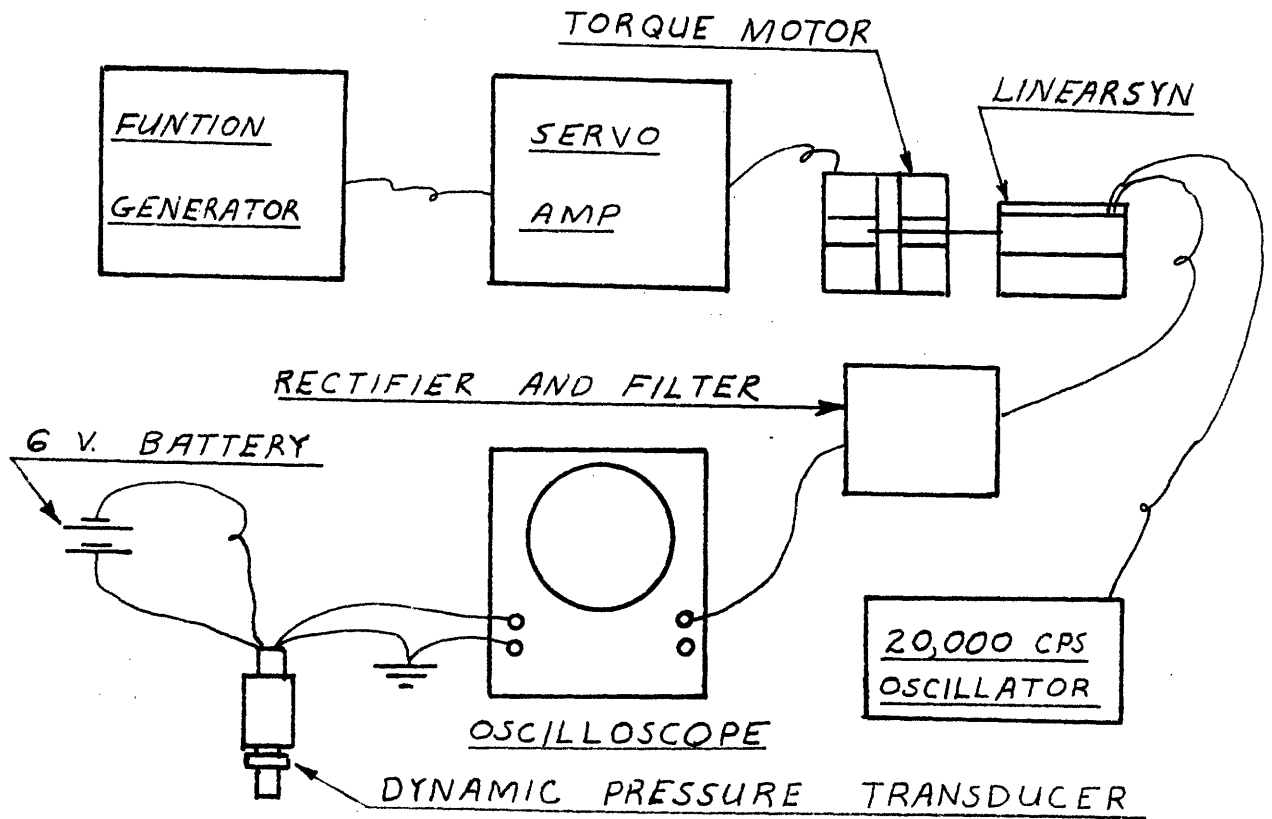
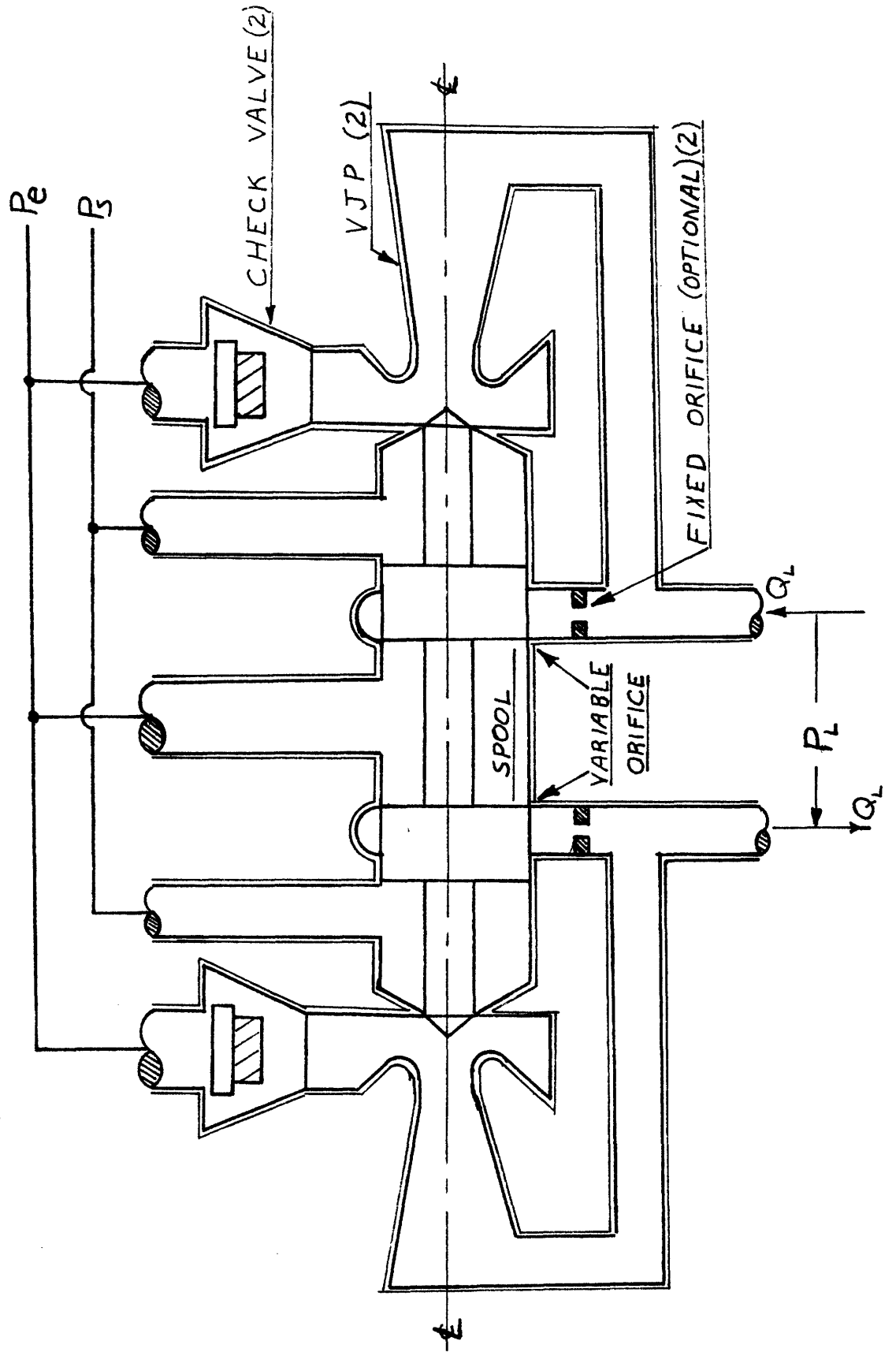


FIG. 2.16 Electronic Apparatus for Dynamic VJP Tests

FIG. 3.1 4-Way VJPV



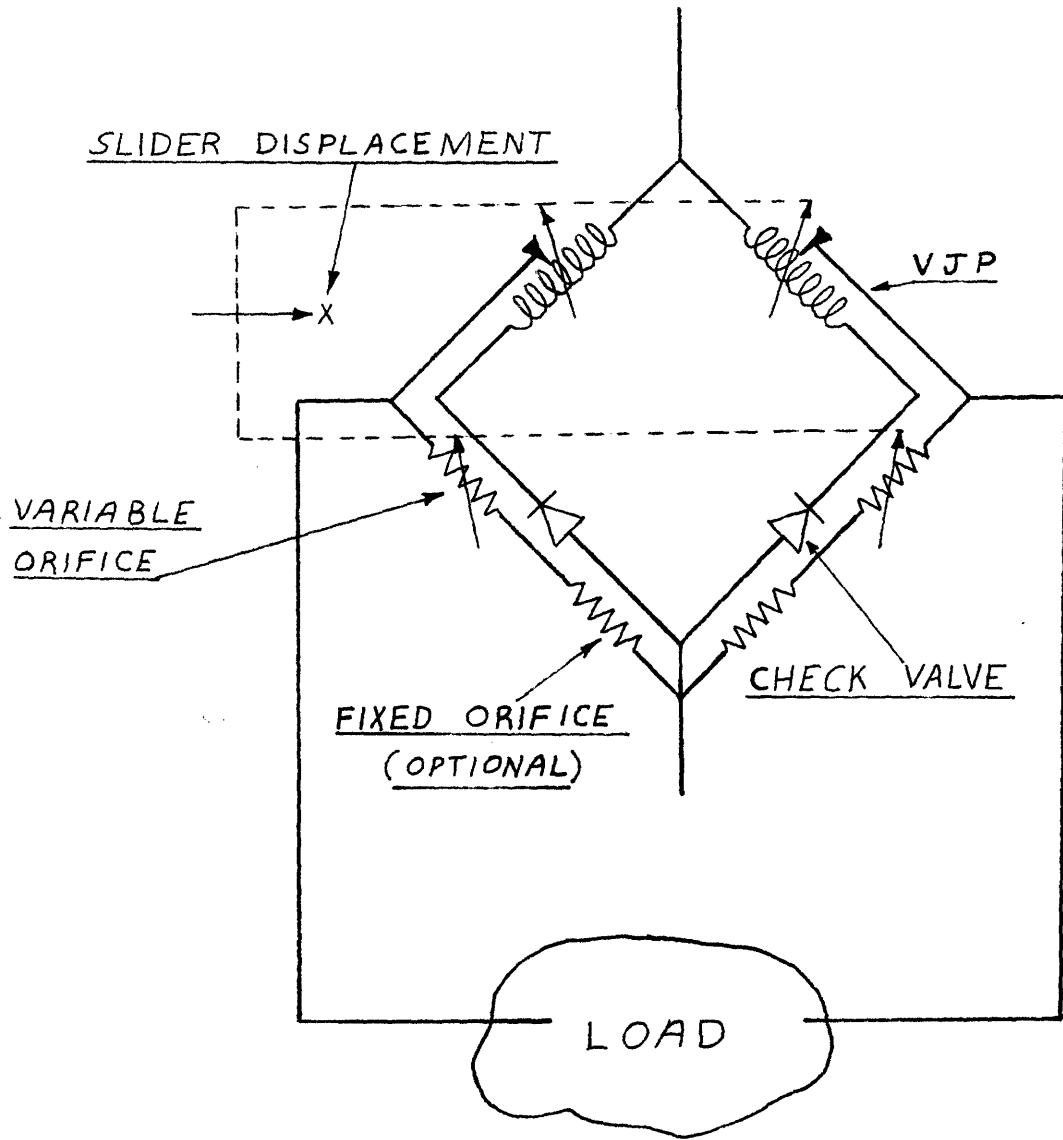
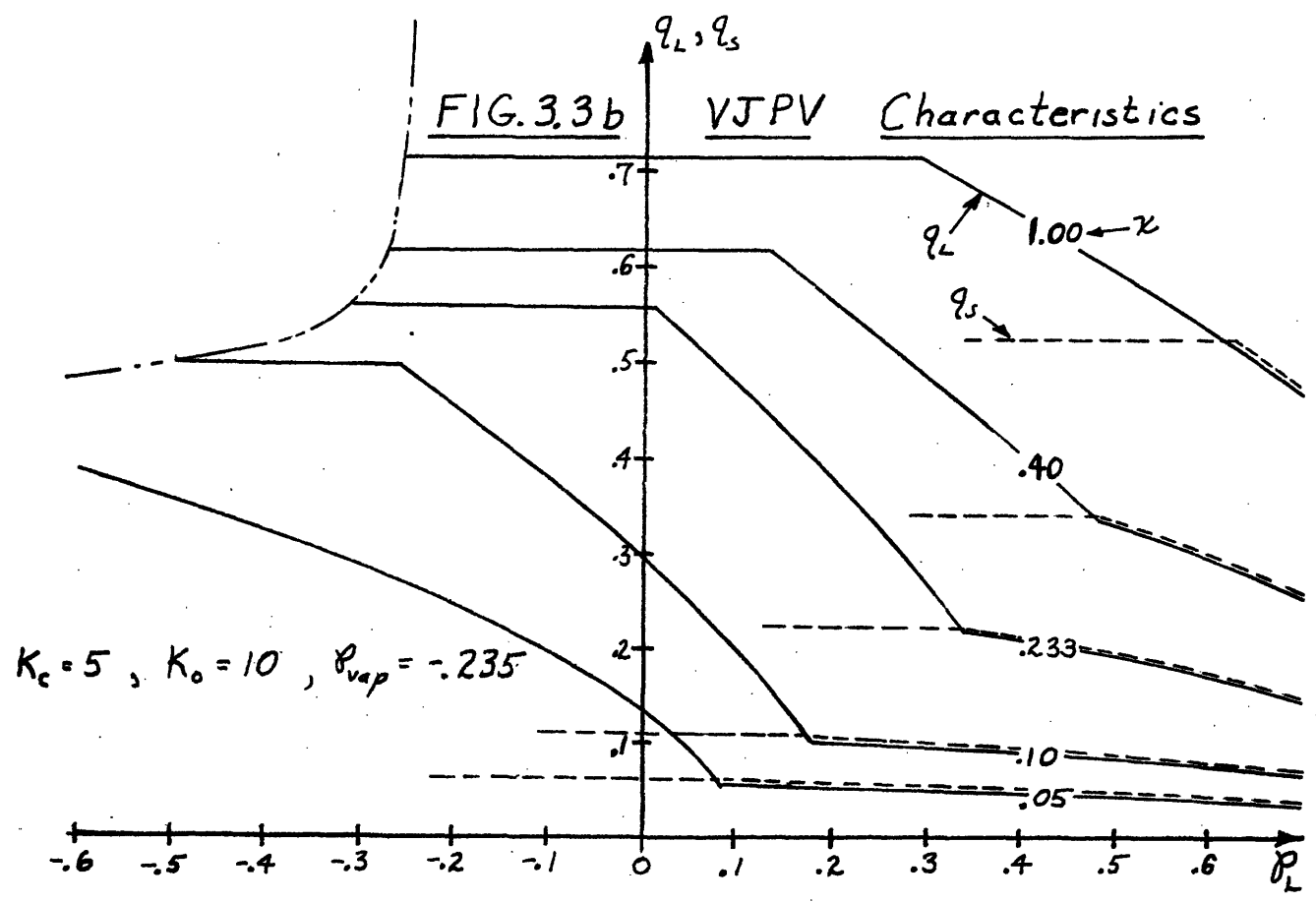
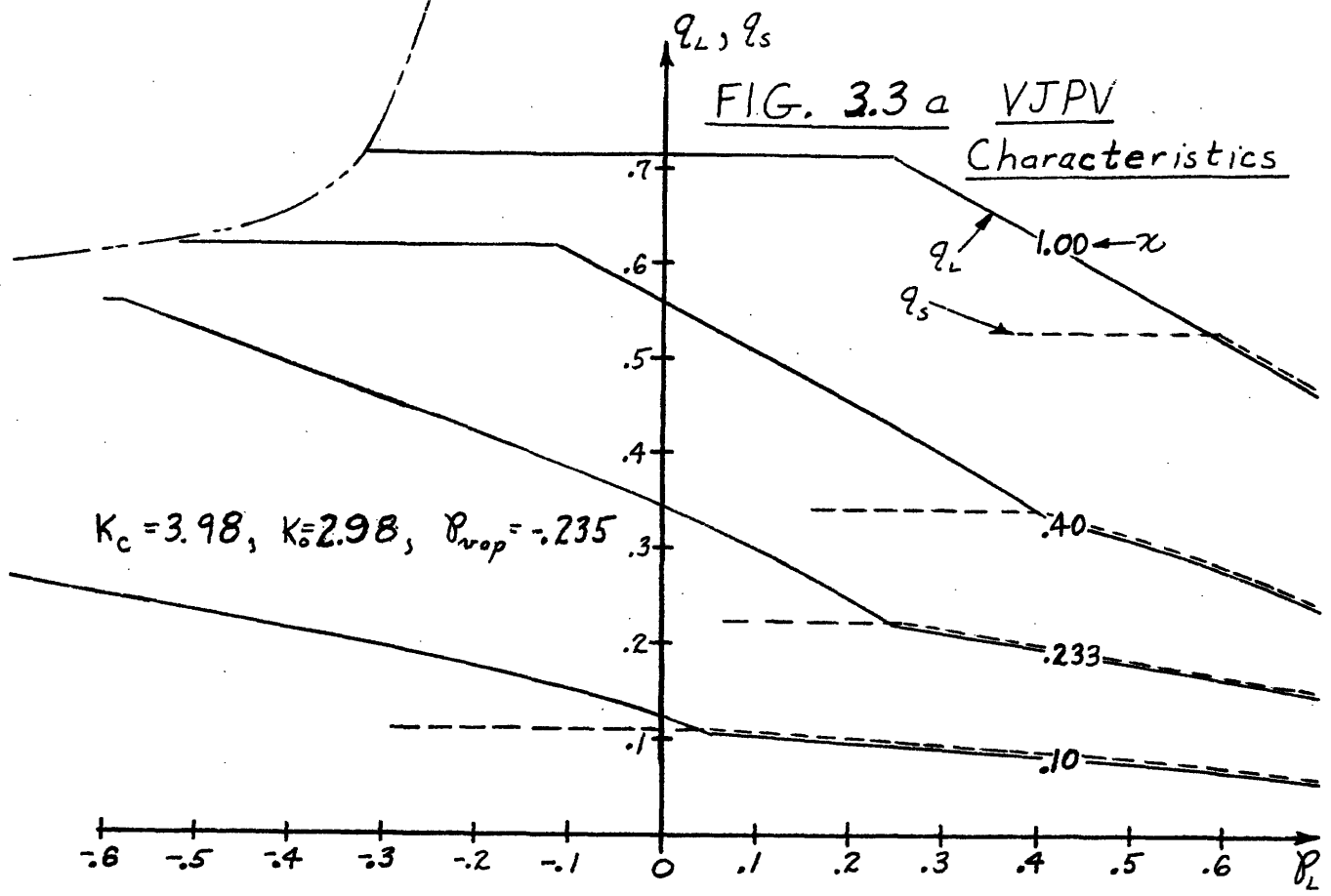


FIG. 3.2 Schematic of VJPV



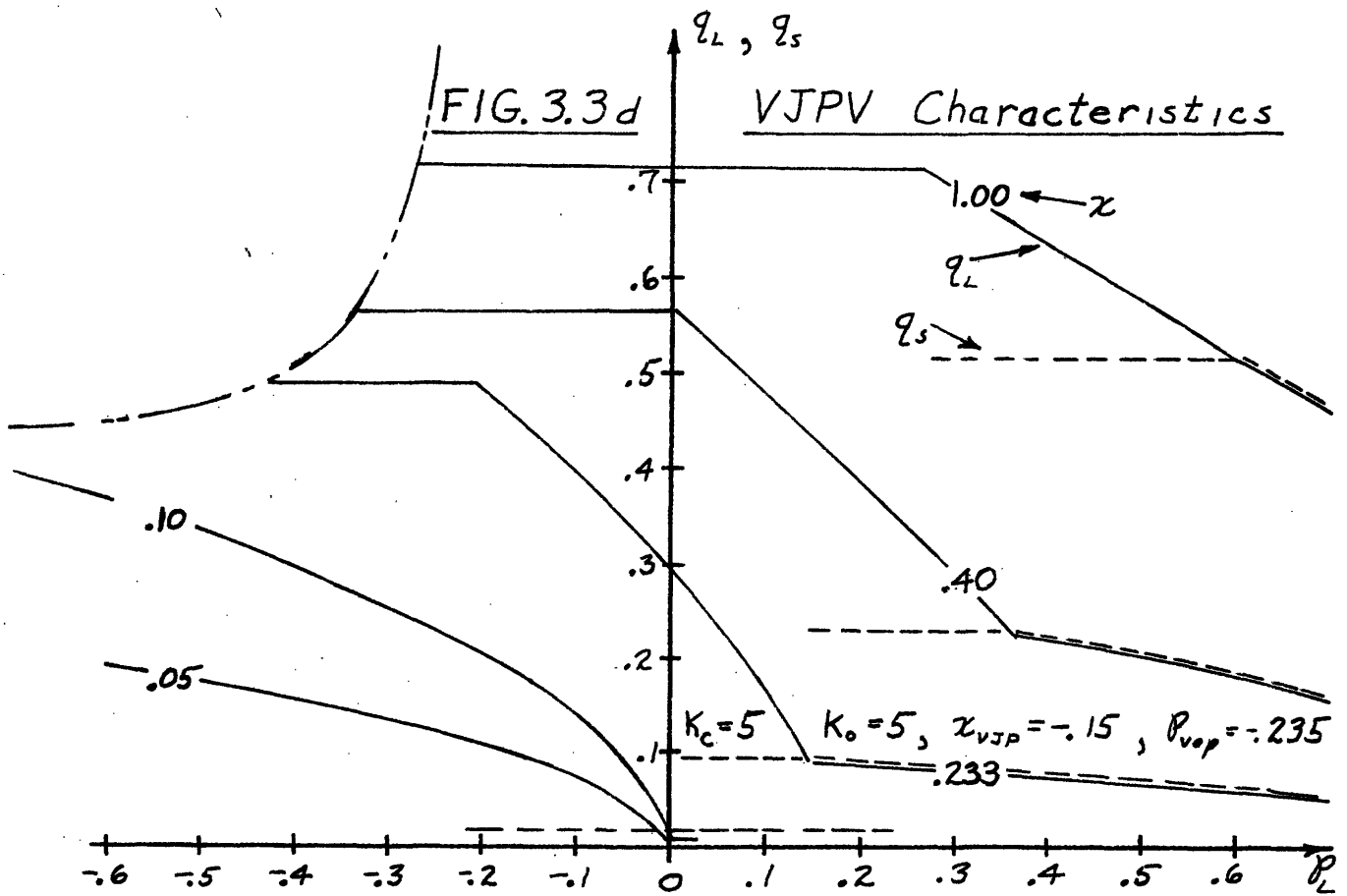
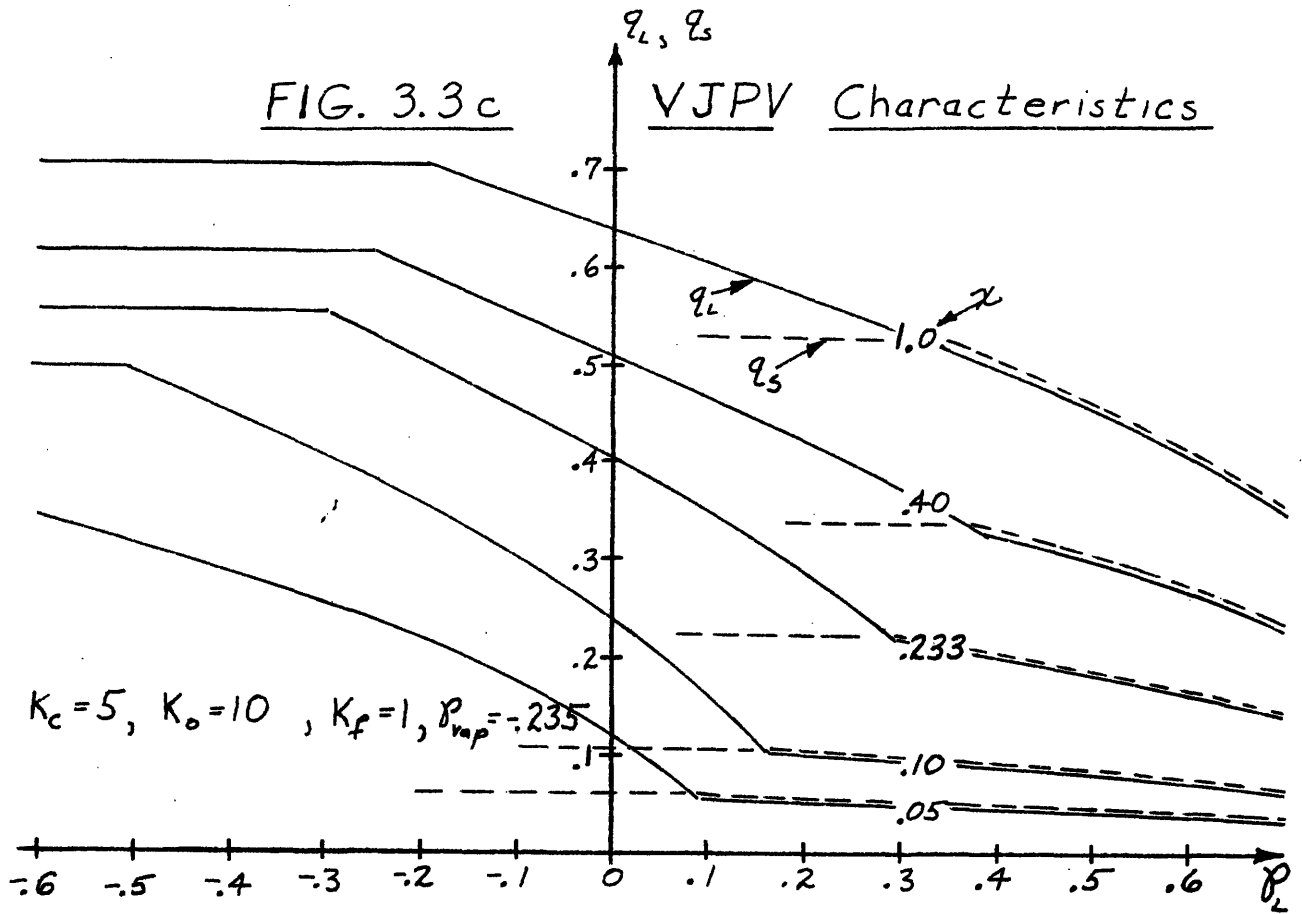




FIG. 3.3e

VJPV Characteristics

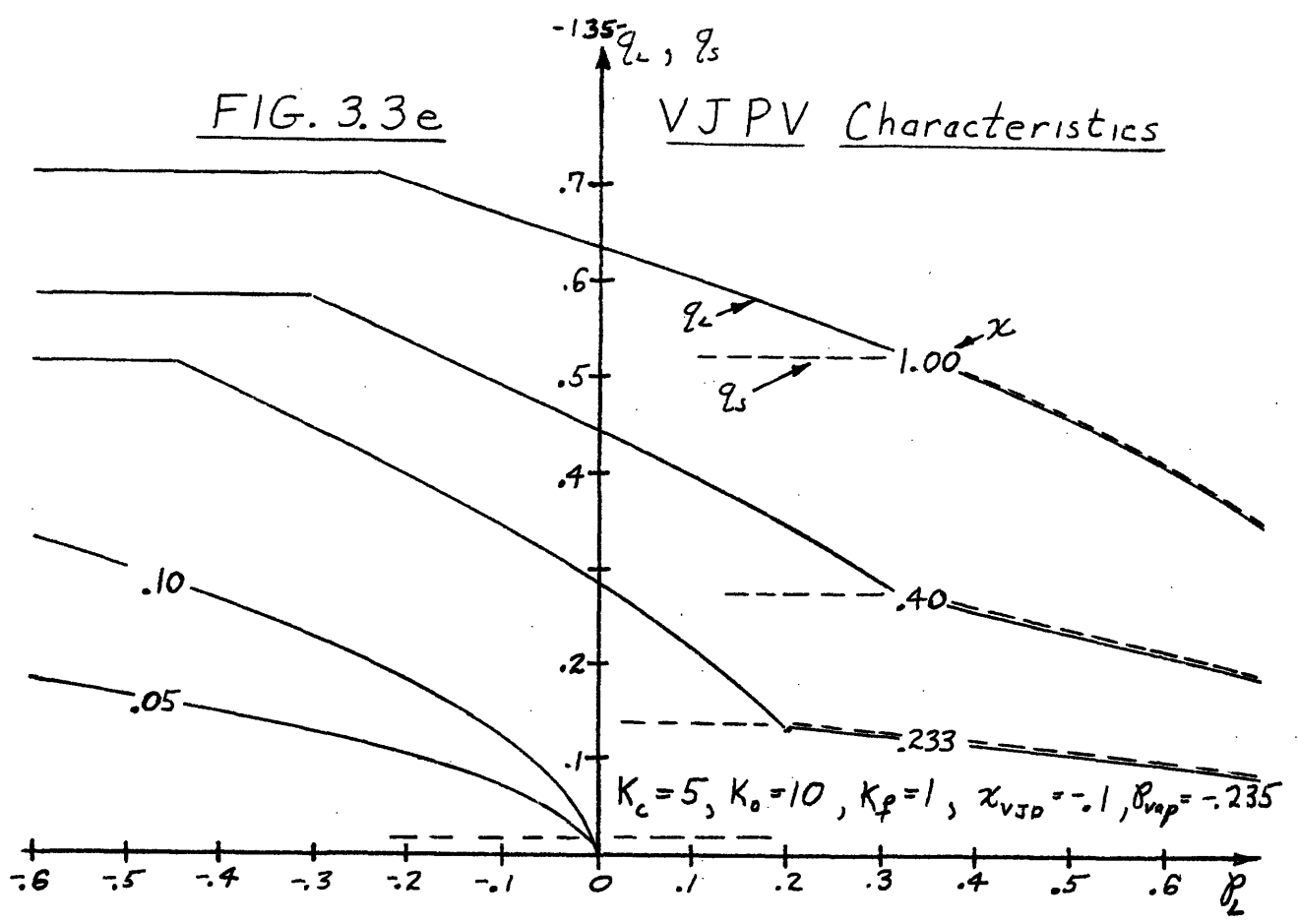
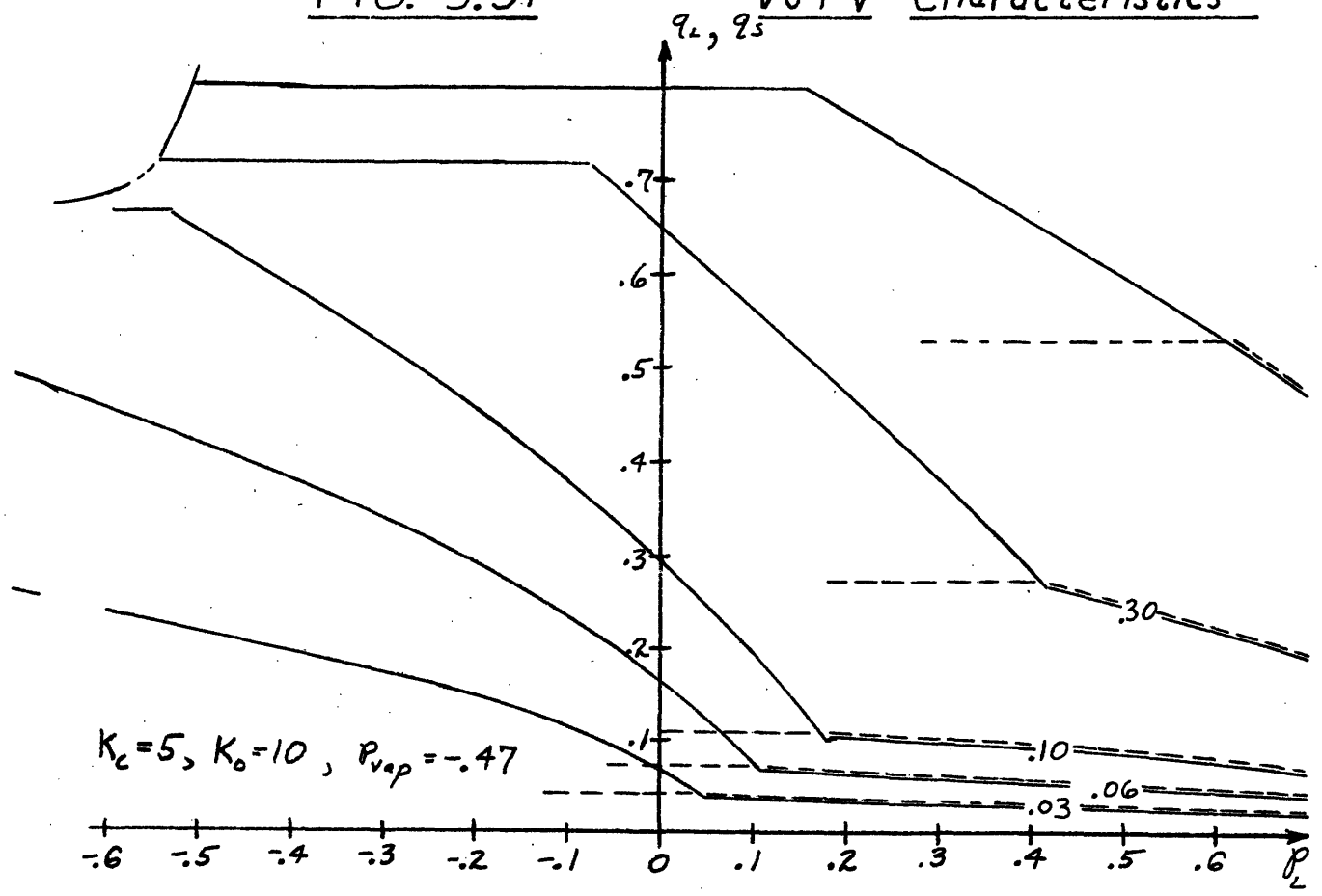


FIG. 3.3f

VJPV Characteristics



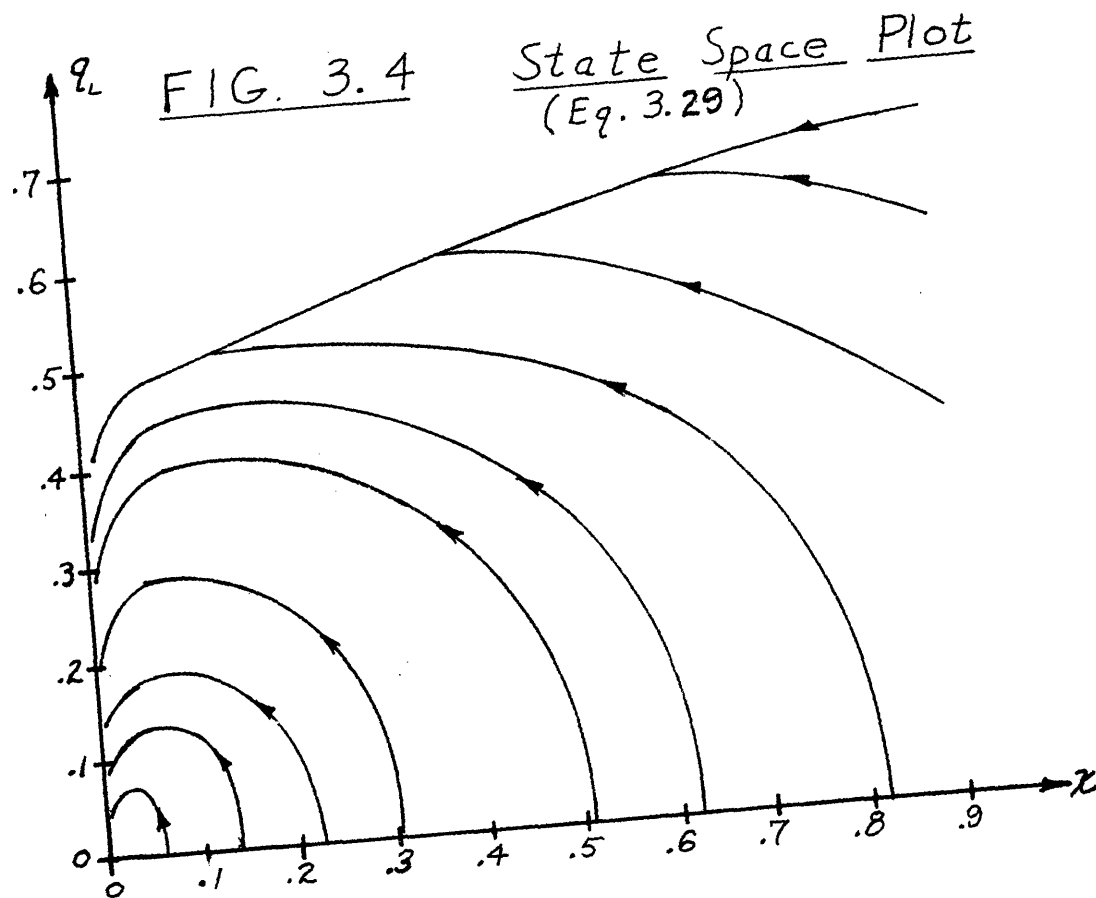
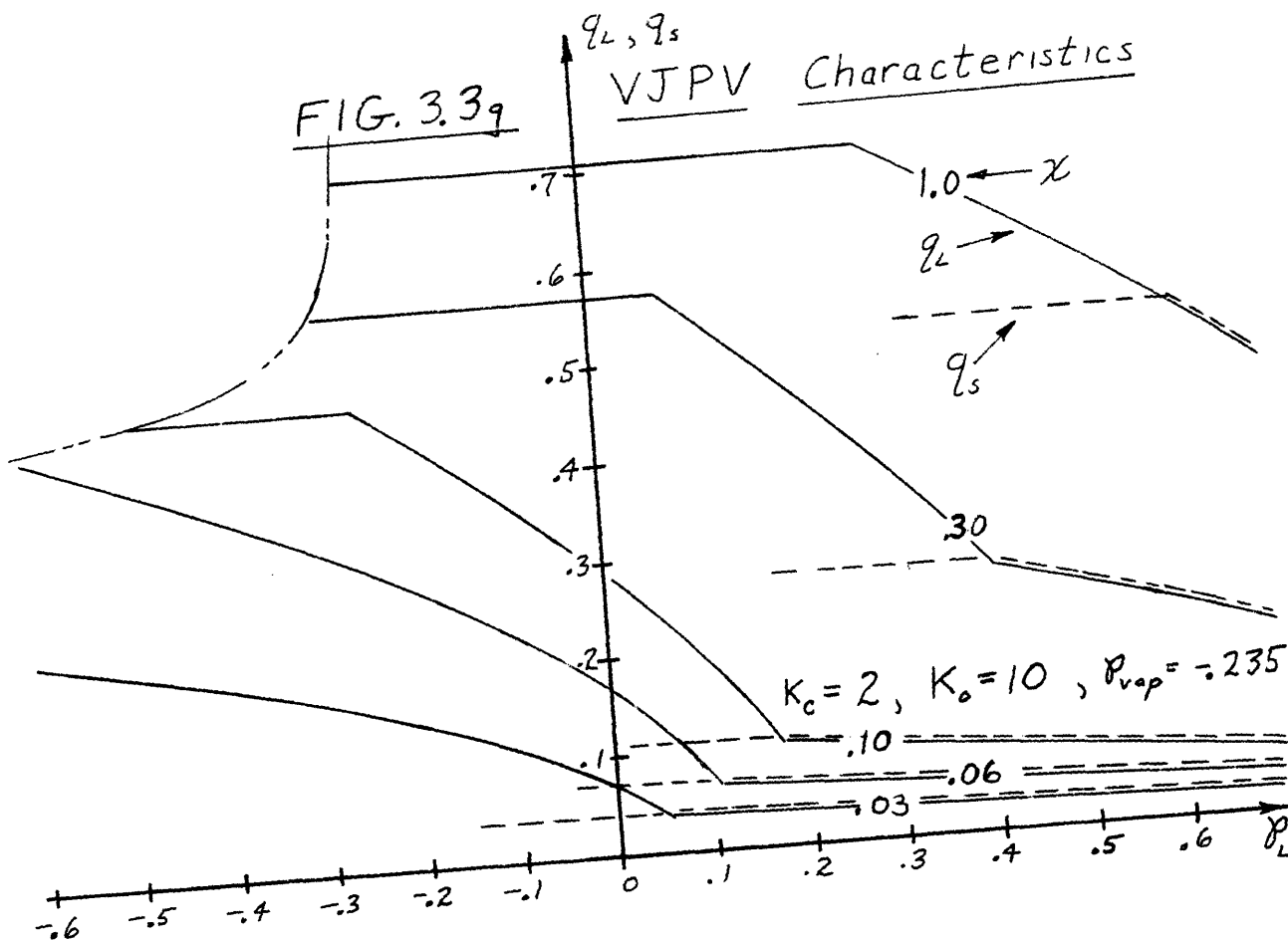


FIG. 4.1a

VJPV Relative Efficiency

$K_c = 3.98, K_o = 2.98, \nu_{vp} = -.235$

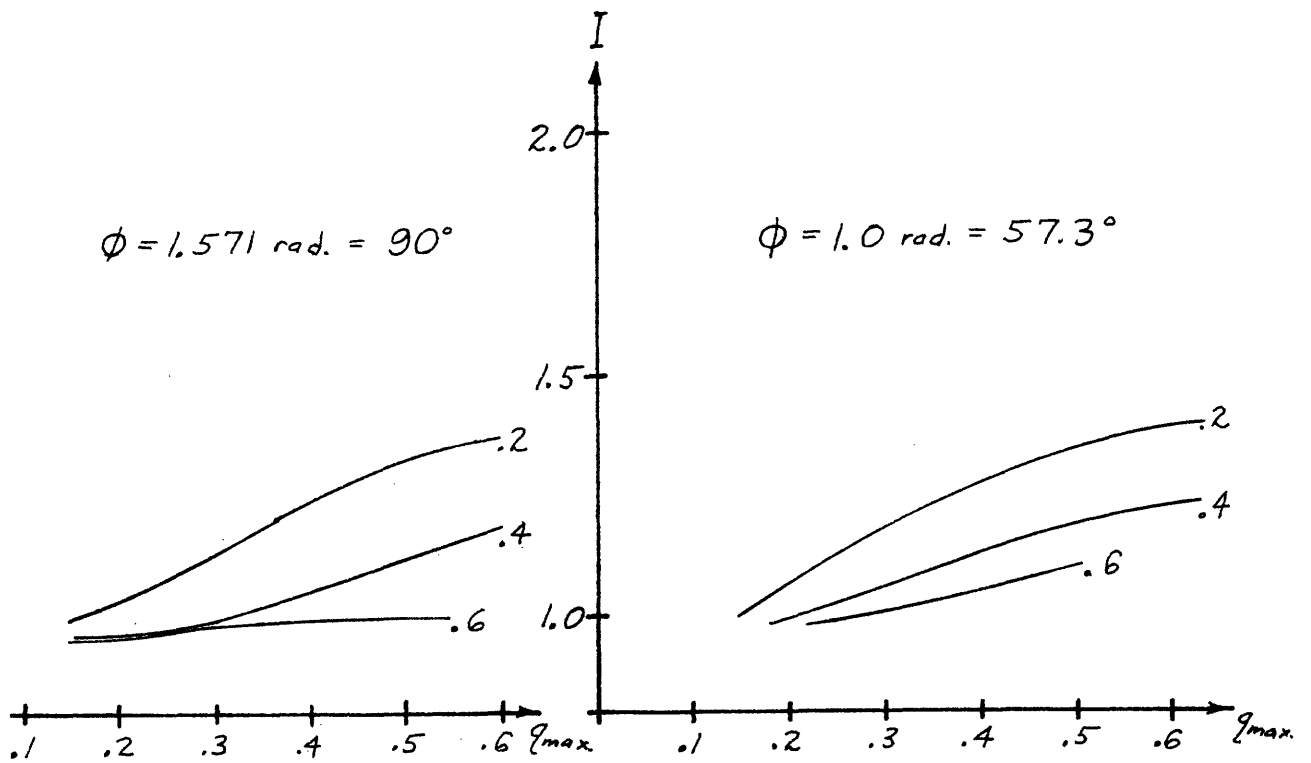
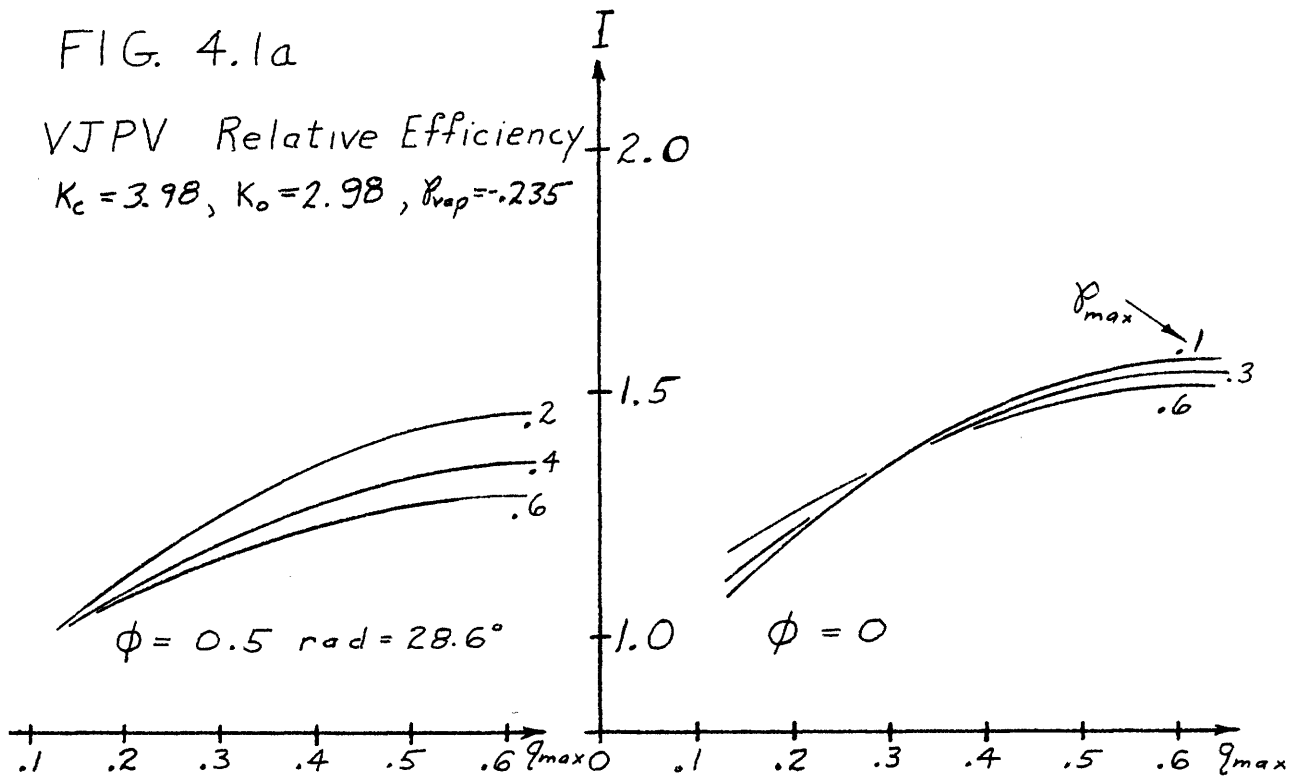


FIG. 4.1 b  
VJPV Relative Efficiency  
 $K_c = 5, K_o = 10, P_{vap} = -.235$

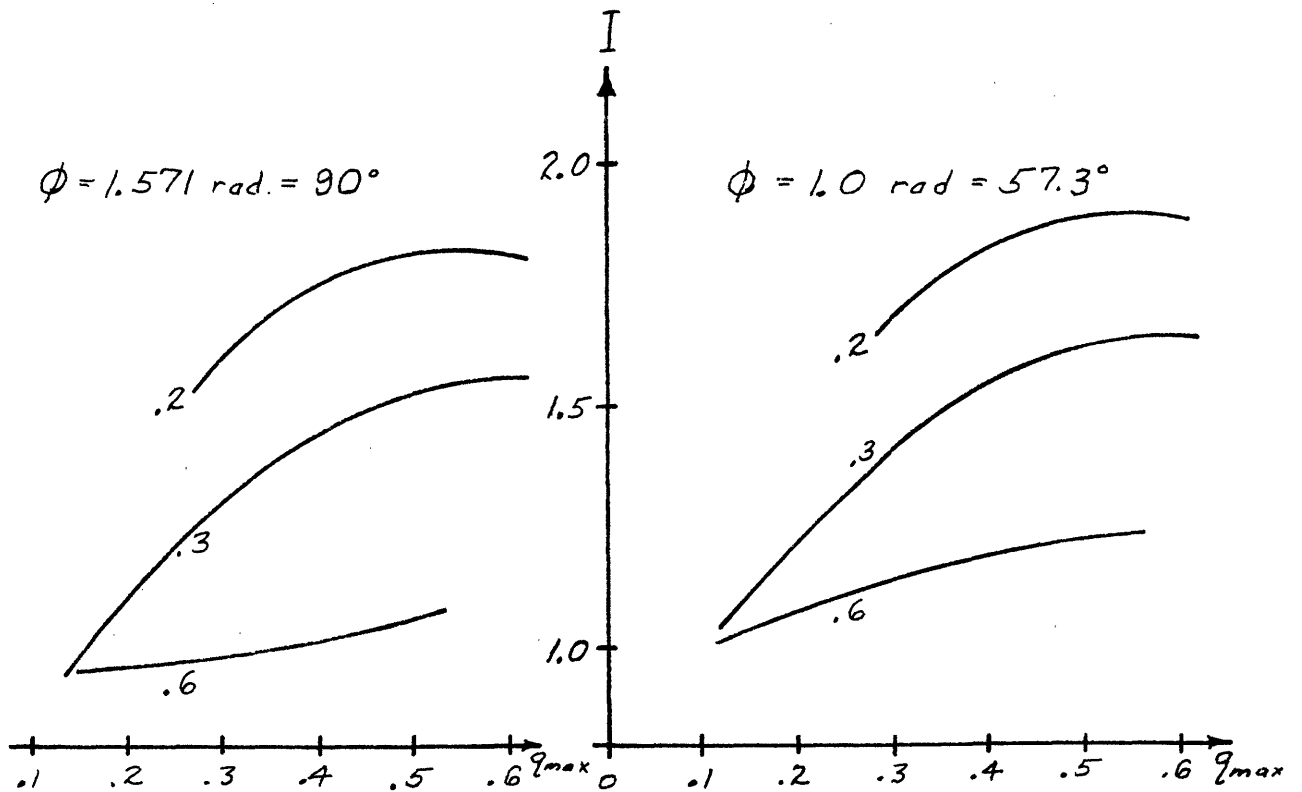
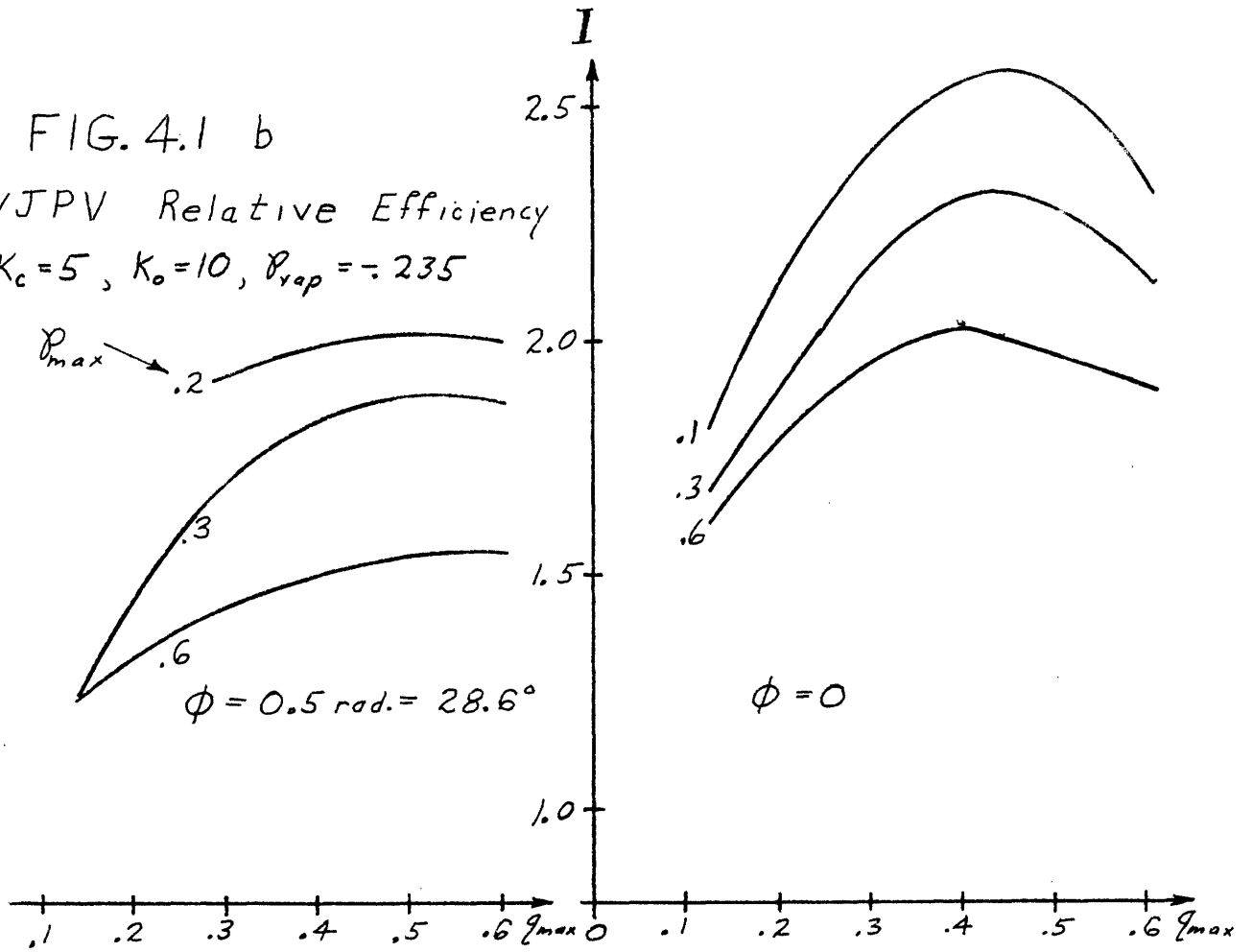


FIG. 4.1c  
VJPV Relative Efficiency

$K_o = 10, K_c = 5, K_p = 1, \rho_{vap} = .235$

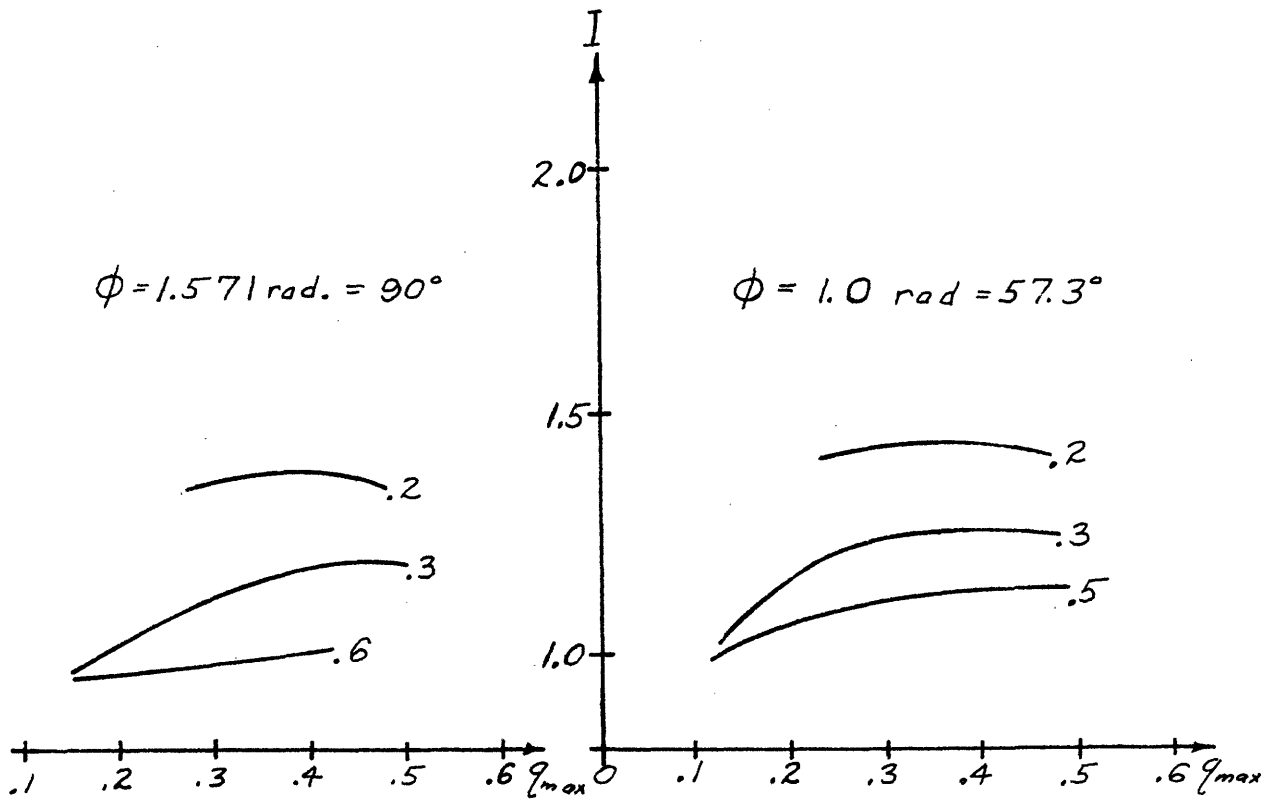
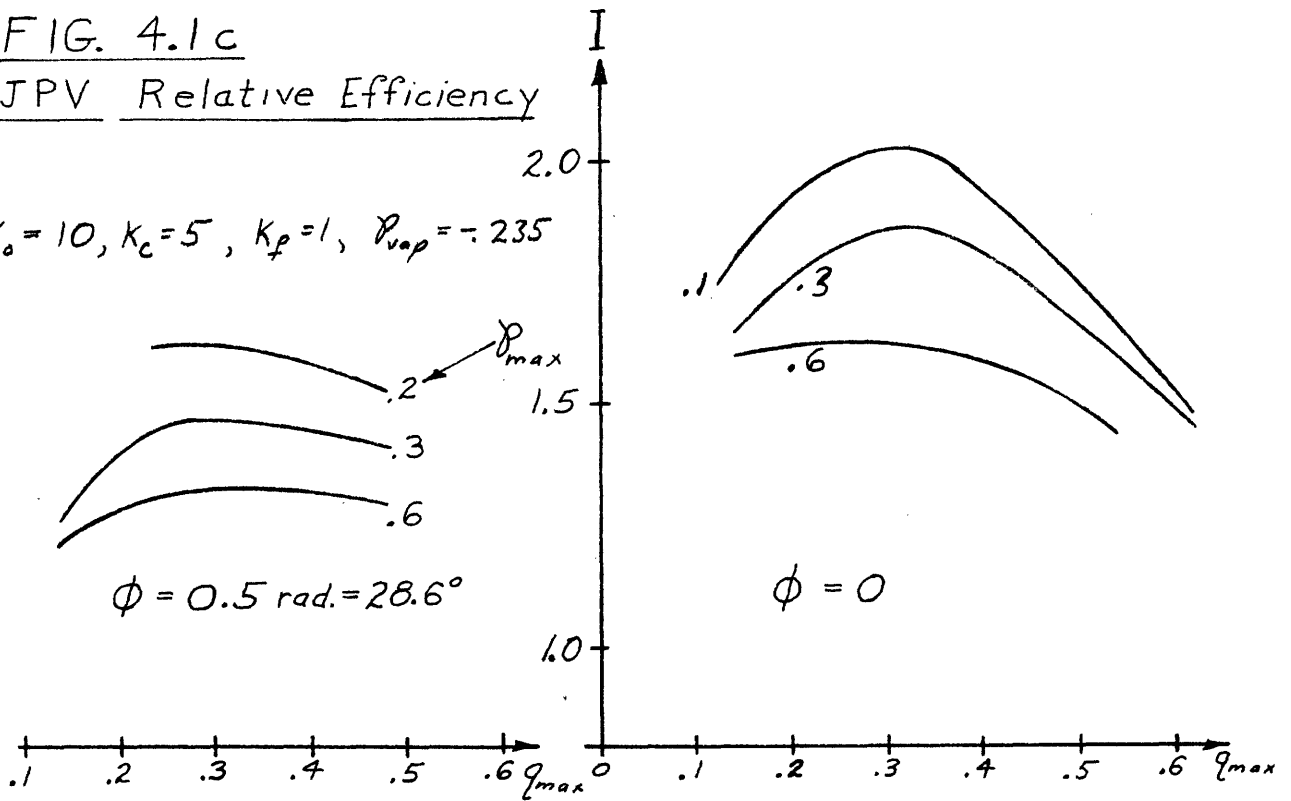


FIG. 4.1d

VJPV Relative Efficiency

$K_c = 5, K_o = 5, x_{VJP} = .15, \rho_{VJP} = -.235$

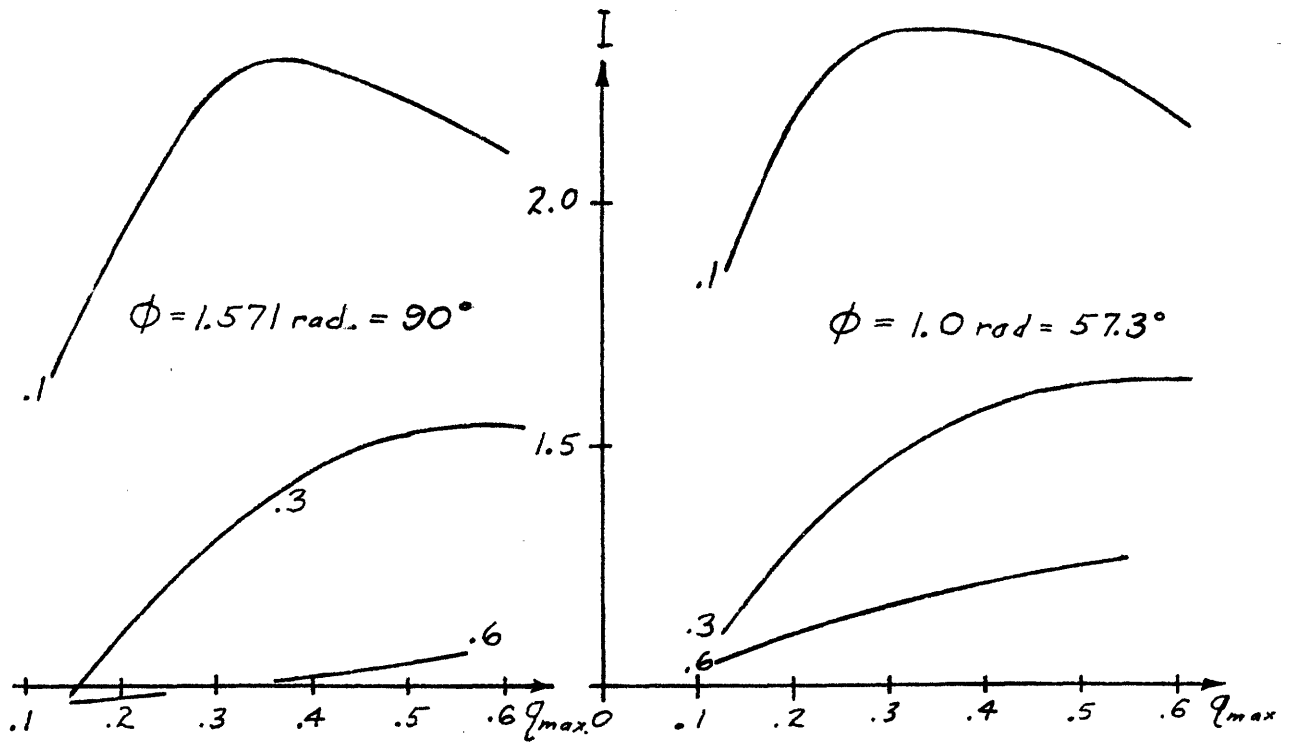
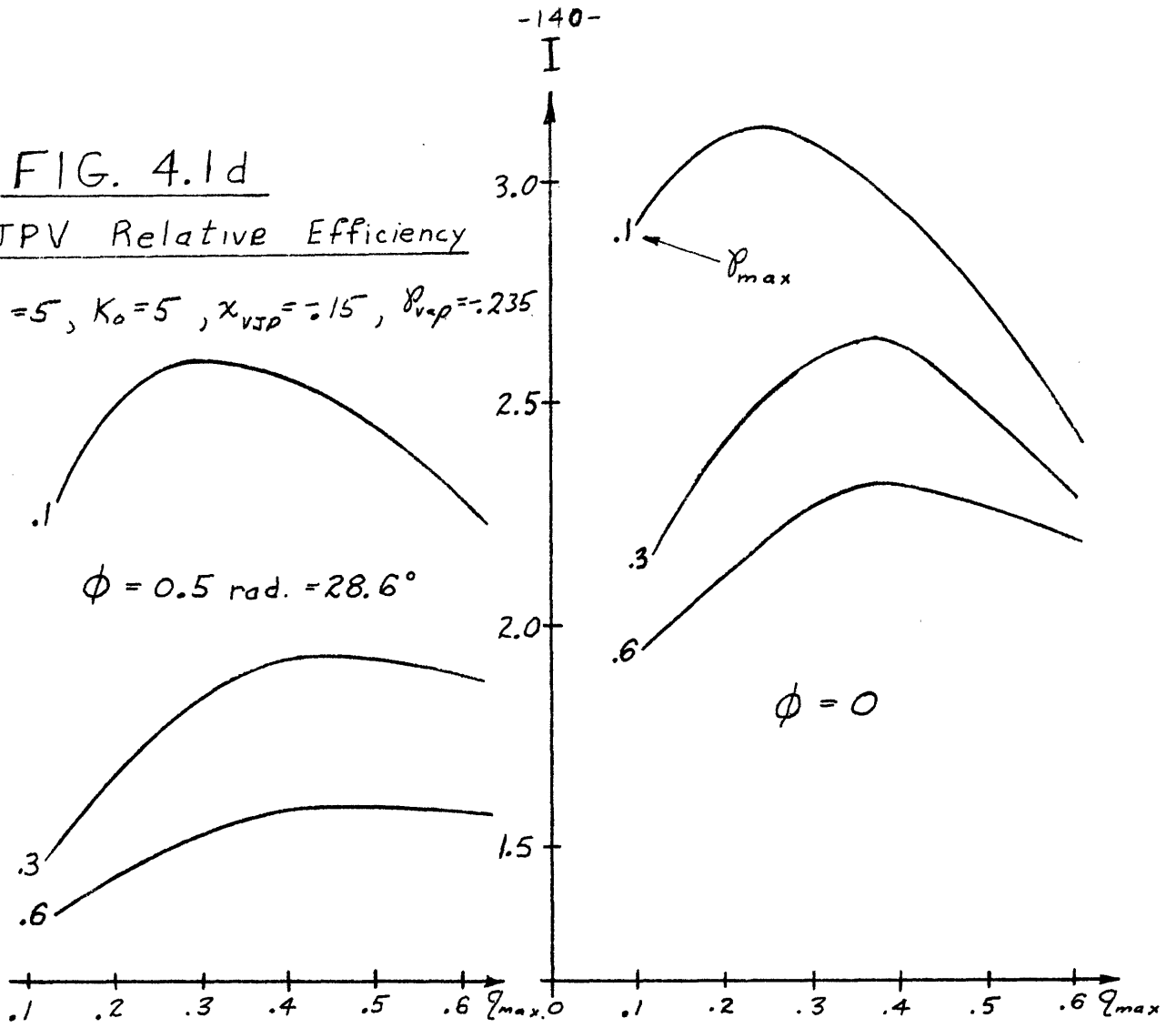


FIG. 4.2 d  
VJPV Relative Efficiency

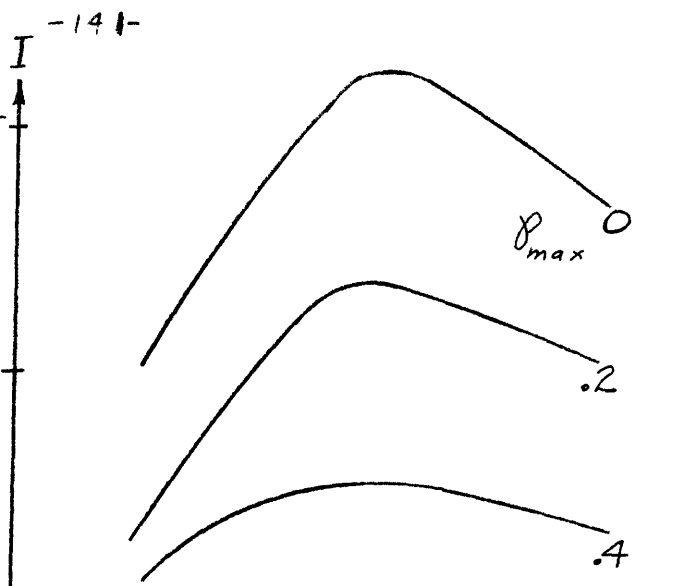
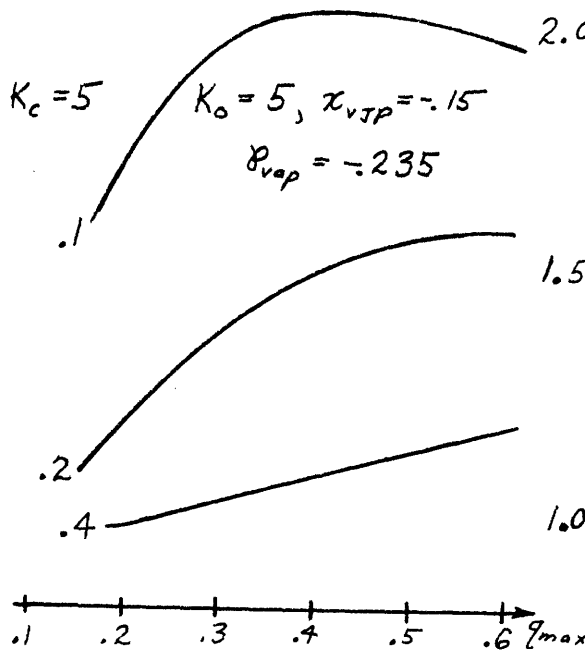
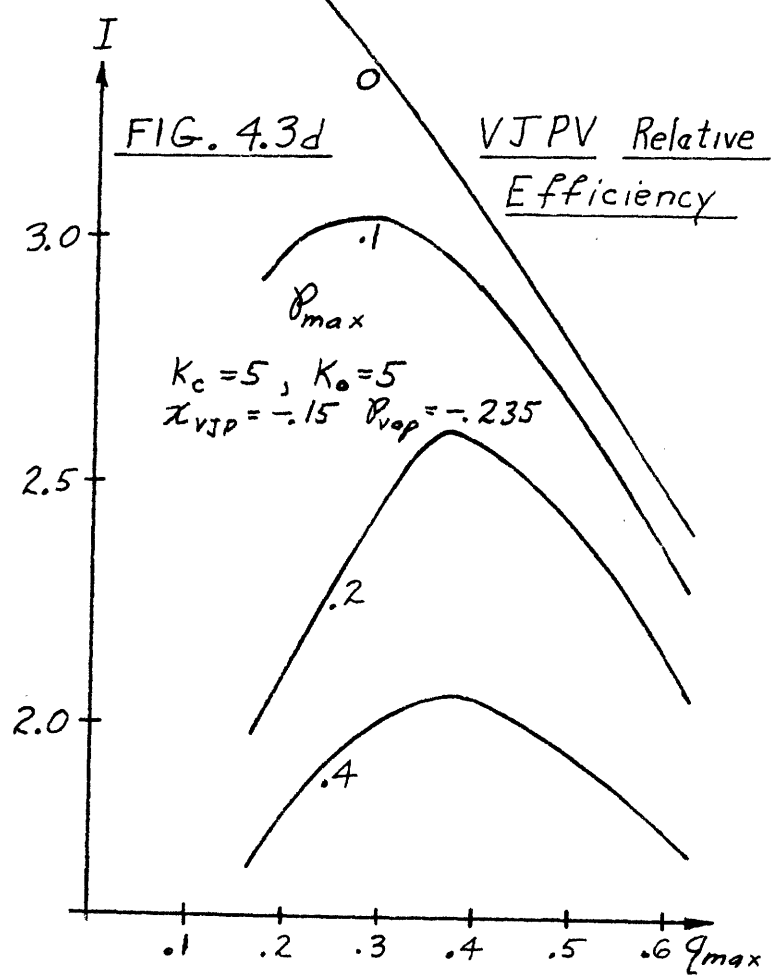


FIG. 4.3 b  
VJPV Relative Efficiency  
 $K_c = 5, K_o = 10, P_{vap} = -.235$

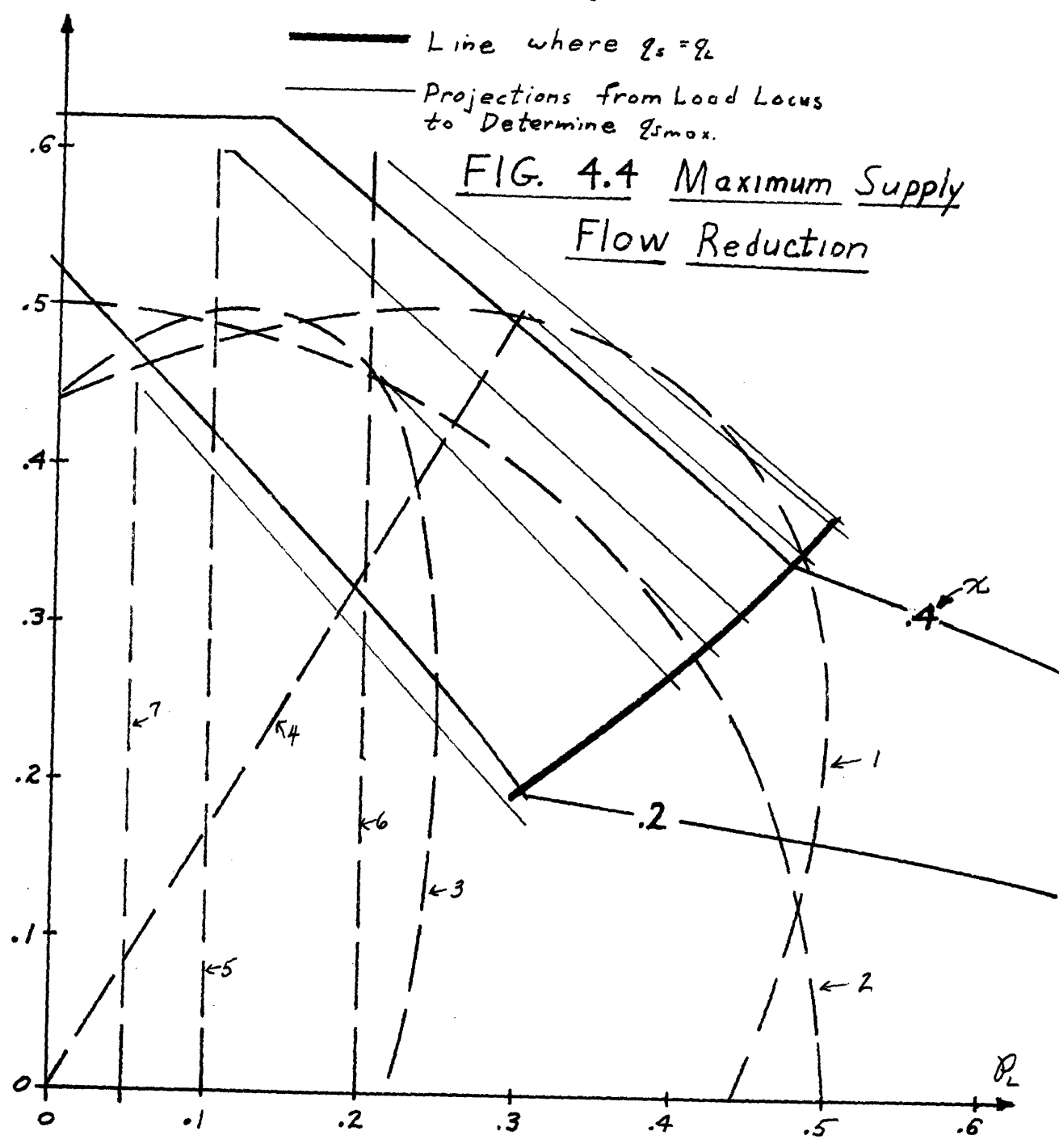


Locus No.	$P_m$	$q_m$	$\phi$	$q_{Lmax}$	$q_{Smax}$	$(q_{Lmax}/q_{Smax})$
1	.5	.5	.5	.5	.37	1.35
2	.5	.5	0	.5	.29	1.72
3	.25	.5	.5	.5	.27	1.85
4	.3	.5	1.571	.5	.35	1.43
5	.1	.6	-	.6	.31	1.93
6	.2	.6	-	.6	.37	1.62
7	.05	.45	-	.45	.19	2.37

Elliptical Loads  
Stiction or Constant Force Loads

- Line of Constant  $\chi$
- Load Locus
- Line where  $q_s = q_L$
- Projections from Load Locus to Determine  $q_{Smax}$ .

FIG. 4.4 Maximum Supply Flow Reduction





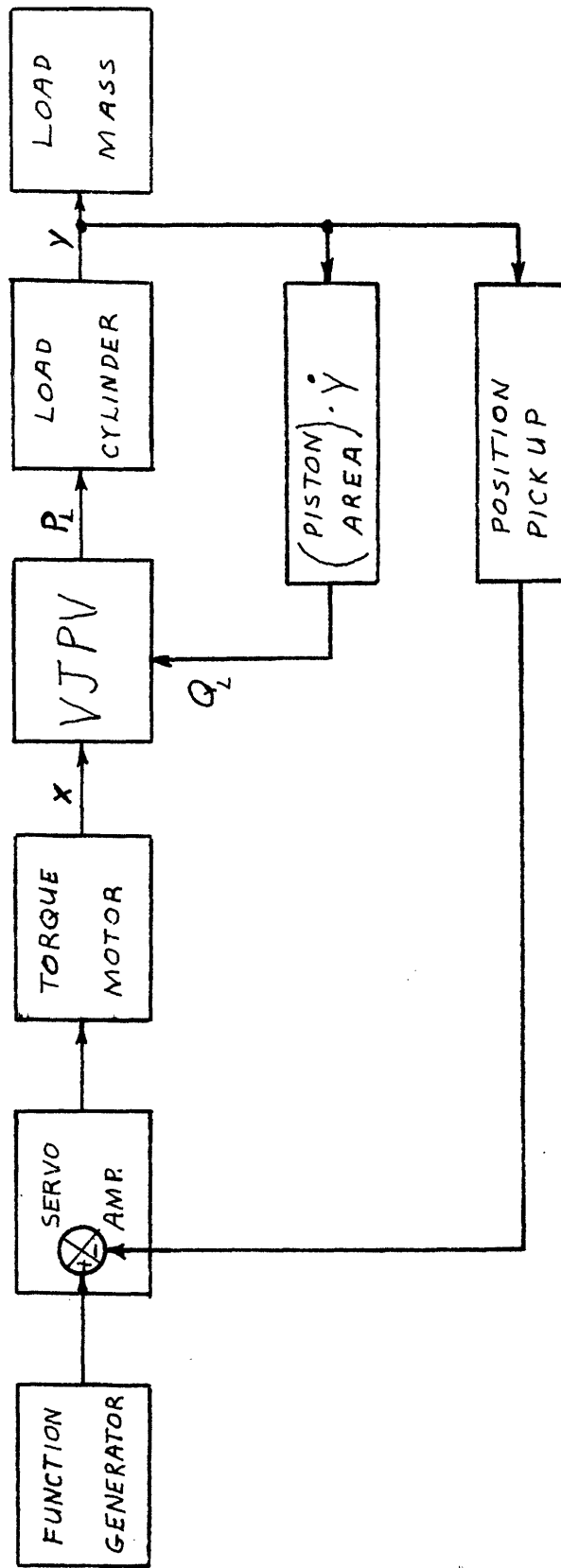


FIG. 5.1 Block Diagram of VJPV  
Position Control System

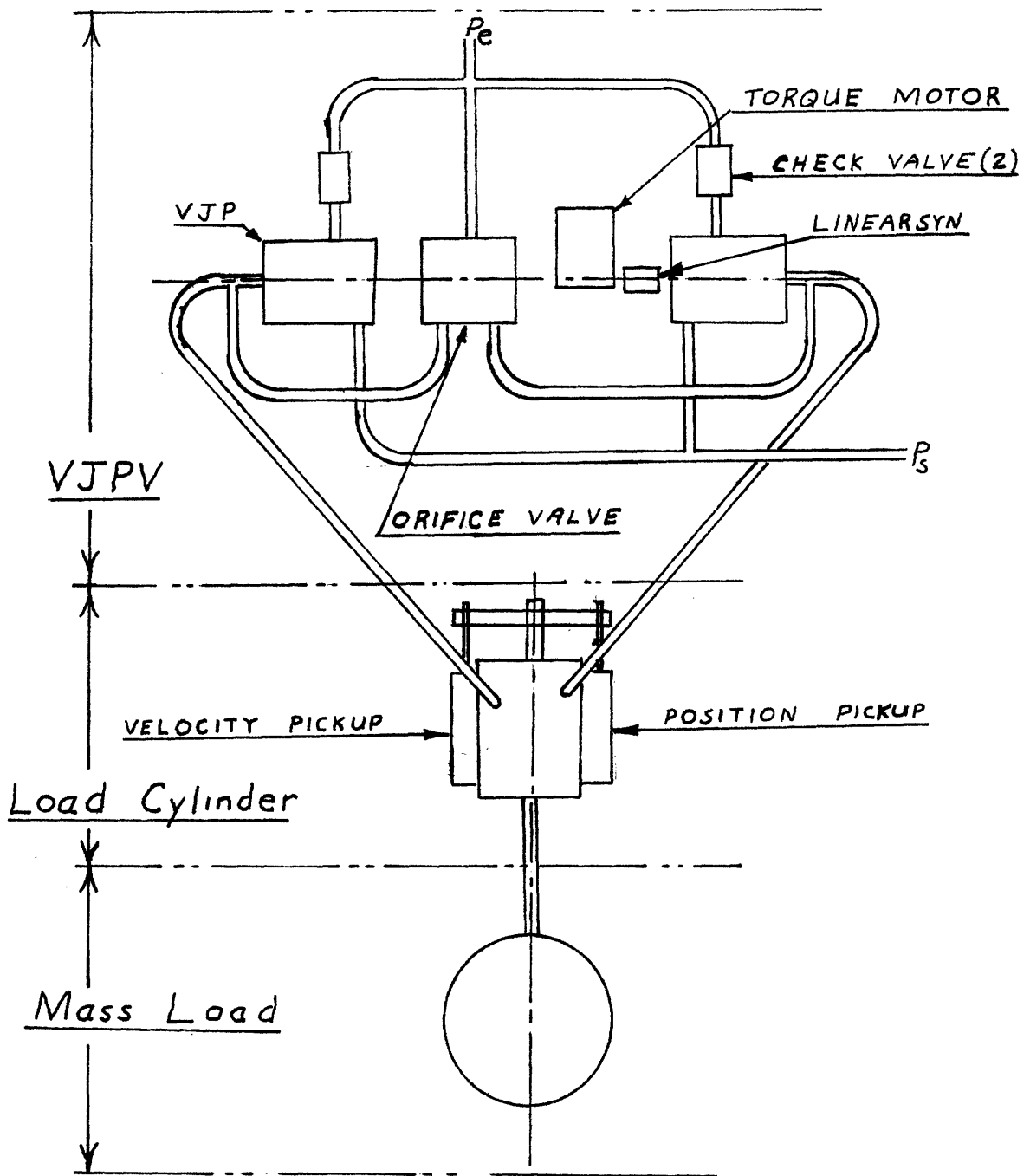


FIG 5.2 a Pictorial of VJPV,  
Load Cylinder, and Load

See: Fig 5.2 b-e for photographs  
Fig. 2.3, 2.4, 2.5 for VJP Design  
Fig. 5.3 for Orifice Valve Design

Fig. 5.2b VJPV test setup

showing

- (1) VJPV
- (2) load cylinder

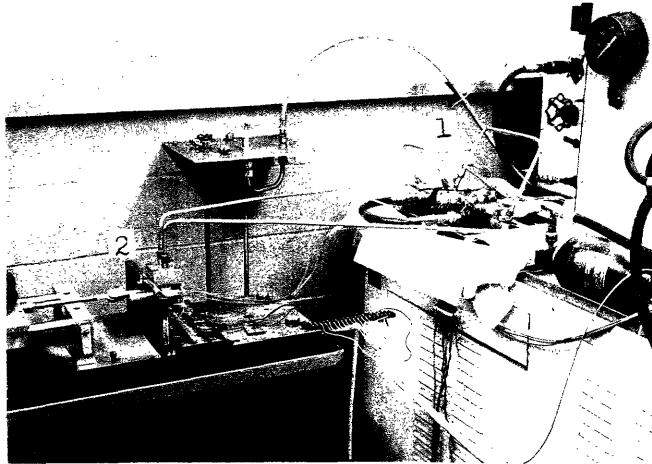


Fig. 5.2c Detail of VJPV

showing

- (1) VJP
- (2) orifice valve
- (3) torque motor
- (4) torque motor position transducer

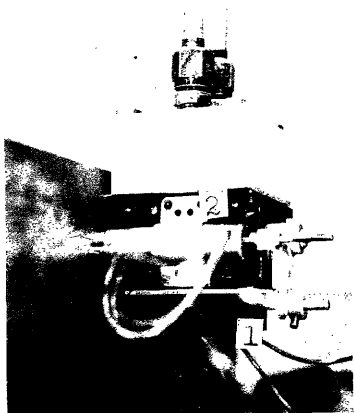
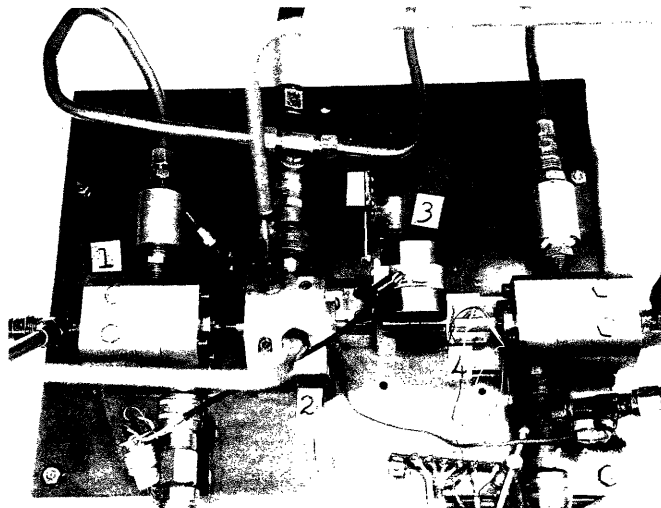


Fig. 5.2d  
Detail of load cylinder

showing

- (1) position transducer
- (2) velocity transducer

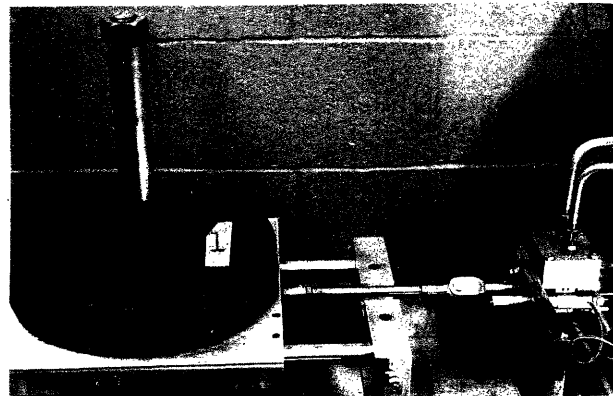


Fig. 5.2e  
Detail of load machine

showing

- (1) load mass

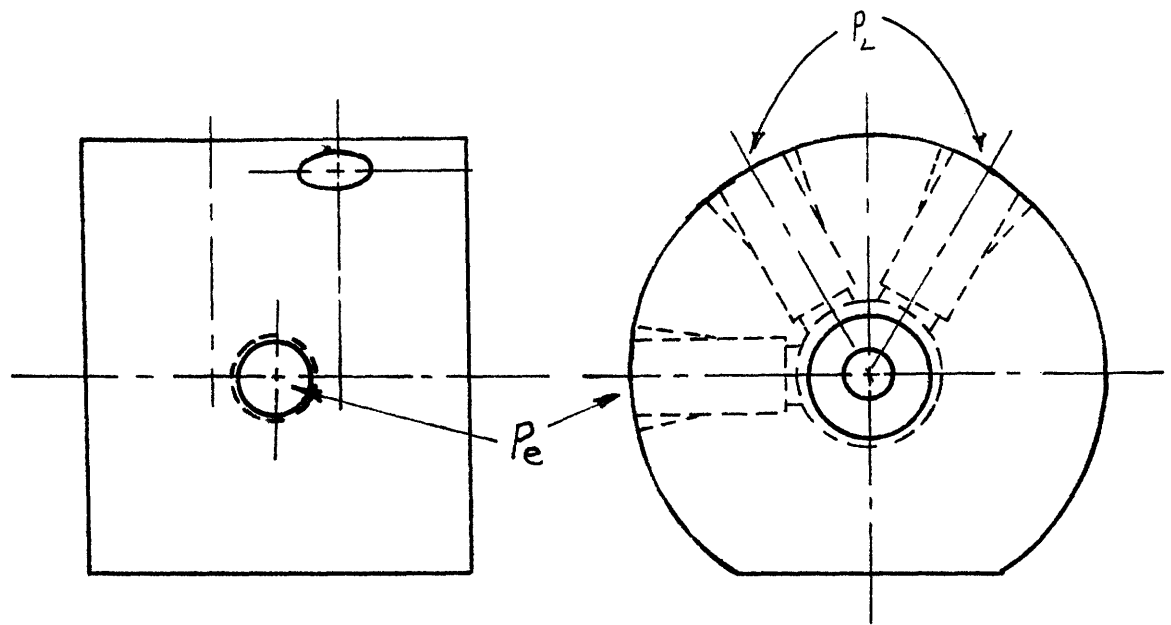
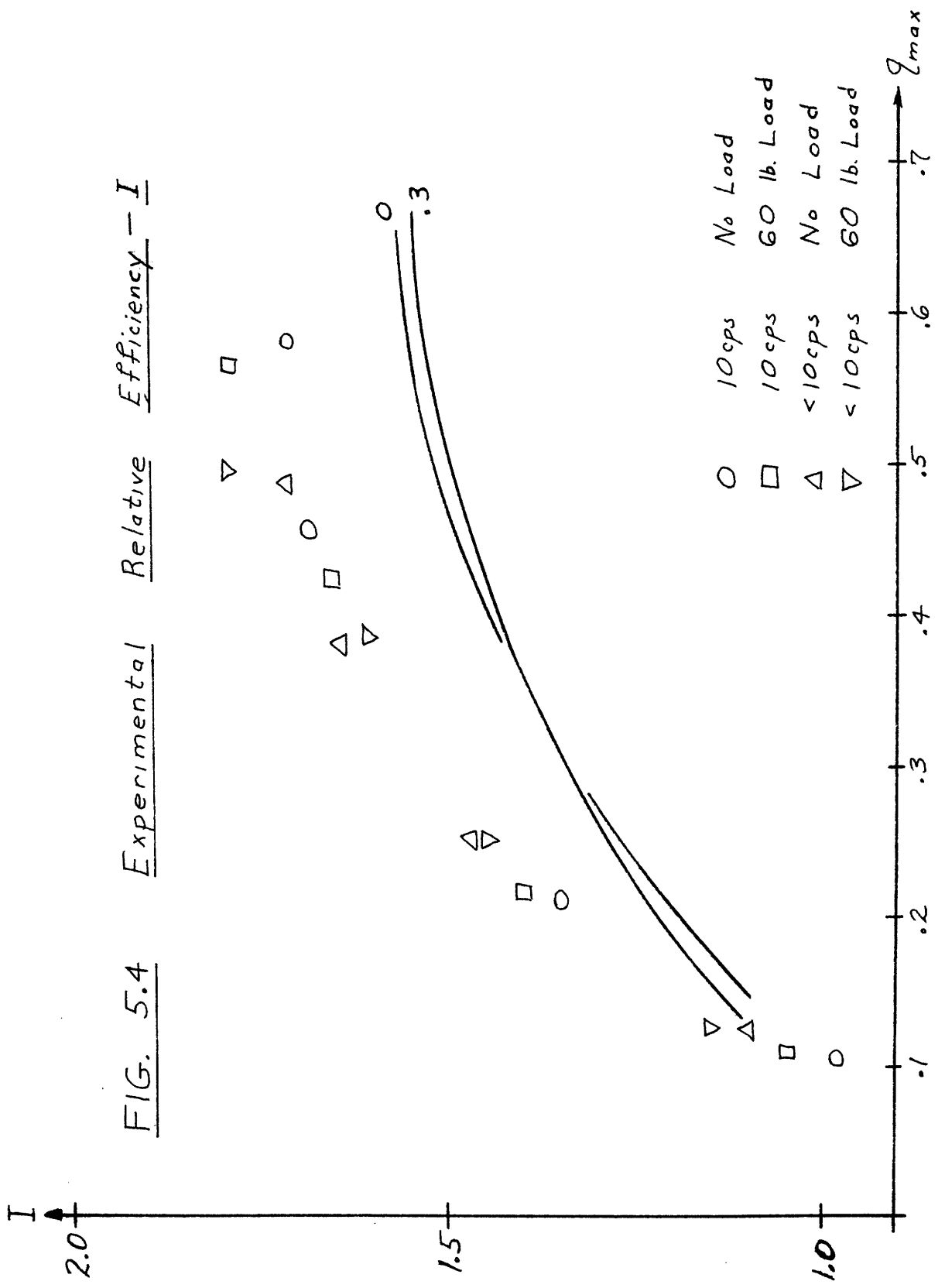
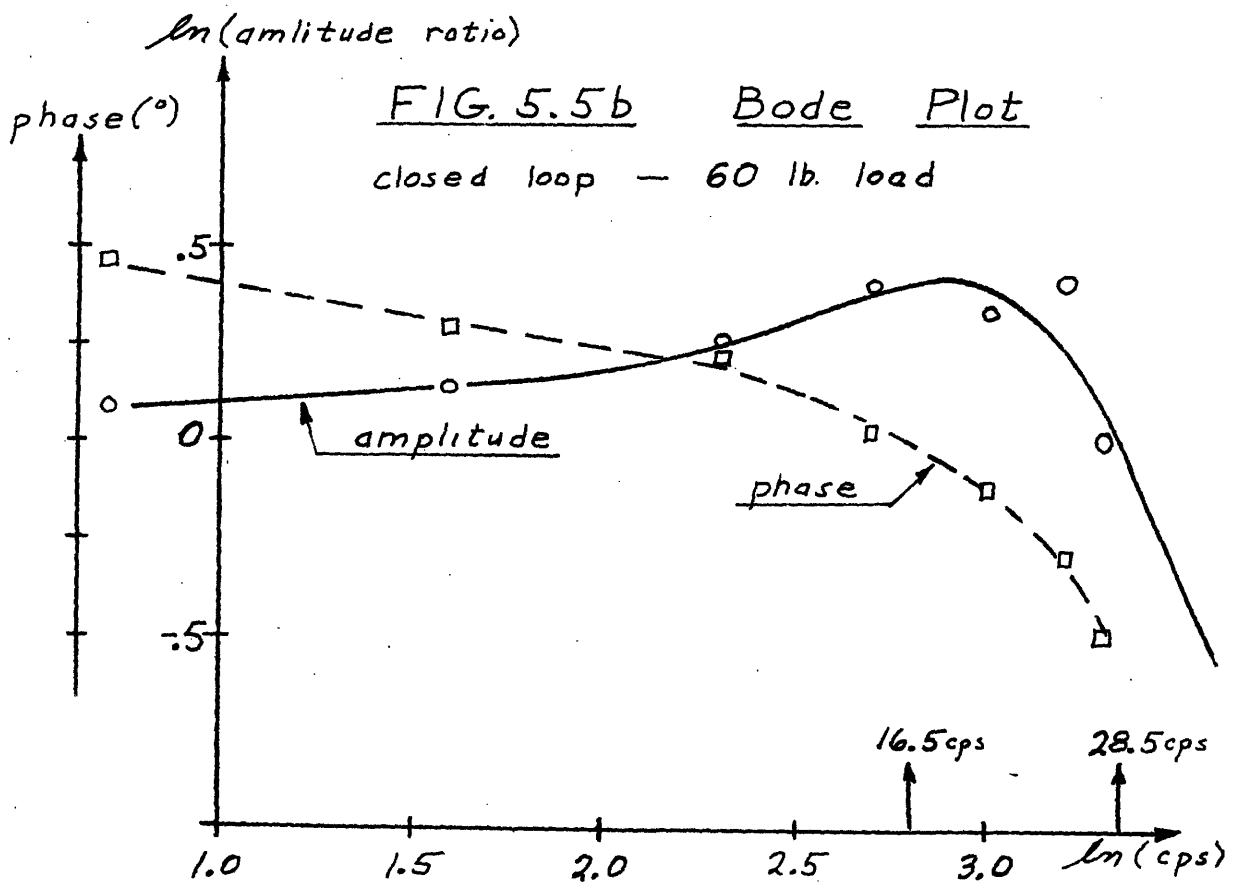
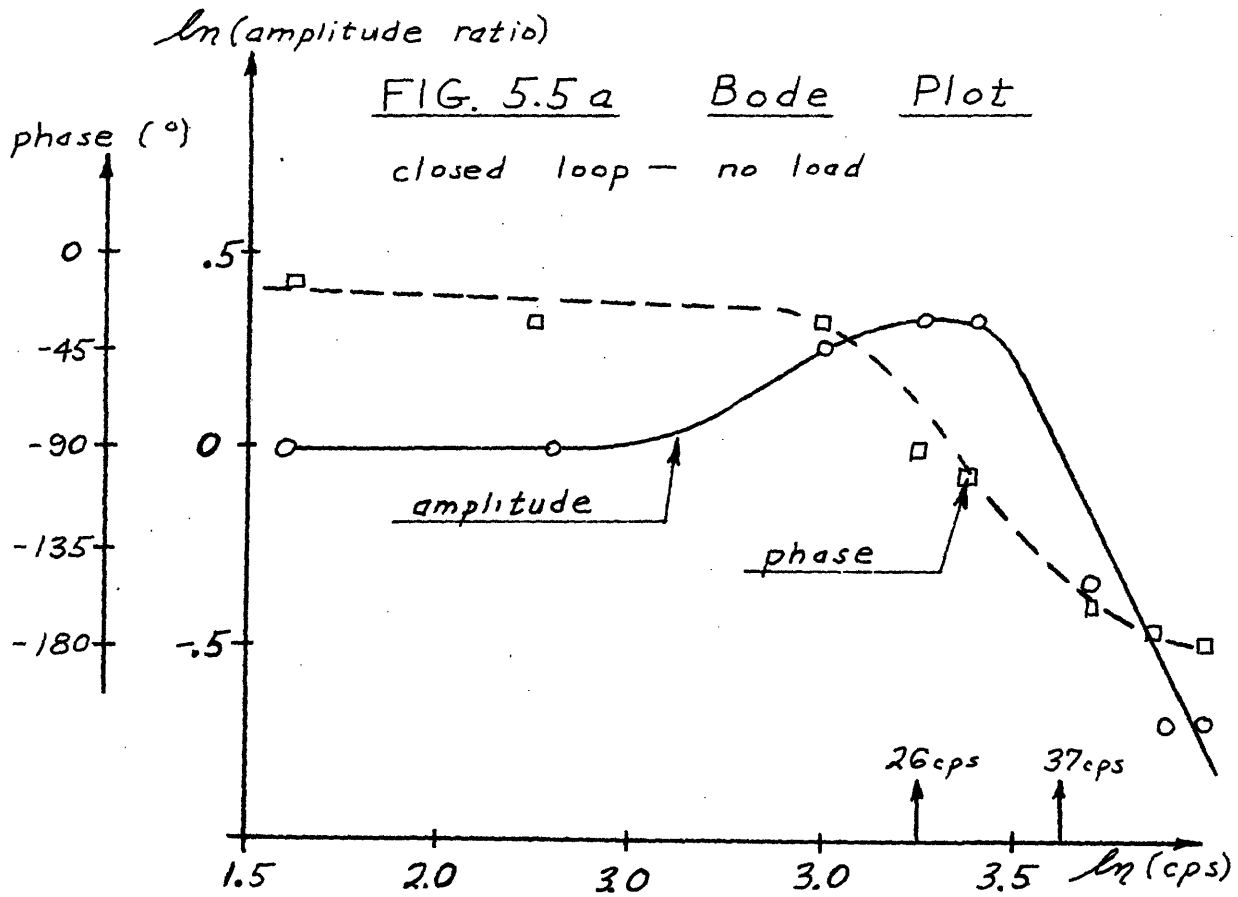


FIG. 5.3    Housing for Orifice Spool  
Valve — Spool 0.250 in. Diameter  
(full size)

FIG. 5.4 Experimental Relative Efficiency - I





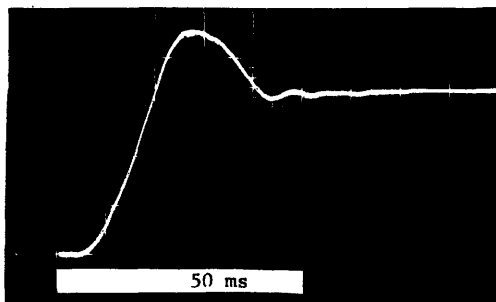


Fig. 5.6a

No-Load Closed-Loop Step-Response  
 $P_s = 1240 \text{ psi}$  ,  $P_e = 220 \text{ psi}$

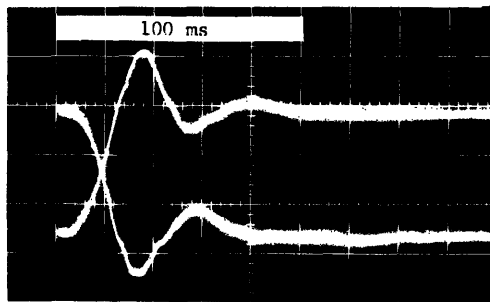


Fig. 5.6b

60 lb.-Load Closed-Loop Step-Response  
 $P_s = 1240 \text{ psi}$  ,  $P_e = 220 \text{ psi}$

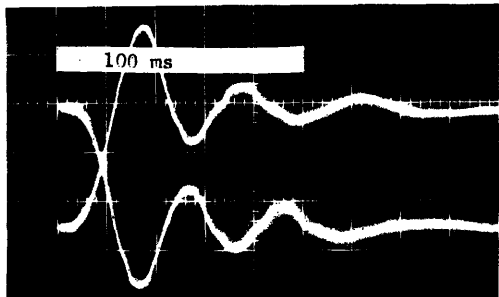


Fig. 5.7

60 lb.-Load Closed-Loop Step-Response  
 Same conditions as Fig. 5.6b except  
 forward loop gain 1/3 greater.

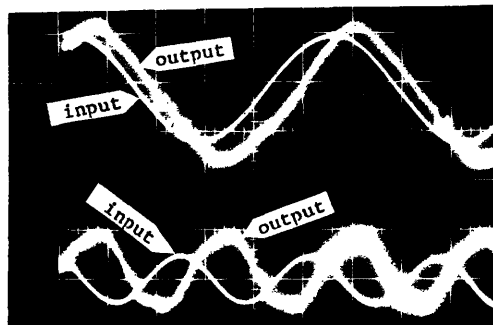


Fig. 5.8

Typical Closed-Loop Wave Forms  
 $P_s = 1240 \text{ psi}$  ,  $P_e = 220 \text{ psi}$   
 Upper: 10 cps    Lower: 20 cps

Fig. 5.9

Lissajous Figures of Torque Motor  
Position (horizontal) and Ram Velocity (1)  
or Ram Displacement (2) at 50 cps  
 No Load,  $P_s = 1240 \text{ psi}$  ,  $P_e = 220 \text{ psi}$

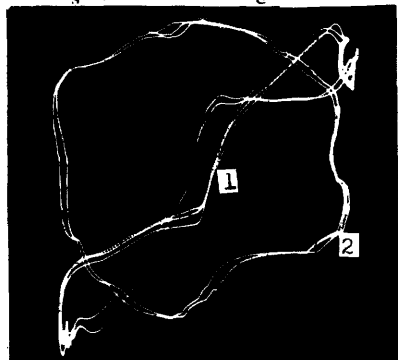
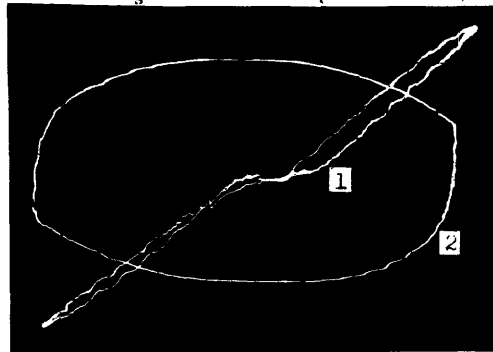


Fig. 5.10

Lissajous Figures of Torque Motor  
Position (horizontal) and Ram Velocity (1)  
or Ram Displacement (2) at 5 cps  
 No Load,  $P_s = 1240 \text{ psi}$  ,  $P_e = 220 \text{ psi}$



## REFERENCES

1. Blackburn, Reetof, and Shearer, Editors: Fluid Power Control, Technology Press of M.I.T., 1960.
2. Cunningham, R. C., The Jet-Pump as a Lubricating Oil Scavenge Pump for Aircraft Engines, ASTIA AD 75184, July 1954, Wright-Patterson AFB.
3. Gasline, and O'Brien, "The Water Jet-Pump," University of California Publications in Engineering, Vol. 3, No. 3, 1934.
4. Graham, D., and McRuer, D., Analysis of Nonlinear Control Systems, John Wiley and Sons, 1961.
5. Hunsaker, J. C., and Rightmire, B. G., Engineering Applications of Fluid Dynamics, McGraw-Hill, 1947.
6. Lewis, E. E., and Stern, H., Design of Hydraulic Control Systems, McGraw-Hill Book Co., 1962.
7. Lung, Kenneth R., "Injector-Impeller Pump," Patent No. 2,457,388, December 28, 1948.
8. Murdock, John, An Investigation into the Use of a Jet-Pump in an Aircraft Fuel System, M.S. Thesis, Course II, M.I.T., January 1964.
9. Shapiro, A. H., The Dynamics and Thermodynamics of Compressible Fluid Flow, Volume 1, Ronald Press Co., 1953.
10. Stepanoff; Centrifugal and Axial Flow Pumps, A. J. Wiley, 1948.



## BIOGRAPHICAL NOTE

The author was born in Rockford, Illinois, on January 6, 1940. He received his Bachelor of Science in Mechanical Engineering from Illinois Institute of Technology in 1962 and a Master of Science in Mechanical Engineering from the University of California at Berkeley in 1963. He is the co-author of ASME paper 63-WA-284, "The Implementation of Linear Time-Optimal Control." The author has been supported in his graduate work by Alfred P. Sloan, Whitney Foundation, and N.S.F. Fellowships and is a member of Phi Eta Sigma, Pi Tau Sigma, and Tau Beta Pi.

## Appendix 1

## GEOMETRY CONSIDERATIONS

Diffusor

Conical diffusors of 7° included angle and area ratio\* of 4 were used in all tests. The literature\*\* shows any angle between 3° and 9° will exhibit about the same pressure recovery and that angles up to 15° degrade performance only slightly. With fully developed turbulent flow a 7° diffusor with area ratio 4 should recover approximately 85% of the dynamic head.

Mixing Section

If wall friction is disregarded, one-dimensional analysis of jet-pumps indicates that converging mixing sections (the so-called constant pressure mixing is a special case of this) are superior to constant diameter mixing sections. This led the author to try 3 converging mixing sections as shown in Fig. 1.10a, b, and c. Except for Fig. 1.10c these performed poorly at the Reynolds number of interest, although it is suspected at very high Reynolds number the longer converging mixing sections, Fig. 1.10a, and b would do quite well. From these tests it was concluded that a very short mixing section was needed. A zero length mixing section model was built, Fig. 1.10d. This unit displayed pressure recovery characteristics similar to the geometry in Fig. 1.10c.

---

\* Ratio of area of diffusor exit area to diffusor inlet area.

\*\* See Eng. Applications of Fluid Dynamics, J. C. Hunsaker and B. G. Rightmire, McGraw-Hill, 1947, p. 348.

It was observed that choking set in at lower values of  $Q_e$  indicating that the exhaust flow separated at the entrance to the diffuser in the manner indicated in Fig. 1.10d. Finally, the standard geometry was tested with substantially the same results as those given by the geometry of Fig. 1.10c. The extremely short mixing section seems to be at variance with the results of other investigators of jet pumps. This may well be because in all other investigations great care is taken to provide a smooth uniform nozzle jet, thus retarding mixing. The nozzle used here is likely to create a great deal of turbulence making mixing a very fast phenomena.

#### Nozzle to mixing section spacing

Cunningham\* indicates that a good spacing to separate the mixing section from the nozzle is  $\frac{D}{2} \cdot \frac{1 - q_s}{\sqrt{q_s}}$  for  $.1 < q_s < .6$ . Because  $q_s$  is not constant in this application but varies from 0 to .55 this formula is hard to apply even if appropriate. A value for this spacing found to be quite good was  $D$ , which in Cunningham's formula corresponds to  $q_s = .17$ . Using much smaller spacing would hinder the exhaust flow. Larger spacing reduces the pressure recovery.

#### Nozzle plate and slider

These elements replace the usual constant diameter nozzle. It is the purpose of these parts to develop a stream of fluid of variable

---

\*I have taken some liberty in translating Cunningham's results to this quite different geometry.

cross sections. The energy losses should be held to a minimum (i.e.,  $C_v$  should be close to 1.0). The stroke of the slider from full open to closed should be short in order to increase the power gain of the VJP. Three different cone angles,  $\alpha$ , (Fig. 1.3) were tried for the sliders. Namely,  $10^\circ$ ,  $25^\circ$ , and  $45^\circ$ .  $C_v$  increased as the angle increased, although  $25^\circ$  and  $45^\circ$  had approximately the same apparent  $C_v$ . The gain,<sup>\*</sup> of course, increases with increasing angle. Thus, the  $45^\circ$  angle was chosen. This problem deserves more detailed attention. The nozzle plate angle,  $\beta$ , Fig. 1.3 was not investigated. It was assumed that  $\beta$  should be much greater than  $\alpha$  so that the flow remains next to the slider cone. However, this assumption may be unnecessary. Of course,  $\beta$  is limited by strength of material considerations. A more sculptured nozzle plate was tried as shown in Fig. 1.11. This made no improvement in performance and in view of its more difficult manufacture it should not be considered.

---

\*By gain is meant the  $\left( \frac{\text{change in nozzle flow}}{\text{change in slider position}} \right)$ .

## Appendix 2

## REYNOLDS NUMBER AND NORMALIZING FACTOR CALCULATIONS

All calculations are based on J-43 at 96°F. Viscosity and density of J-43 versus temperature are given by Fig. 1.4. The 3 Reynolds numbers of interest are:

$$R_N \equiv \frac{\sqrt{2P_s \rho}}{\mu} d$$

$$R_T \equiv \frac{\sqrt{2P_s \rho}}{\mu} D$$

$$R_{\text{vap}} \equiv \frac{\sqrt{-2P_{\text{vap}} \rho}}{\mu} D$$

In all experimental work of Chapters 1 and 2,  $d = .108$  in.  $D = .125$  in.

From Fig. 1.4:

$$\rho = 7.8 \times 10^{-5} \frac{\text{lb. sec}^2}{\text{in}^4}$$

$$\mu = 2.2 \times 10^{-6} \frac{\text{lb. sec.}}{\text{in}^2}$$

thus,

$$\frac{\sqrt{2\rho}}{\mu} = 5.63 \times 10^3$$

$$R_N = 613 \sqrt{P_s}$$

$$R_T = 710 \sqrt{P_s}$$

$$R_{\text{vap}} = 710 \sqrt{-P_{\text{vap}}}$$

The normalizing flows of interest are

$$\frac{\pi}{4} d^2 \sqrt{\frac{2P_s}{\rho}} \quad \text{and} \quad \frac{\pi}{4} D^2 \sqrt{\frac{2P_s}{\rho}}$$

since  $\frac{\pi}{4} \sqrt{\frac{2}{\rho}} = 126$

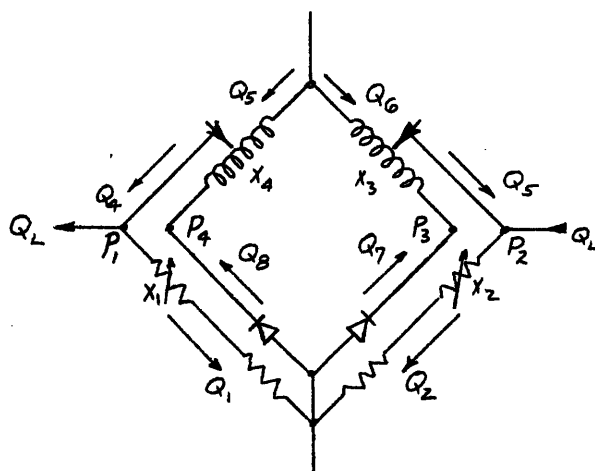
$$\frac{\pi}{4} d^2 \sqrt{\frac{2P_s}{\rho}} = 1.47 \sqrt{P_s}$$

$$\frac{\pi}{4} D^2 \sqrt{\frac{2P_s}{\rho}} = 1.97 \sqrt{P_s}$$

## Appendix 3

## VJPV PRESSURE-FLOW EQUATIONS

In Chapter 3 the equations describing the pressure-flow characteristics of a 4-way constant-supply-pressure VJPV were presented. In that derivation  $P_s$  and  $P_4$  were taken



as zero and it was shown that under ordinary conditions this would lead to only a small error in the VJPV characteristics. If this error cannot be tolerated Eq. 3.13 no longer is valid and the following relationships must be substituted.

As in Chapter 3 define:

$$g(x) \equiv \left(\frac{d}{D}\right)^2 (C_d f(x) + q_{No}) \quad \text{III.1}$$

If  $P_1 \leq 2C_v g(x_4) - (2 - \eta) g^2(x_4)$  then the VJP is not in the blocked condition. To apply the equations given in the "Summary of VJP Characteristics," p. 29, some care must be taken. In these equations it is assumed

that the exhaust pressure is zero in the induced and choked flow condition. If the check valve pressure drop is to be considered, then the exhaust pressure in the induced and choked flow condition is less than zero. Thus, while the equations are still correct it must be remembered that all pressures must now be referred to  $P_4$  rather than zero (i.e.,  $P_e$ ). The original induced flow equations are:

$$\begin{aligned} \mathcal{P}_L &= 2C_v q_s - (2 - \eta)q_s^2 - [2(2 - \eta)q_s + (2 - \eta - \psi)q_{eo}] q_e \\ q_s &= g(\chi) \end{aligned} \quad \text{III.2}$$

(Valid only for exhaust pressure equal to zero)

Putting these in unnormalized form with pressures referred to  $P_4$  they become:

$$\begin{aligned} \frac{P_1 - P_4}{P_s - P_4} &= 2C_v \frac{Q_s}{A_T \sqrt{\frac{2(P_s - P_4)}{\rho}}} - (2 - \eta) \left[ \frac{Q_5}{A_T \sqrt{2(P_s - P_4)/\rho}} \right]^2 \\ &\quad - [2(2 - \eta) \frac{Q_5}{A_T \sqrt{2(P_s - P_4)/\rho}} + (2 - \eta - \psi)q_{eo}] \frac{Q_s}{A_T \sqrt{2(P_s - P_4)/\rho}} \end{aligned} \quad \text{III.3}$$

$$\frac{Q_5}{A_T \sqrt{2(P_s - P_4)/\rho}} = g(\chi_4)$$



then substituting:

$$\gamma \equiv \sqrt{1 - \mathcal{P}_4} = \sqrt{\frac{P_s - P_4}{P_s}} \quad \text{III.4}$$

III.3 becomes:

$$\begin{aligned} \mathcal{P}_1 - \mathcal{P}_4 &= 2C_v \gamma q_5 - (2 - \eta) q_5^2 - \\ &[2(2 - \eta) q_5 + (2 - \eta - \psi) \gamma q_{e0}] q_8 \end{aligned} \quad \text{III.5}$$

$$q_5 = \gamma g(x_4)$$

One also has the relationships from Eq. 3.8 that:

$$q_8 = K_c \sqrt{-\mathcal{P}_4} \quad \text{III.6}$$

Eq. III.4, III.5, and III.6 are four equations in four unknowns,  $\mathcal{P}_4$ ,  $q_5$ ,  $q_8$ , and  $\gamma$ , which when solved, replace the induced flow portion of Eq. 3.13.  $\mathcal{P}_1$  and  $x_4$  are considered given.

For the choked condition, the original equations are:

$$1 = \frac{q_s}{C_v} \sqrt{\frac{P_s}{P_s - P_{\text{vap}}}} + \frac{q_e}{k_v} \sqrt{\frac{P_s}{-P_{\text{vap}}}} \quad \text{III.7}$$

$$q_5 = g(x)$$

(Valid only for exhaust pressure equal to zero)

Again referring all pressures to  $P_4$  Eq. III.7 writes:

$$1 = \frac{q_s}{C_v A_T \sqrt{2(P_s - P_4)/\rho}} \sqrt{\frac{P_s - P_4}{P_s - P_4 - (P_{\text{vap}} - P_q)}} + \frac{q_e}{k_v A_T \sqrt{2(P_s - P_q)/\rho}} \sqrt{\frac{P_s - P_4}{-(P_{\text{vap}} - P_4)}} \quad \text{III.8}$$

or

$$1 = \frac{q_5}{C_v \sqrt{1 - \rho_{\text{vap}}}} + \frac{q_8}{k_v \sqrt{\rho_1 - \rho_{\text{vap}}}} \quad \text{III.9}$$

and as before:

$$q_5 = \gamma g(x_4) \quad \text{III.10}$$

$$q_8 = k_c \sqrt{-\rho_1}$$

$$\gamma \equiv \sqrt{1 - \rho_4}$$

Eq. III.9 and III.10 replace the choked flow portion of equation 3.13.